TECHNISCHE UNIVERSITÄT MÜNCHEN
DEPARTMENT CHEMIE
LEHRSTUHL FÜR BIOCHEMIE

Discovery and Characterization of Novel Proteasome Ligand Binding Sites

Philipp Beck

Vollständiger Abdruck der von der Fakultät für Chemie der Technischen Universität München zur Erlangung des akademischen Grades eines Doktors der Naturwissenschaften (Dr. rer. nat.) genehmigten Dissertation.

Vorsitzender: Univ.-Prof. Dr. J. Buchner

Prüfer der Dissertation

1. Univ.-Prof. Dr. M. Groll
2. Univ.-Prof. Dr. L. Hintermann
3. Univ.-Prof. Dr. F. E. Kühn

Die Dissertation wurde am 03.07.2014 bei der Technischen Universität München eingereicht und durch die Fakultät für Chemie am 15.09.2014 angenommen.

Für Laura und Katharina

Table of Contents

1 Summary 1

2 Zusammenfassung 3

3 Introduction 7

3.1 The ubiquitin-proteasome-system 7

3.1.1 Polyubiquitin-tags label proteins for degradation by the 26S proteasome 7

3.1.2 Architecture and workflow of the 26S proteasome 8

3.2 The 20S core particle as a drug target 12

3.2.1 First generation of CP inhibitors 12

3.2.2 Second generation of CP inhibitors 14

3.2.3 Current developments: plasma stability and tissue targeting 16

3.3 Screening methods for the discovery of novel CP ligands 18

3.3.1 Biochemical methods 18

3.3.2 Biophysical methods 19

3.3.3 X-ray crystallography-based screening methods 21

4 Objective 23

5 Materials and Methods 25

5.1 Materials 25

5.1.1 Chemicals 25

5.1.2 Strains 25

5.1.3 Flurogenic Substrates 25

5.1.4 Instruments 25

5.2 Protein chemistry 28

5.2.1 Purification of the yeast 20S proteasome (yCP) 28

5.2.2 Determination of protein concentrations 29

5.3 Protein crystallography 29

5.3.1 Crystallization and sample preparation of the yeast 20S proteasome (yCP) ... 29

5.3.2 Data collection, processing and structure determination 30

5.4 Yeast mutagenesis 30

5.5 *In vitro* activity assays 31

5.5.1 Determination of yCP inhibition and & IC_{50} measurements 31
5.5.2 HPLC-MS substrate digestion assay 31
5.5.3 Determination of the β5 activity in yeast cells 32
5.5.4 Halo assay for growth inhibition of yeast cells 32
5.6 Cell culture experiments 33
5.6.1 Cell viability assays 33
5.6.2 Proteasome-Glo® assays 34
5.7 Synthesis of sulfonamide derivatives 34
5.8 Synthesis of peptidic substrates 43
5.8.1 Solid phase synthesis 43
5.8.2 Resin cleavage and purification 44
6 Results 45
6.1 Collection of a focused library for crystallographic screening 45
6.1.1 Steroids (A) 48
6.1.2 Polyketides (B) 48
6.1.3 Natural and synthetic alkaloids (C) 49
6.1.4 Cyclic Peptides (D) 49
6.1.5 Metal complexes (E) 49
6.1.6 Assorted natural products (F) 50
6.1.7 Synthetic compounds (G) 50
6.2 Evaluation of screening hits 53
6.3 Screening hit I: Sulfonamides (SA) 54
6.3.1 Discovery of SA by in silico screening 54
6.3.2 Crystal structure of SA bound to the yCP 54
6.3.3 Synthesis of SA and derivatives 57
6.4 Screening hit II: kendomycin (KM) 61
6.4.1 Discovery & cytotoxicity of KM 61
6.4.2 KM inhibits the CP in the presence of SDS 61
6.4.3 Crystal structure of KM bound to the yCP 64
6.4.4 *In vivo* effect of KM on HeLa and yeast cells 68

6.5 Screening hit III: Phakellin Derivative (PD) 71
6.5.1 Origin and discovery of phakellins and phakellstatins as CP inhibitors 71
6.5.2 Crystal structure of PD bound to the yCP 72
6.5.3 Influence of the halogen bond for ligand stabilization 75
7 Discussion 77
7.1 Discovery of three CP ligands with novel binding modes 77
7.2 Guidelines for the rational design of CP inhibitors 79
7.2.1 SA: CP subtype specificty and dual targeting of β1 and β2 80
7.2.2 PD: a scaffold for β5-selective inhibitors 81
8 Bibliography 83
9 Appendix 93
10 Abbreviations 94
11 Publications 97
12 Acknowledgement 99
13 Declaration 101

1 Summary

The 20S proteasome is the proteolytic core particle (CP) of the ubiquitin-proteasome-system (UPS) and represents a key control enzyme for most of biological pathways in eukaryotic cells. Moreover, it plays a pivotal role in many disease-associated processes, such as cell proliferation, apoptosis, the regulation of gene transcription and immune response.[1,2] In the last decade, two drugs (*Velcade*® and *Kyprolis*®) received FDA-approval and evolved to blockbuster drugs for the treatment of multiple myeloma. Furthermore, current studies indicate that CP inhibitors are by far not limited to blood cancer, but can also be applied against solid tumors, inflammatory diseases and autoimmune disorders.

However, the rapid development of resistances, severe side-effects as well as unfavorable pharmacokinetic and -dynamic properties of the applied CP inhibitors highlight the need for novel ligands. The development of new inhibitors is hampered by a lack of structural knowledge from ligands that target different binding sites and/or have a non-covalent binding mode. In addition, current screening methods for CP drug discovery suffer from low sensitivity and are limited to the detection of irreversible inhibitors.

The present thesis presents the discovery and characterization of new CP ligands *via* direct crystallographic screening of a focused compound library (Figure 1). Crystal soaking and data collection with subsequent automated search of the respective F_O-F_C-difference electron density maps identified three unique non-peptidic reversible and irreversible screening hits from natural as well as synthetic origin: i) the sulfonamide (SA), ii) the natural product kendomycin (KM) and a synthetic phakellin derivative (PD) (Figure 1C). The ligands exhibit distinct chemotypes and display a hitherto unparalleled mode of action. In addition, each hit molecule populates a previously unidentified CP binding site and hence, the structural and biochemical characterization of the ligands are discussed as separate case studies.

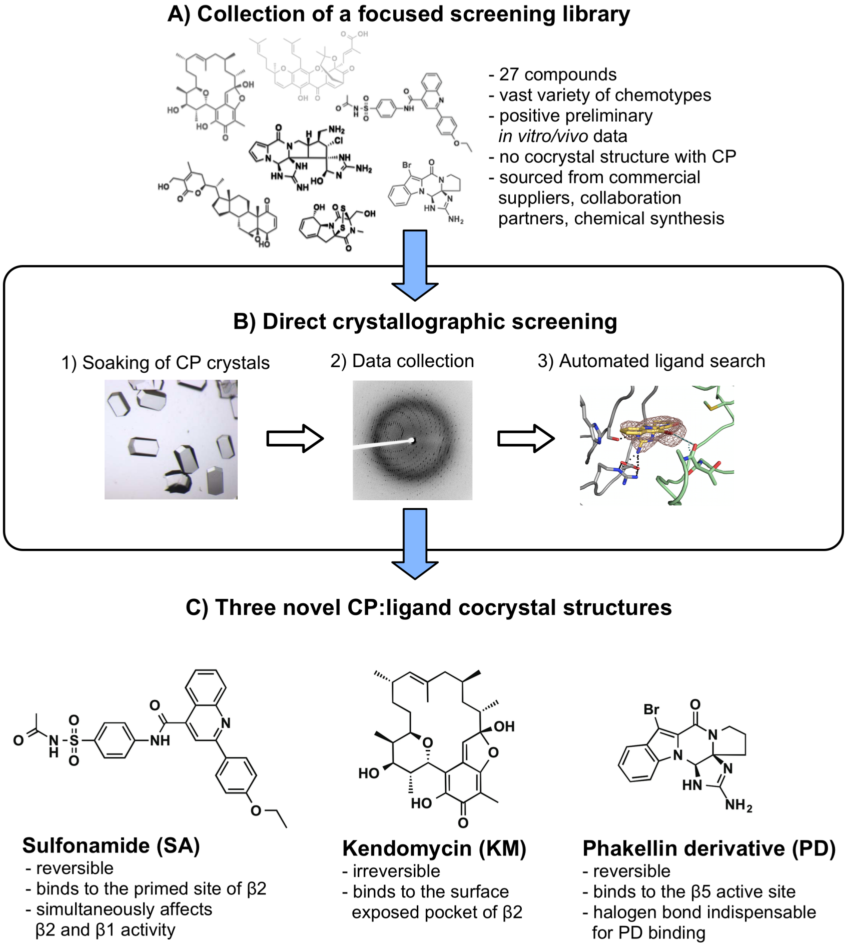
A) Collection of a focused screening library
- 27 compounds
- vast variety of chemotypes
- positive preliminary in vitro/vivo data
- no cocrystal structure with CP
- sourced from commercial suppliers, collaboration partners, chemical synthesis
B) Direct crystallographic screening
1) Soaking of CP crystals
2) Data collection
3) Automated ligand search
C) Three novel CP:ligand cocrystal structures
Sulfonamide (SA)
- reversible
- binds to the primed site of β2
- simultaneously affects β2 and β1 activity
Kendomycin (KM)
- irreversible
- binds to the surface exposed pocket of β2
Phakellin derivative (PD)
- reversible
- binds to the β5 active site
- halogen bond indispensable for PD binding

Figure 1: Direct crystallographic screening of a focused compound library. A) Collection of compounds through commercial sources, synthesis or collaborations resulted in a focused screening library with 27 highly diverse molecules. B) yCP crystals are soaked with the screening compounds and the resulting datasets are subsequently evaluated by automatic search of the difference electron density maps. C) Three novel CP:ligand cocrystal structures with distinct chemotypes and mode of actions were identified. All inhibitors populate hitherto unknown binding sites of the CP.

The first case study examines the yCP crystal structure in complex with the synthetic sulfonamide ligand that reversibly interacts with the primed β2 substrate binding channel. As a consequence, SA exhibits an unusual inhibition profile that affects both, the β1 as well as the β2 catalytic activity. In addition, the ligand addresses a so far unidentified binding pocket that differs significantly among mammalian CP subtypes. Thus, SA provides a synthetically accessible scaffold for generation of CP subtype specific ligands.

The second screening hit is represented by the yCP:KM complex structure. KM is a highly cytotoxic fungal metabolite from *Streptomyces violaceoruber* and comprised of an ansa-polyketide scaffold with a reactive quinone methide. The natural product covalently binds to β2-His141N$^{\gamma}$ into a surface exposed pocket formed by the subunits β2 and β7'. Thorough hit validation *via* crystallographic, mutagenesis and cell culture studies revealed that the CP is not the primary target of KM, which rather exhibits a polypharmacologic mode of action *in vivo.* These findings highlight the importance of using a broad and orthogonal set of methods for careful validation of screening hits that give promising but ambiguous results.

The third case study describes the yCP crystal structure in complex with a synthetic phakellin-derivative (PD, Figure 1C) that is closely related to the highly publicized palau'amine, bearing characteristic pyrrole-2-carboxyamide and 2-aminoimidazoline moieties. The ligand solely binds to the *sub*-P3 pocket of the β5 substrate binding channel with an IC_{50} of 3.5 μM, stabilized by tight coordination of the 2-aminoimidazole ring and formation of a C=O···Br halogen bond to β5-Thr21. Remarkably, the binding affinity of a debrominated PD analogue was decreased by one order of magnitude (IC_{50} = 25 μM), thus underlining the important influence of the halogen bond for ligand stabilization.

In summary, the herein described screening hits expand the druggable space that can be targeted by proteasome inhibitors. In addition, the structural insights from the presented complex structures can be exploited as starting points for the structure-based design of novel drugs with potential application for the treatment of cancer, inflammatory and autoimmune diseases as well as tool compounds for biochemical research.

2 Zusammenfassung

Das 20S Proteasom ist das proteolytische Kernelement (core particle, CP) des Ubiquitin-Proteasom-Systems (UPS) und ist ein essentielles Kontrollenzym für die Zellteilung und -differenzierung. Durch diese Schlüsselposition im zellulären Stoffwechsel stellt die Inhibition des Proteasoms eine wirkungsvolle Therapiemöglichkeit verschiedener Krebserkrankungen dar. In den letzten 10 Jahren erhielten zwei CP-Blocker (Velcade® und Kyprolis®) die Marktzulassung und entwickelten sich zu Blockbustern im Einsatz gegen Krebserkrankungen des Knochenmarks (Multiples Myelom). Aktuelle Studien zeigen zudem, dass die Anwendung von CP Inhibitoren nicht auf Blutkrebsarten beschränkt ist,

sondern auch gegen solide Tumoren, chronischen Entzündungserkrankungen und Autoimmunkrankheiten ein wirksames Mittel darstellt.

Die rasche Resistenzentwicklung in der Tumortherapie, starke Nebenwirkungen und die ungünstigen pharmakokinetischen und -dynamischen Eigenschaften der vermarkteten CP Inhibitoren unterstreichen die Notwendigkeit zur Entwicklung von Liganden mit neuer Wirkungsweise. Trotz umfangreicher Forschungen ist die Entwicklung neuer Inhibitoren limitiert, da keine strukturellen Kenntnisse über neuartige Leitstrukturen vorliegen. Zusätzlich wird die Entdeckung neuer Wirkstoffe durch die geringe Empfindlichkeit aktueller Screeningverfahren eingeschränkt.

Die vorliegende Arbeit behandelt die Entdeckung und Charakterisierung von neuen CP-Liganden durch ein direktes kristallographisches Screening einer fokussierten Substanzbibliothek. Kristallisation, Röntgenbeugung, Datensammlung und automatisierte Absuche der entsprechenden F_O-F_C-Differenzelektronendichtekarten führte zur Identifizierung von drei nicht-peptidischen, reversiblen und irreversiblen Screening Hits mit natürlichem als auch synthetischen Ursprung (Abbildung 2): a) das Sulfonamid (SA), b) das Naturprodukt Kendomycin (KM) und c) ein synthetisches Phakellin-Derivat (PD) (Abbildung 2C). Alle Liganden besitzen unterschiedliche Chemotypen und zeichnen sich durch einen neuartigen Bindemodus aus. Darüber hinaus wechselwirkt jede der Substanzen in einer bisher nicht beschriebenen Art und Weise mit dem CP, weshalb die einzelnen Screening Hits in separaten Fallstudien besprochen werden.

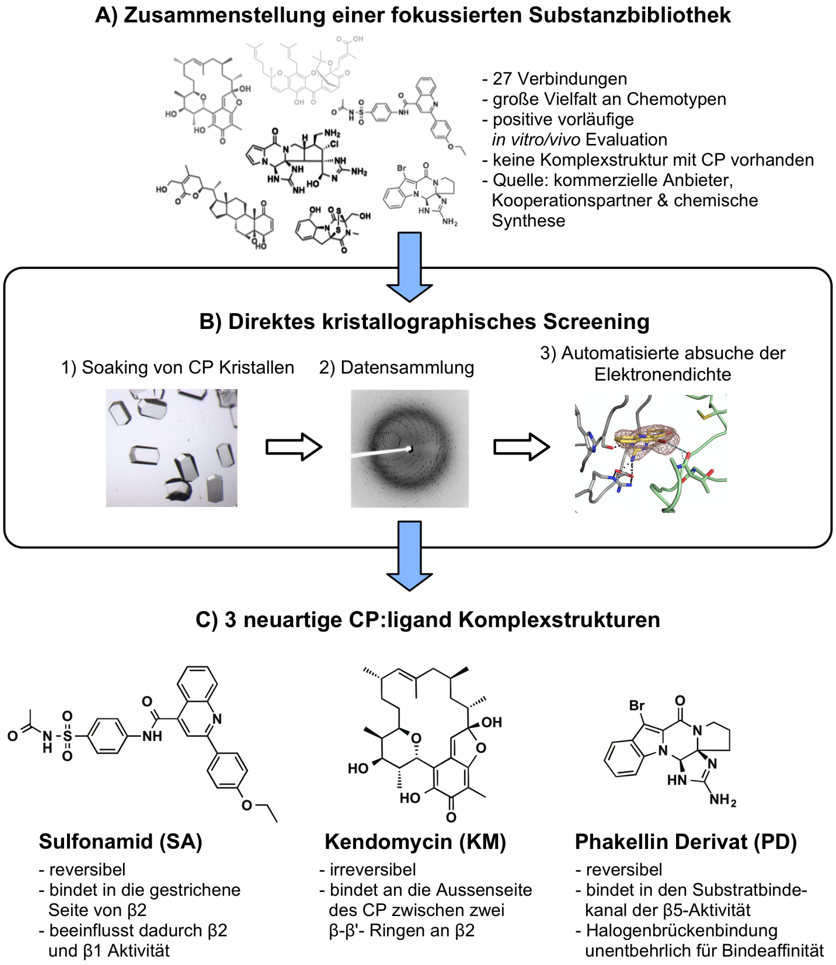
A) Zusammenstellung einer fokussierten Substanzbibliothek
- 27 Verbindungen
- große Vielfalt an Chemotypen
- positive vorläufige in vitro/vivo Evaluation
- keine Komplexstruktur mit CP vorhanden
- Quelle: kommerzielle Anbieter, Kooperationspartner & chemische Synthese
B) Direktes kristallographisches Screening
1) Soaking von CP Kristallen
2) Datensammlung
3) Automatisierte absuche der Elektronendichte
C) 3 neuartige CP:ligand Komplexstrukturen
Sulfonamid (SA)
- reversibel
- bindet in die gestrichene Seite von β2
- beeinflusst dadurch β2 und β1 Aktivität
Kendomycin (KM)
- irreversibel
- bindet an die Aussenseite des CP zwischen zwei β-β'- Ringen an β2
Phakellin Derivat (PD)
- reversibel
- bindet in den Substratbindekanal der β5-Aktivität
- Halogenbrückenbindung unentbehrlich für Bindeaffinität

Abbildung 2: Kristallographisches Screening einer fokussierten Verbindungsbibliothek. A) Eine fokussierte Substanzbibliothek mit 27 vielfältigen Substanzen bildet den Grundstein für das kristallographische Screening. B) Kristalle des Hefe 20S Proteasoms wurden mit den Screeningkandidaten behandelt; Aufnahme von Beugungsdaten und anschließende automatisierte Absuche der F_O-F_C-Differenzelektronendichtekarten führte zur Identifizierung von drei neuartigen CP Liganden (C), die alle bislang nicht beobachtete und individuelle Wechselwirkungen mit dem CP eingehen.

Die erste Fallstudie untersucht die Komplexstruktur aus yCP und dem synthetischen Sulfonamid-Liganden (SA), der reversibel in die gestrichene Seite des β2 Substratbindekanals wechselwirkt. Dieser Bindemodus erklärt die ungewöhnliche Doppelwirkung von SA auf die β1- und β2-Aktivität des Proteasom *in vitro*. Die yCP:SA Komplexstruktur zeigt, dass der Chinolinring des Inhibitors tief in eine Bindeasche ragt, die in den verschiedenen Säugerproteasom-Subtypen hinsichtlich Polarität und Größe unterschiedlich ausgeprägt ist. Somit stellt SA ein synthetisch zugänglicher Ausgangspunkt für die Entwicklung von selektiven CP Inhibitoren dar.

Der zweite Screening Hit wird mit der yCP:KM Komplexstruktur vorgestellt. KM ist ein sekundärer Metabolit aus *Streptomyces violaceoruber*, der aus einem Ansa-Polyketidgerüst mit reaktivem Chinonmethid besteht. Die starke cytotoxische Substanz bindet an der Grenzfläche zwischen zwei β-β' Ringen des CP kovalent an β2-His141N^{γ}. Die Bindetasche liegt exponiert an der Oberfläche des Proteasoms und wird durch die β2- und β7' Untereinheiten gebildet. Im Validierungsprozess konnte durch Mutations- und Zellkulturstudien jedoch gezeigt werden, dass das CP nicht das molekulare Target von KM *in vivo* ist und einen unspezifischen, polypharmakologischen Wirkmechanismus besitzt. Diese Ergebnisse unterstreichen die Bedeutung von orthogonalen Analysemethoden für die sorgfältige Validierung von vielversprechenden Kandidaten.

Die dritte Fallstudie beschreibt eine yCP Kristallstruktur im Komplex mit einem synthetischen Phakellin-Derivat (PD), das durch die charakteristischen Pyrrol bzw. 2-Aminoimidazol-Ringen in enger Verwandtschaft mit dem vielbeachteten Naturprodukt Palau'amine steht. PD wechselwirkt ausschließlich mit der *sub*-S3 Bindetasche des β5 Substratbindekanals (IC_{50} = 3.5 μM) und ist durch starke Koordination des 2-Aminoimidazols und der Ausprägung einer $C{=}O\cdots Br$ Halogenbrückenbindung mit dem Proteinrückgrat stabilisiert. Dehalogenierung des Liganden führt zu einem bemerkenswerten Abfall der Bindeaffinität (IC_{50} = 25 μM), was den Einfluss der $CO\cdots Br$ Bindung unterstreicht.

Die in dieser Arbeit beschriebenen Methoden und identifizierten Proteasomliganden leisten einen wichtigen Beitrag zum Wissensstand über CP Inhibitoren, da der Großteil der bisherigen kristallographischen Studien hauptsächlich peptidische Verbindungen behandelt. Die strukturellen Erkenntnisse aus den vorgestellten Komplexstrukturen dienen somit als Ausgangspunkte sowohl für ein strukturbasiertes Design neuer Wirkstoffe als auch der Optimierung bereits verwendeter Proteasominhibitoren zur Behandlung von Krebserkrankungen.

3 Introduction

3.1 The ubiquitin-proteasome-system

3.1.1 Polyubiquitin-tags label proteins for degradation by the 26S proteasome

The life cycle of all intracellular proteins begins with the ribosomal synthesis and is terminated by degradation into smaller peptides and single amino acids by proteases. The equilibrium of formation and destruction of proteins serves as a control system that is deeply integrated in various cellular processes, for instance cell proliferation, antigen production and signaling cascades.[3] In eukaryotic cells, the ubiquitin-proteasome-system (UPS) is the main non-lysosomal pathway for the terminal recycling step of redundant, damaged and regulatory proteins.[4,5] Degradation of substrates by the UPS is highly specific, since only ubiquitin-flagged proteins are unfolded and digested by the 26S proteasome. Thus, the UPS can be divided into two processes, i) polyubiquitination of proteins by ligases and ii) their subsequent degradation by the 26S proteasome.[6]

A sequential multistep process of three distinct enzymes (E1-E3, Figure 3) facilitates the conjugation of ubiquitin (Ub) to protein substrates.[7] Action of all three enzymes is required for covalent attachment of Ub to the ε-amino residue of surface-exposed lysine side chains *via* isopeptide bond formation.[8] Once a protein is tagged with one Ub molecule, it serves as a platform for the conjugation of further Ub units with repeated procedures of Ub-activation (E1),[9] -conjugation (E2)[10] and -ligation (E3).[11] Each Ub molecule comprises seven accessible Lys moieties and thus, polyubiquitination can proceed in a dendrimeric or linear fashion.[7,12] As a result, the configuration of polyUb-tags is highly diverse and conveys different information such as translocational directions or signaling.[13] Amongst the plethora of polyubiquitinated proteins, however, only linear chains of at least four Lys48-linked Ub molecules are recognized by the 26S proteasome.[14]

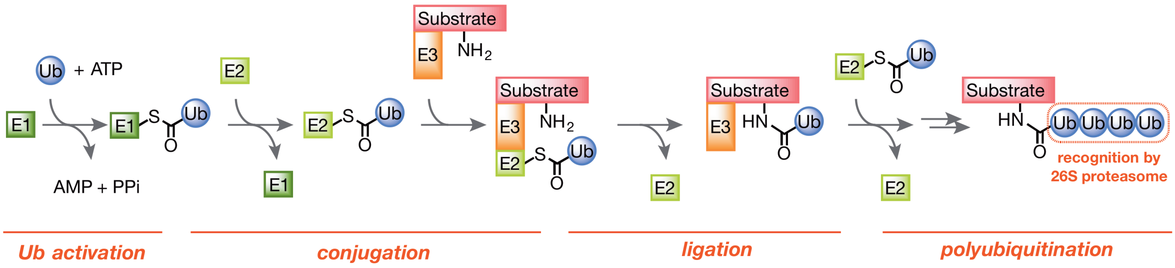

Figure 3: Polyubiquitination is facilitated by three distinct enzymes that activate (E1, dark green), conjugate (E2, light green) and ligate (E3, orange) an Ub molecule (blue) to a growing chain attached at a suitable substrate molecule (red). Linear polyubiquitin chains of at least four K48-linked Ub molecules are recognized by the 26S proteasome.[7]

3.1.2 Architecture and workflow of the 26S proteasome

The 26S proteasome is a multicatalytic, multisubunit protease complex that facilitates the recognition, de-ubiquitination, unfolding and proteolytic degradation of polyubiquitinated substrates. The 2.5 MDa complex is comprised of the cylindrical 20S core particle (CP) with two 19S regulatory units at either end (Figure 6).[15] The latter consists of at least 17 different subunits with ATPase and non-ATPase functionalities that are required for substrate recognition, deubiquitination, unfolding and translocation into the CP.[16] The CP itself is assembled of four stacked heptameric rings, each consisting of either α- or β-type subunits, following an $\alpha_{1\text{-}7}\beta_{1\text{-}7}\beta'_{1\text{-}7}\alpha'_{1\text{-}7}$ stoichiometry.[17] The proteolytically active sites of the CP are located at the β-subunits in the inner cavity of the barrel-like structure, whereas the α-subunits serve as adapters for regulatory complexes and guard the entry to the active sites by restricting access to unfolded proteins only. Compared to archaebacterial proteasomes, which have 14 identical and 14 proteolytically active sites, eukaryotic CPs only contain three active β subunits per β ring (subunits β1, β2 and β5).[18] Each catalytic center comprises a threonine residue (Thr1) and assigns the proteasome to the family of N-terminal nucleophilic (Ntn) hydrolases.[19,20]

Analysis of the cleavage products at different times has revealed a processive degradation mechanism and a length distribution of oligopeptides ranging from three to 25 amino acids, thus classifying the CP as an endoprotease.[21] The resulting peptide fragments can either be further degraded by downstream proteases into single amino acids or be loaded on major histocompatibility complex class I (MHC-I) receptors and presented on the cell surface to immune cells.[22]

Whereas the mechanism of peptide bond cleavage follows a universal principle among all CPs, it is the singularity of each substrate binding channel which determines the chemical nature of the specificity (S) pockets that accommodate the substrate's side chains (P sites, Figure 4). Although all substrates are primarily stabilized by the formation of an antiparallel β-strand with the substrate binding channel, the distinct preferences of the various active subunits were shown to be solely determined by the composition of the substrate binding pockets, which are termed non-primed (S1, S2, S3,..., Sn) and primed (S1', S2' , S3',..., Sn') sites, depending on their proximity to the active centers (Figure 4). Residues in the substrate that interact with the proteasomal specificity pockets are referred to as P1, P2, P3,..., Pn and P1', P2' , P3',..., Pn', accordingly.[23]

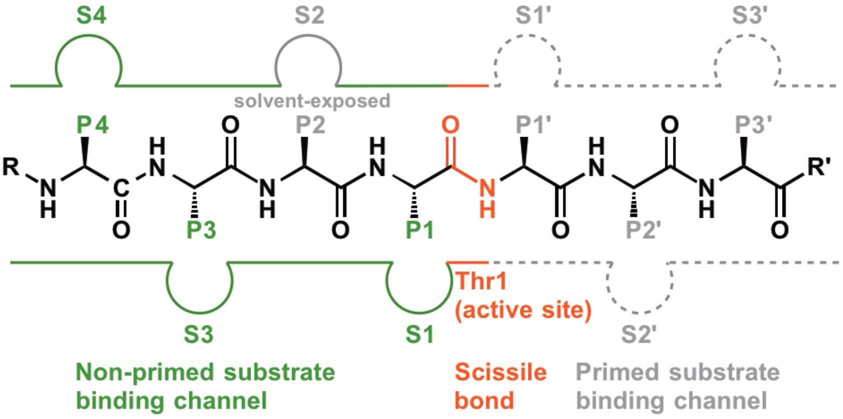

Figure 4: Schematic representations of the proteasomal substrate-binding channel. The non-primed specificity pockets (S) and the interacting substrate residues (P) are shown in green; S2 is colored in gray since the proteasome lacks a prominent pocket. The primed specificity pockets (S') have so far not been identified experimentally and are therefore drawn as gray dashed lines, whereas the corresponding substrate residues (P') are in gray. The scissile peptide bond and the active site including Thr1 are highlighted in red. Figure adopted from Beck *et al.*[24]

The proteasomal cleavage specificities were assigned with respect to the preferred P1 amino acid of chromogenic screening substrates:[25] subunit β1 cleaves peptide bonds after acidic side chains, which equates to caspase-like (CL) activity. Although the β2-subunit has been attributed to trypsin-like (TL) activity, its rather large substrate binding pocket endows it with broad substrate specificity. The S1 site of subunit β5 is of non-polar nature and hence its substrate specificity was termed chymotrypsin-like (ChTL) activity.

However, it was later revealed that not only the P1, but also the P2, P3 and P4 sites of substrates form specific interactions with the respective binding pockets.[26–28] A particular interest in current proteasomal research is the investigation of the poorly understood primed substrate binding pockets.[28]

Once an unfolded polypeptide chain is translocated into the CP, nucleophilic attack by Thr1O$^{\gamma}$ at the carbonyl carbon atom of the scissile peptide bond initiates the catalytic cycle (Figure 5). The tetrahedral intermediate is stabilized by the oxyanion hole and subsequently forms an acyl-enzyme complex by releasing the N-terminus of the substrate. The carbonyl carbon atom of resulting ester-intermediate is perfectly pre-orientated for a second nucleophilic attack by an activated water molecule that is pre-orientated in the Bürgi-Dunitz trajectory.[29,30] Extrusion of the free acid regenerates the nucleophilic Thr1O$^{\gamma}$ for the next catalytic cleavage.

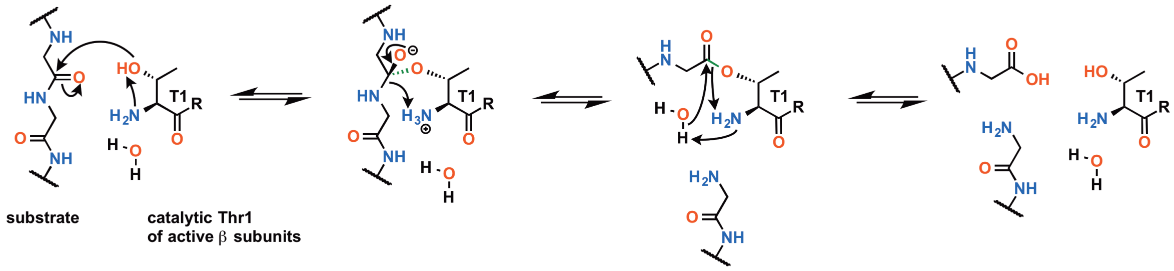

Figure 5: Mechanism of catalytic peptide bond hydrolysis in proteasomes. Nucleophilic attack of Thr1O$^{\gamma}$ on the carbonyl carbon of the scissile peptide bond results in an acyl-enzyme intermediate, thereby releasing the first cleavage product. In a second step, the activated water molecule is pre-orientated in a Bürgi-Dunitz trajectory for hydrolysis of the ester and regeneration of the catalytic Thr1.

In vertebrates a diverged set of three CPs are expressed in different tissues: the thymoproteasome (tCP) is exclusively found in cortical thymic epithelial cells;[31] the immunoproteasome (iCP) is predominantly present in mono- and lymphocytes and its production is stimulated by cytokines such as γ-interferon.[32] The constitutive proteasome (cCP), however, has to be distributed in each cell type to accommodate protein recycling to individual amino acids and hereby facilitating the building blocks for protein synthesis (Figure 6).[31,33]

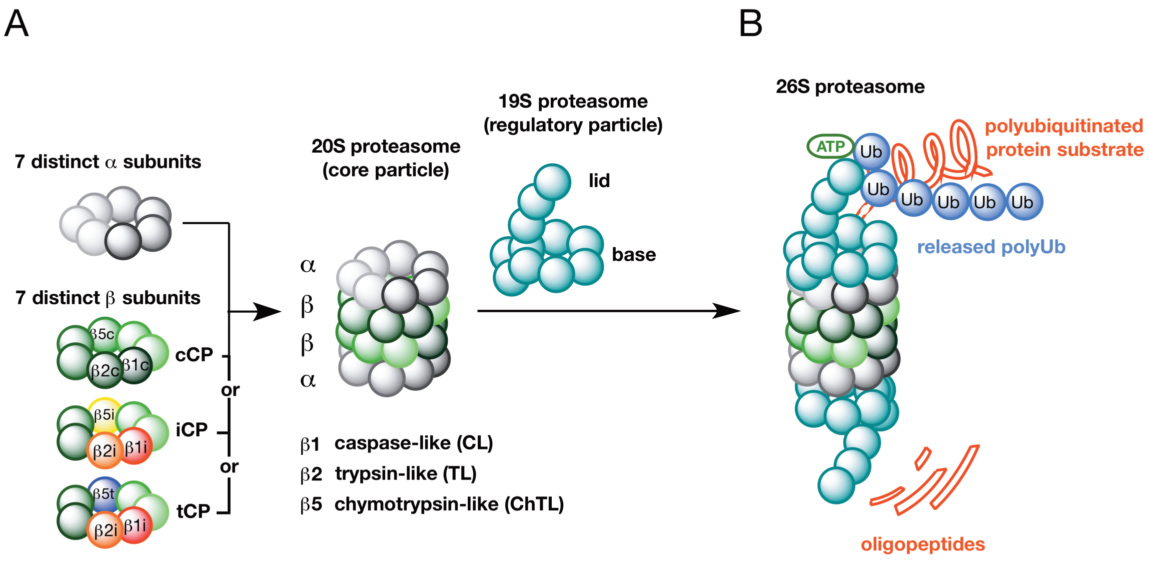
A
B
7 distinct α subunits
7 distinct β subunits
β5c
β2c
β1c
cCP
or
β5i
β2i
β1i
iCP
or
β5t
β2i
β1i
tCP
20S proteasome
(core particle)
α
β
β
α
β1 caspase-like (CL)
β2 trypsin-like (TL)
β5 chymotrypsin-like (ChTL)
19S proteasome
(regulatory particle)
lid
base
26S proteasome
ATP
Ub
Ub
Ub
Ub
Ub
Ub
polyubiquitinated
protein substrate
released polyUb
oligopeptides

Figure 6: Architecture of the 26S proteasome. A: The 20S core particle consists of four stacked heptameric rings with an $\alpha_{1\text{-}7}\beta_{1\text{-}7}\beta'_{1\text{-}7}\alpha'_{1\text{-}7}$ stoichiometry. The subunits are encoded by different genes and only the β1, β2 and β5 subunits are enzymatically active.[18] In vertebrates, three subtypes of 20S proteasomes have evolved, namely the cCP, iCP and tCP. These particles are implemented in different biological pathways and incorporate distinct sets of catalytic β subunits with slightly adjusted cleavage specificities.[31,34,35]

The major feature of iCPs compared to cCPs is the amplified production of oligopeptides with hydrophobic C-termini. N-terminal trimming to smaller fragments of eight to ten amino acids allows their loading on MHC-I receptors that are presented to cytotoxic T cells in order to trigger immune responses.[36] In turn, the tCP is thought to play an essential role in positive selection of MHC-I restricted T cells.[31]

The diverse biological functions of cCPs, iCPs and tCPs are exerted by incorporation of unique sets of catalytic β-type subunits, leading to individual but overlapping peptide cleavage repertoires: cCPs incorporate β1c, β2c and β5c; iCPs consist of β1i, β2i and β5i, while tCPs harbor β1i, β2i and β5t (Figure 6). Notably, all remaining subunits do not alter among CP-subtypes. Based on their high structural similarity, both β2c and β2i are capable of generating MHC-I epitopes with neutral or basic C-terminal anchor residues.[37] Consequently, the rationale for incorporating subunit β2i into the iCP remains elusive, and β2 subunits may play an additional, hitherto unknown functional role.[38] In contrast, most residues forming the S1 specificity pocket of subunit β1c are replaced in β1i. The size of the S1 pocket is thereby reduced and the CL activity of β1c is changed to a branched chain amino acid preferring (BrAAP) activity in β1i.[25] Interestingly, subunits β5c and β5i are both non-polar in nature and hence, their substrate specificities were attributed to ChTL activity. Nevertheless, murine cCP and iCP crystal structures revealed that the S1 specificity pocket of β5c is significantly reduced in size compared to its β5i-counterpart.[38] Therefore, β5c exerts rather an elastase-like or small neutral amino acid-preferring activity (SnAAP), whereas subunit β5i more resembles a classical ChTL activity by preferentially hydrolyzing oligopeptides C-terminally after bulky hydrophobic amino acids.[38]

3.2 The 20S core particle as a drug target

The UPS is responsible for more than >80% of cellular protein degradation. The 20S core particle is the centerpiece of the machinery and regulation of its activity is of exceptional importance for most biological processes in all eukaryotic cells. Moreover, the proteasome plays a pivotal role in disease-associated processes, such as cell proliferation, apoptosis, the regulation of gene transcription and immune response.[1,2] Consequently, inhibition of proteasomal degradation leads to the accumulation of missfolded proteins and the formation of toxic reactive oxygen species. In comparison to healthy tissue, malignant transformed cells thus display elevated CP expression levels, since chromosomal instability results in defective protein synthesis.[39] Thus, application of proteasome inhibitors preferentially triggers apoptosis in cancerous tissue and thereby, the CP holds promising potential as a drug target for the therapy of cancer.[40,41] More recently, the focus of CP drug discovery has broadened, as selective inhibition of the iCP has demonstrated therapeutic benefit in autoimmune disorders by downregulation of multiple proinflammatory mediators (NF-κB, interleukin-6 and tumor necrosis factor α).[42–44]

3.2.1 First generation of CP inhibitors

The CP is categorized as a highly druggable biological target since it is known to bind substrates/inhibitors with high affinity and provides a rapid therapeutic feedback due to its deep integration in crucial cellular processes. Determination of the yCP crystal structure in complex with various ligands provided the basis for rational, structure based drug design for the CP.[18,45,46]

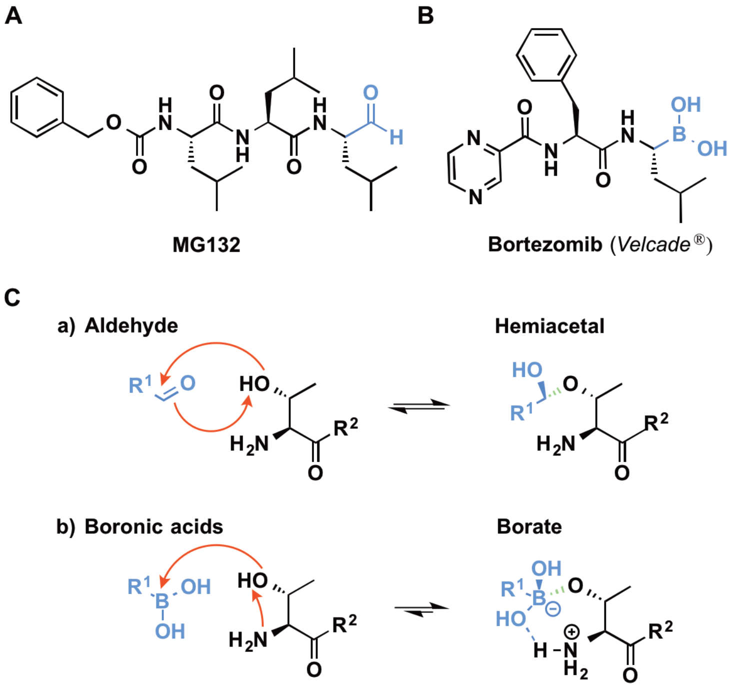

Figure 7: Structure and mechanism of action of the 1st generation CP inhibitors MG132 and bortezomib. A: MG132 comprises a Cbz-capped tripeptidic peptide backbone with an aldehyde headgroup (blue) and is used as a tool compound for CP inhibition *in vitro*. B: The FDA-approved dipeptidic bortezomib employs an electron-deficient boronic acid warhead (blue) and is used for therapy of multiple myeloma. C: Mechanism of covalent Thr1 modification with aldehydes (a) and boronic acids (b). Notably, formation of both the hemiacetal and borate adducts are reversible, whereas the residence time of the borate adduct is significantly prolonged compared to the hemiacetal. Thr1 is marked in black and R^2 denotes the main protein chain of the active β-subunit. Newly formed bonds are colored in green.

The first generation of CP inhibitors emerged from laboratory tool compounds such as MG132 (
Figure 7A) and targeted the nucleophilic Thr1O$^{\gamma}$ with electrophilic aldehyde headgroups at the C-terminal end of peptide backbones. Thus, the inhibitors form covalent yet reversible adducts with Thr1 and substantially impair substrate cleavage at nanomolar concentrations. Although early cell culture studies demonstrated the broad spectrum anti-proliferative and pro-apoptotic effect of CP inhibitors, peptide aldehydes suffered from undesired cross reactivity, instability and lack of potency *in vivo*.[47,48] Thus, these compounds never sparked the interest of the pharmaceutical industry.

However, the promising potential of the CP as a drug target was exploited by the first-in-class drug bortezomib (

Figure 7B), a dipeptidyl boronic acid approved for the treatment of multiple myeloma as well as relapsed and refractory mantle cell lymphoma.[49,50] The electrophilic warhead binds to the nucleophilic Thr1O$^{\gamma}$ to form a covalent tetrahedral adduct that mimics the oxyanion during peptide cleavage (Figure 5).[51] On the other hand, the drug's severe adverse events include neurodegenerative effects and gastrointestinal disorders, both resulting from off-target effects against several serine proteases such as cathepsin A, cathepsin G, chymase and dipeptidyl peptidase II.[52] In spite of these drawbacks, bortezomib emerged as a first-line treatment option for multiple myeloma and thus validated the CP as a drug target for cancer therapy.

The unfavorable pharmacokinetic and pharmacodynamic profile of bortezomib lead to the development of second-generation peptide boronic acids, namely CEP-18770[53] and MLN2238[54,55] (Figure 8A/B). Both feature a dipeptidic scaffold and enhanced anti-tumor activity, whereas MLN9708 was specially engineered to display deeper tissue penetration by increasing the dissociation rate.[54] While bortezomib has to be applied intravenously, the advanced drugs are orally available and currently investigated for hematologic and even solid tumors.

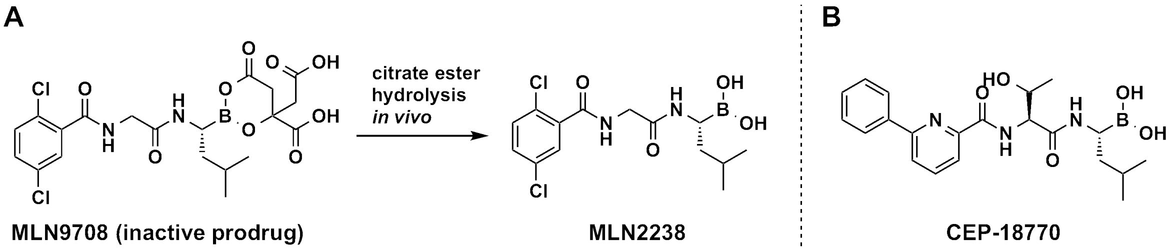

Figure 8: Orally available successors of bortezomib. A: MLN2238 is applied as its citrate ester MLN9708 that is immediately hydrolyzed after application. B: CEP-18770 bears a threonine side chain in P2 and a biaryl N-cap to provide specificity for the CP.

3.2.2 Second generation of CP inhibitors

The second generation of CP inhibitors was developed to improve the unspecific mode of action of the boronic acid head group and was therefore tailored to target the small group of N-terminal threonine hydrolases.[56] The bivalent α',β'-epoxyketone warhead of carfilzomib is inspired by the highly cytotoxic natural product epoxomicin by forming an irreversible morpholine adduct with Thr1 (Figure 9A-C).[57] Compared to bortezomib, carfilzomib exhibits a vastly improved safety profile and better response rates in clinical trials.[52] Consequently, the compound was granted accelerated approval by the FDA for multiple myeloma in 2012. Now, a variety of related α',β'-epoxyketones against immune disorders and even solid tumors are in clinical trials.[58,59]

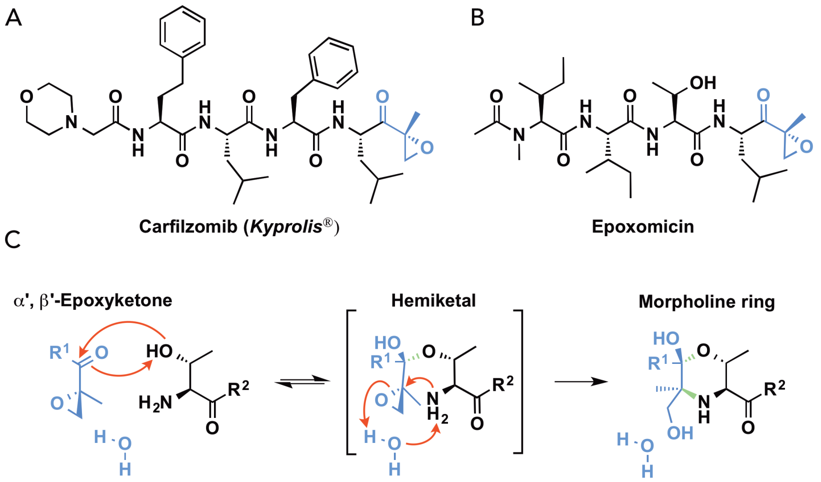

Figure 9: Structure and mechanism of action of the 2nd generation CP inhibitors. A: Carfilzomib consists of a tetrapeptidic peptide backbone and employs the α',β'-epoxyketone headgroup (blue) that is inspired by the natural product epoxomicin.[60] B: Structure of the natural product epoxomicin. B: Reaction of the α',β'-epoxyketone headgroup with the nucleophilic Thr1O$^{\gamma}$.[45] Thr1 is marked in black and R^2 denotes the main protein chain of the active β-subunit. Newly formed bonds are colored in green. Figure adopted from Beck *et al.*[24]

The poor oral availability of carfilzomib sparked the development of tripeptidic inhibitors that allow for cellular update *via* peptidase transporters.[61] ONX 0912 represents the only orally available α',β'-epoxyketone inhibitor to date and exhibits comparable potency as carfilzomib (Figure 10A). The compound is being evaluated in phase I clinical trials against solid tumors and hematologic malignancies.[39]

Further screening efforts identified α',β'-epoxyketone inhibitors that specifically target the iCP and thus provide the possibility to interfere with certain cellular pathways, e.g. presentation of antigenic peptides on MHC-I molecules at the cell surface and production of proinflammatory cytokines.[42] ONX 0914 represents the first iCP-selective compound (Figure 10B) and was shown to prevent the progression of rheumatoid arthritis, experimental colitis and lupus erythematodes.[44] Remarkably, recent crystallographic studies revealed that the main molecular cause for the iCP selectivity of ONX0914 is found in a more spacious S1 pocket of iβ5 subunits compared to the cβ5 counterpart.[38] Although it was demonstrated that neither β5c- nor β5i-selective compounds have anti-tumor activity,[62] PR-924 (Figure 10B) was revealed to block multiple myeloma cell growth both *in vitro* and *in vivo*.[63] In addition, the compound displayed strong anti-leukemic activity towards normal and bortezomib-resistant leukemia cells. However, the anti-leukemic effect was only achieved at concentrations that blocked both β5c and β5i subunits.[64]

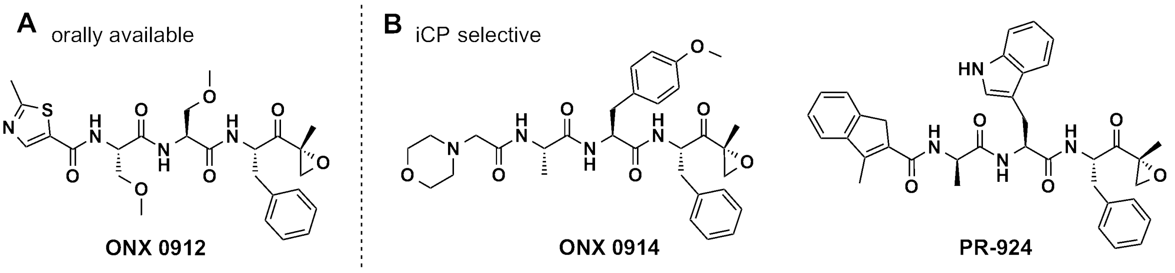

Figure 10: Structures of orally available and iCP selective CP inhibitors. A: The tripeptidic scaffold of ONX 0912 enables active cellular uptake *via* peptide transporters.[39,61,65] B: iCP specific CP inhibitors ONX 0914 and PR-924 feature comparably large and hydrophobic P1 and P2 moieties, whereas the P2 residue remains small.

3.2.3 Current developments: plasma stability and tissue targeting

The encouraging clinical outcome of bortezomib and carfilzomib in multiple myeloma patients triggered the decisive stimulus for further development of CP inhibitors and their application in a broad range of malignancies. The conjugation of bortezomib or MG132 into polymeric micelles aimed to improve plasma stability and tissue specificity, but both approaches did not address the various off-target effects of boronic acid- or aldehyde-based inhibitors.[66,67] However, a recent patent by Onyx Pharmaceuticals (Patent No. WO 2014/011695 A29) gives insights into the ongoing investigations of the company to broaden the scope of CP inhibitors. The document details various possibilities to derivatize the carfilzomib scaffold in order to increase its plasma stability, solubility and tissue specificity. For example, the warhead can be replaced with an activated diol that reacts to the epoxyketone pharmacophore upon intramolecular S_N2 reaction. This process can be controlled with pH-sensitive leaving groups and thus the active drug is only released when the inhibitor enters certain cell compartments, such as lysosomes. In addition, attachment of PEG residues increases the solubility and plasma stability of the CP inhibitors, therefore allowing more convenient dosing schemes since the compound can be administered in higher concentrations.

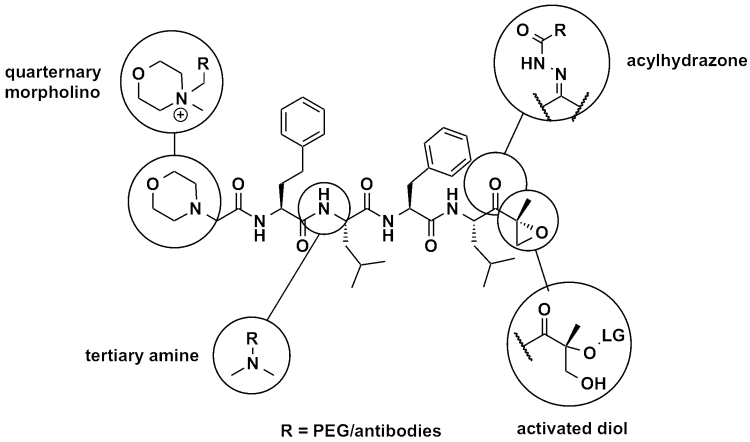

Figure 11: Third generation CP inhibitors. Prodrug approach that allows the reversible attachment of PEG or bioconjugates to CP inhibitors for improvement of plasma stability or tissue specificity.

Furthermore, the patent covers the application of carfilzomib in antibody-drug conjugates (ADCs). ADCs are a class of therapeutics that harnesses the selectivity of monoclonal antibodies to deliver highly potent cytotoxic drugs to antigen-expressing tumor receptors. Hitherto, only anti-tubulin[68,69] and DNA-damaging agents[70] are employed as the cytotoxic payload, but CP inhibitors are thought to provide a comparably cytotoxic alternative

3.3 Screening methods for the discovery of novel CP ligands

The clinical application of CP inhibitors suffers from the development of resistances as well as unfavorable pharmacokinetic and -dynamic profiles. Thus, screening for compounds with novel structural scaffolds and mode of actions remains a priority in CP drug discovery. The application of multiple screening technologies in parallel is crucial for the identification of novel chemical entities that have the potential for emerging to lead structures in drug development.[71] The diverse set of high-throughput screening (HTS) methods can be divided into biochemical and biophysical methods. X-ray crystallography is generally not considered as a high-throughput method, although current developments indicated the use of direct crystallographic screenings as the primary screening technique.[72,73]

3.3.1 Biochemical methods

The most frequently used assay systems rely on biochemical methods to screen large libraries of compounds for biological activity. CP impairment can be measured either *via* direct evaluation of CP cleavage activity or analysis of upstream/downstream signals that indicate proteasomal dysfunction.

A widespread method for the detection of proteasome activity is based on tetra- or tripepidic non-natural substrates that carry a C-terminal chromophore, such as 7-amino-4-methylcoumarin (AMC) or para-naphtylamine (Figure 12). The amino acid scaffold can be adjusted to address the different proteasomal activities and a variety of specific substrates are commercially available. Cleavage of the scissile bond releases the chromogenic moiety that can be quantified by UV-Vis spectrometry.[74,75]

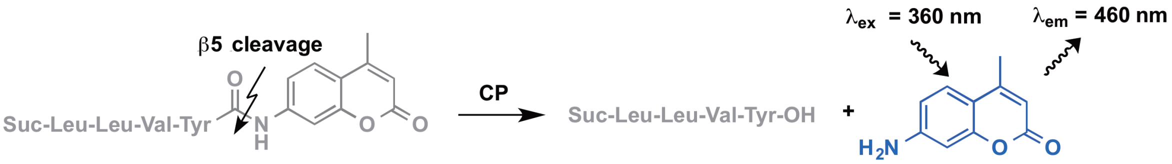

Figure 12: Cleavage of a β5-specific AMC substrate by the CP. Most CP inhibitor screening assays use subunit-specific peptides that contain a chromogenic headgroup at the C-terminus. The chromophore is internally quenched in the bound form and develops its fluorescent properties upon proteasomal cleavage.

However, the chromogenic substrates are also cleaved by non-proteasomal proteases and are thus limited to *in vitro* screenings with purified proteasome. In addition, the UV-Vis read-out is influenced by fluorescence quenching or autofluorescence and represents the major source of false-positive assay results that are reported in literature.[76,77]

In contrast, site specific activity probes (SSAP) allow the detection of proteasomal activity in crude mixtures of cell lysate. The probes consist of a reactive warhead for covalent attachment to Thr1 and a fluorescent dye for visualization such as BODIPY or rhodamine.[78,79] Addition of SSAPs to cell lysate tags all present proteasomes with the fluorescent dye and after submission to SDS-PAGE, fluorescence gel scanning provides a rough estimate of CP inhibition. If the sample contained an irreversible inhibitor, the fluorescent probe is unable to tag the CP, resulting in weaker labeling and surpressed fluorescence after SDS-PAGE development. However, the method is not suitable for the detection of reversible ligands, since SSAPs have to react covalently and irreversibly with the CP to allow assay read-out.

Other applied biochemical screening methods measure upstream signals of CP inhibition, such as accumulation of ubiquitinated proteins in general,[80,81] direct evaluation of IκB, p53[82] or blockage of NFκB activation.[83] Although these techniques are important for the evaluation of CP blockage *in vivo,* they are lacking sensitivity for weakly binding or subunit specific inhibitors and are thus less likely to detect ligands with a non-covalent mode of action.

3.3.2 Biophysical methods

In comparison to the biochemical techniques, biophysical screening methods provide a more reliable alternative that remained underrepresented in CP inhibitor discovery until the recent development of an NMR-based assay by Stein *et al.*[84] Here, a native proteasomal substrate was labeled at the scissile peptide bond with a ^{13}C-carbonyl carbon, which displayed a distinct shift in the NMR spectrum after proteasomal hydrolysis (Figure 13). The sequence of the peptide can be adjusted for subunit selectivity and thus allows the detection of different CP activities, whereas non-covalent or reversible inhibitors can be detected through variation of incubation times. In addition, any diffraction or quenching effects of crude mixtures do not hamper the methodology and even concentrated mixtures can be evaluated with one measurement. Thus, the technique is superior to most biochemical screening assays.

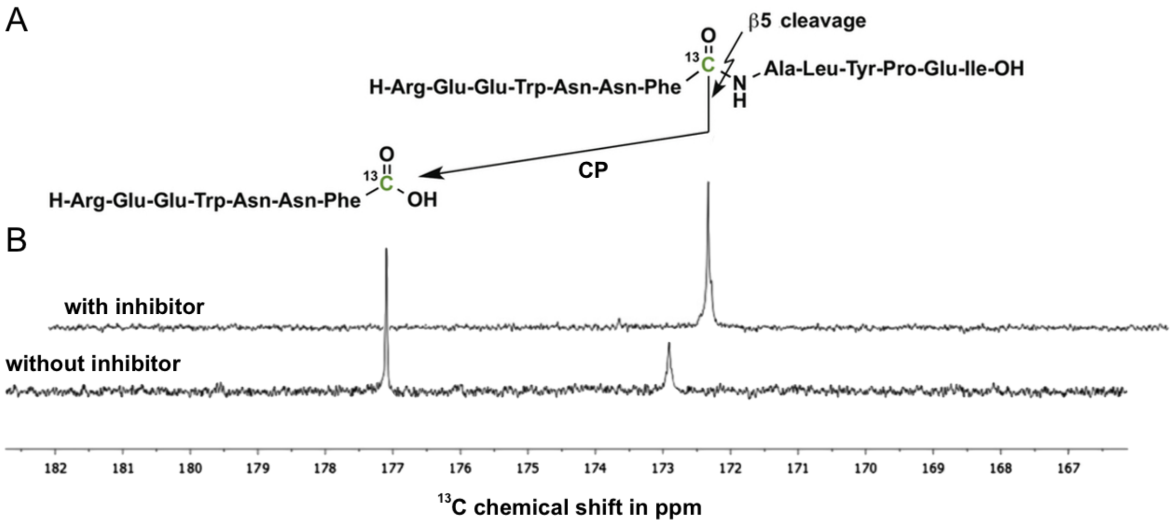

Figure 13: NMR screening assay with ^{13}C-labeled substrate. A: Primary sequence of the substrate with the scissile peptide bond and the ^{13}C label (173 ppm). The peptide is specifically cleaved by the β5 activity of the CP and the product fragment is released with a free C-terminus (177 ppm). B: NMR spectrum of microbial broths with (upper) and without (lower) CP inhibitor. The uncleaved peptide gives an intense signal at 173 ppm, whereas in the absence of a CP inhibitor proteasomal digestion yields the cleaved peptide (177 ppm). Figure adopted from Stein *et al.*[84]

In principle, NMR-based screening methods are highly versatile since one or more parameters can be changed rapidly, such as the observed core (^{1}H, ^{15}N, ^{13}C, ^{19}F), relaxation of the ligand or protein, cross relaxation in the protein–ligand complex, or cross relaxation between the ligand and the protein bound water-molecule.[85–87] However, the large size of the CP practically limits NMR-guided drug discovery to ligand-observed experiments that deliver only data about whether the ligand binds or not. The identity of the ligand then remains to be elucidated.

Other biophysical methods for high-throughput CP drug discovery suffer technical difficulties that arise from the large size of the proteasome. Although isothermal calorimetry[88,89] and surface plasmon resonance[90,91] are highly sensitive and widely applied analytical methods, the overall ratio of the size of the CP versus its binding sites is too large to give interpretable results in the event of ligand binding. As a result, successful applications of the above mentioned screening methods against the CP have not been reported to date.

In comparison, mass spectrometry (MS) is not limited by particle size and provides a highly sensitive tool for the simultaneous observation of all CP subunits in one measurement.[92,93] Nevertheless, MS relies on covalent modification of the target and is thus not suitable for the discovery of non-covalent inhibitors. In addition, single-subunit resolution can only be achieved in combination with liquid chromatography and thus, the method requires extensive sample preparation.

3.3.3 X-ray crystallography-based screening methods

Structural knowledge obtained through X-ray crystallography is indispensable in every screening campaign to supply precise information for the rational optimization of initially identified hits. Moreover, for targets whose 3D structure is so far not available, a screening often is not considered at all.

Despite huge technological advances of the past years, crystallography still counts as a secondary method to verify hit molecules from initial high-throughput screenings due to the requirement of vast resources regarding material (i.e. purified protein) as well as human input.[72] In the case of the CP, evaluation of crystals with satisfactory resolution (>2.6 Å) demands synchrotron radiation and takes at least two minutes per crystal. As a result, the screening library size is limited and direct X-ray crystallographic HTS against the CP have hitherto not been undertaken. The discovery of truly innovative chemical leads against the CP is thus hampered by incomplete utilization of X-ray crystallography in the early stages of screening campaigns.

4 Objective

Proteasome inhibitors recently emerged from a last-resort treatment option to a first-line therapy of multiple myeloma. However, the application of the FDA-approved CP inhibitors bortezomib (Velcade®) and carfilzomib (Kyprolis®) are limited by severe side-effects and intrinsic drawbacks that arise from i) the peptidic molecular scaffold that is rapidly metabolized and ii) the reactive electrophilic head group, which gets successively inactivated once the drug is applied *in vivo*. In addition, a rapid development of adaptive resistances highlights the need for novel agents to treat medical conditions that are susceptible to proteasome inhibition.

Therefore, the aim of this thesis was to characterize and evaluate structurally novel types of reversible and irreversible non-peptidic CP ligands. Most importantly, information gained via elucidation of CP-ligand complex structures by X-ray crystallography was of high interest, since biostructural techniques are less prone to produce false-positives compared to commonly used biochemical assays that rely on fluorogenic substrates. Furthermore, cocrystal structures allow the detection of weakly binding ligands with few but strong interactions that otherwise would have been overlooked, since traditional in-vitro assay conditions often require action of strong ligands or covalent modification of the CPs catalytic Thr1 residues.

So far, only inhibitors that bind to the proteasomal substrate binding channel were further developed for clinical use, mostly because structural data on other possible binding sites were lacking. Thus, a thorough literature search for putative CP inhibitors of natural and synthetic origin together with subsequent crystallographic screening was aimed to identify ligands that populate hitherto untargeted regions of the CP. Due to the large size of the CP, automated evaluation of the obtained difference electron density maps was envisioned to find small molecules that coordinate at novel ligand binding sites. In the event of a screening hit, identification of the most crucial protein-ligand interactions by fragment-growing or -merging approaches with existing inhibitors were intended to produce leads with a higher affinity.

In order to avoid biochemical artifacts by compounds that interfere with common assay read-out methods, development of a set of orthogonal in-vitro characterization methods was mandatory for unambiguous identification of false-positive CP inhibitors or ligands that would only bind to the yeast proteasome. Hence, promising hits from the crystallographic screening were to be subjected to hit validation by HPLC-MS coupled substrate digestion assays, mutagenesis experiments with the model organism *S. cerevisiae* and cytotoxicity as well as Proteasome-Glo activity assays with cancer cell lines.

In summary, a multidisciplinary approach for the discovery of novel proteasome ligands was undertaken, combining X-ray crystallography, chemical synthesis, yeast mutagenesis and in-vitro as well as cellular inhibition assays to provide new insights for the development of potential lead structures.

5 Materials and Methods

5.1 Materials

5.1.1 Chemicals

All applied compounds and solvents were acquired from the following companies: Bachem (Bubendorf, SWI), Enzo Life Sciences (Lörrach, GER), Fluka (Neu-Ulm, GER), Merck (Darmstadt, GER), Santa Cruz (Heidelberg, GER), Sigma-Aldrich (Steinheim, GER), Roth (Karlsruhe, GER) and VWR (Darmstadt, GER).

5.1.2 Strains

Organism	Strain	Genotype	Source
S. cerevisiae	WCG-4a	MATa, ura3 leu2-3,112 his3-11, 15Can^S GAL1	Heinemeyer *et al.*[94]
S. cerevisiae	YHei032 WCG-4a	MATa, ura3 leu2-3,112 his3-11, 15Can^S GAL1, pup1Δ::His3, pRS315-PUP1	Donation from Dr. W. Heinemeyer
S. cerevisiae	YHei032 WCG-4a	MATa, ura3 leu2-3,112 his3-11, 15Can^S GAL1, pup1Δ::His3, pRS315-PUP1-H141A/K/R	Donation from Dr. W. Heinemeyer

5.1.3 Flurogenic Substrates

Suc-Leu-Leu-Val-Tyr-AMC	Enzo Life Science (Lörrach, GER)
Z-Leu-Leu-Glu-AMC	Enzo Life Science (Lörrach, GER)
Boc-Leu-Arg-Arg-AMC	Enzo Life Science (Lörrach, GER)

All substrates were dissolved in DMSO at concentrations of 50 mM and stored at -20 °C.

5.1.4 Instruments

Balances

Analytical Balance TE124S	Sartorius (Göttingen,GER)
Precision Balance BP3100 P	Sartorius (Göttingen, GER)

Centrifuges

Biofuge Pico	Heraeus Instruments (Hannau, GER)
SIGMA 4K15 rotor 11150/13220 & rotor 11150/13350	SIGMA Laborzentrifugen (Osterode am Harz, GER)

Crystallography

Crystal CAP HT für CryoLoop	Hampton (Aliso Viejo, USA)
Crystal CAP HT Vial	Hampton (Aliso Viejo, USA)
Foam Dewar	Spearlab (San Francisco, USA
Magnetic Caps, Pins and Vials	Molecular Dimensions (Newmarket, UK)
Micro Tool Box	Molecular Dimensions (Newmarket, UK)
Mounted CryoLoop	Hampton (Aliso Viejo, USA)
Siliconized Glass Cover Slides	Hampton (Aliso Viejo, USA)
Storing Dewar HC20	Taylor Wharton Germany (Mildestedt, GER)
Super Clear Pregreased 24 Well Plate	Crystalgen (New York, USA)
Vial Clamp	Molecular Dimensions (Newmarket, UK)
Zoom stereo microscope SZX10/KL1500LCD	Olympus (Tokyo, JP)

Peptide Synthesis

Alpha 2-4 LD plus lyophilisator	Christ (Osterode, GER)
Peptide synthesizer PS3	Protein Technologies (Tucson, USA)
Rotavapor R215	Büchi (Essen, GER)

Liquid chromatography

Reveleris X1 Flash Chromatography System	Grace (Deerfield, USA)
GraceResolv 4g – 80 g	Grace (Deerfield, USA)

HPLC and mass spectroscopy

Binary pump system 1525	Waters (Eschborn, GER)

Column selector	Waters (Eschborn, GER)
Flex Inject Loop	Waters (Eschborn, GER)
Fraction collector II	Waters (Eschborn, GER)
HPLC system Ultimate 3000	Dionex (Idsetin, GER)
LCQ Fleet MS	Thermo Fisher (Schwerte, GER)
Xbridge BEH C18, 10 mm x 250 mm	Waters (Eschborn, GER)

NMR

Proton (^{1}H) and carbon (^{13}C) nuclear magnetic resonance (NMR) spectra were recorded at 250, 360 and 500 MHz on the following spectrometers:

Cryo NMR Ultrashield 500 plus	Bruker (Billerica, USA)
AV-250	Bruker (Billerica, USA)
AV-360	Bruker (Billerica, USA)
NMR Ultrashield 500	Bruker (Billerica, USA)

NMR spectra were acquired in $CDCl_3$ with chemical shifts (δ) reported in parts per million (ppm) relative to TMS (^{1}H: $\delta = 0$ ppm) and $CDCl_3$ (^{13}C: $\delta = 77.0$ ppm). Alternatively, where stated, spectra were acquired in (DMSO-D_6) with δ values relative to TMS (^{1}H: $\delta = 0$ ppm) as an internal standard. Coupling constants (*J*) are reported in Hertz (Hz). *J* values listed in ^{1}H NMR spectral data refer to coupling between hydrogen nuclei. Multiplicities are reported as singlet (s), broad singlet (bs), doublet (d), doublet of doublets (dd), triplet (t), quartet (q), pentet (p) or multiplet (m).

All spectra were recorded with the following NMR tube:

NMR Tubes 5 mm Professional	Schott (Mainz, GER)

Additional equipments and materials

Cary Eclipse Fluorescence spectrometer	Varian (Darmstadt, GER)
Constant Cell Disruption System E106	Constant Systems (Northants, UK)
Cold trap CT 02-50 SR	Buch and Holm (Herlev, DEN)
MR Hei-Standard Magentic stirrer	Heidolph (Schwabach, GER)

NanoPhotometer	Pearl IMPLEN (München, GER)
Speedvac, centrifuge RVC 2-25 CO plus	Christ, (Osterode, GER)
Vortex Genie 2	Scientific Industries (New York, USA)
Vacuum pump MZ 2C NT	VacuBrand (Wertheim, GER)
White 96 well plate NUNC	Thermo scientific (München, GER)

Computer software and bioinformatics tools

Breeze	Waters (Eschborn, GER)
CCP4 Software Suite	www.ccp4.ac.uk[95]
ChemBioOffice	Perkin Elmer (Cambridge, USA)
Chromäleon	Dionex (Idstein, GER)
COOT	Emsley, P.[96]
CorelDraw X5	Corel (Ottawa, CA)
Graph Pad Prism 5/6	Graph Pad Software (La Jolla, USA)
Mendeley	Mendeley, UK
MestReNova 7	Mestre Lab Research S.L. (Santiago de Compostela, SPA)
Microsoft Office	Microsoft (Redmond, USA)
Adobe Photoshop	Adobe (CA, USA)
Pymol	Schrödinger, LLC[97]
Xcalibur	Thermo Scientific (Waltham, USA)
XDS program package	Kabsch, W. (Heidelberg, Germany)[98]

5.2 Protein chemistry

5.2.1 Purification of the yeast 20S proteasome (yCP)

Purification of WT and mutant yCPs was carried out by Richard Feicht according to published procedures.[18,99] Yeast cells were solubilized in approximately 2 times the volume of the pellet weight of 50 mM KH_2PO_4/K_2HPO_4 buffer, pH 7.5. DNAse I was added and the cells were disrupted with a French press. The lysate was centrifuged for 30 min at 21 000 rpm at 4 °C. The resulting supernatant was filtered and 30 % of saturated ammonium sulfate was added. Subsequently, the solute was loaded on a Phenyl Sepharose™ 6 Fast Flow column pre-equilibrated with 1 M ammonium sulfate in 20 mM KH_2PO_4/K_2HPO_4, pH 7.5. The yCP was eluted by applying a linear gradient from 1 M to 0 M ammonium sulfate in 4 column volumes. Collected fractions were tested for proteolytic activity using the fluorogenic substrates Suc-Leu-Leu-Val-Tyr-AMC (for WT yCP): 30 µl of each fraction were incubated for 1 h with 1 µl of 10 mM substrate and the resulting fluorescence was measured (λ_{ex} = 360 nm and λ_{em} = 460 nm). Active samples were pooled and applied to a hydroxyapatite column, which has been equilibrated with 20 mM KH_2PO_4/K_2HPO_4 pH 7.5. Using a linear gradient from 20 mM to 500 mM KH_2PO_4/K_2HPO_4 in 20 column volumes, the yCP was eluted. Proteolytically active fractions were loaded on a Resource Q column and a sodium chloride gradient from 0 mM to 500 mM in 20 mM Tris-HCl pH 7.5 was applied over 10 column volumes. For crystallization the buffer was exchanged for 10 mM MES pH 6.8 using a HiPrep™ 26/10 desalting column.

5.2.2 Determination of protein concentrations

UV/VIS spectra of protein solutions were recorded with the nanophotometer of IMPLEN. The absorption at a wavelength of 280 nm was used to calculate protein concentrations via the Lambert-Beer law. The required theoretical molar extinction coefficient was computed with the ProtParam tool (yCP: 727.3 cm·l/mmol).

5.3 Protein crystallography

5.3.1 Crystallization and sample preparation of the yeast 20S proteasome (yCP)

Crystals of the yeast wildtype and mutant CP were grown in hanging drops at 20 °C as described previously.[18,99] The protein concentration was 40 mg/mL in Tris / HCl (20 mM, pH 7.5) and EDTA (1 mM). The drops contained 1 µL of protein and 1 µL of the reservoir solution (30 mM magnesium acetate, 100 mM MES (pH 7.2) and 10% (wt/vol) 2-methyl-2,4-pentanediol). Crystals appeared after two days and were then incubated with either KM, SA or PD in DMSO at final concentrations of 2 mM for at least 24 h. Droplets were complemented with a cryoprotecting buffer (30% (wt/vol) MPD, 20 mM magnesium acetate, 100 mM MES, pH 6.9) and supercooled in a stream of liquid nitrogen gas at 100 K (Oxford Cryo Systems).

5.3.2 Data collection, processing and structure determination

The datasets from the CP:SA, CP:KM and CP:PD complexes were collected by using synchrotron radiation ($\lambda = 1.0$ Å) at the X06SA-beamline (Swiss Light Source, Villingen, Switzerland). X-ray intensities and data reduction were evaluated using the XDS program package.[98] Conventional crystallographic rigid body, positional, and temperature factor refinements were carried out with REFMAC5[100] using coordinates of the yCP structure as starting model (PDB ID code 1RYP).[18] For model building, the programs SYBYL[101], COOT[96] and MAIN[102] were used. The completed crystal structures yielded excellent R factors, as well as RMSD bond and angle values. Coordinates were confirmed to fulfill the Ramachandran plot. Graphical illustrations of the structures was performed with PyMOL.[97] The coordinates of the yCP:KM complex was deposited in the PDB under the accession code 4Q1S.

5.4 Yeast mutagenesis

Mutations of the H141 codon in the *PUP1* gene encoding the β2 yCP subunit were introduced by recombinant PCR techniques. The resulting fragments were ligated into the centromeric, *LEU2*-marked shuttle vector pRS315. Strain YWH10,[103] which carries a deletion of the chromosomal *PUP1* ORF and harbors the *PUP1* gene on a *URA3*-marked plasmid, was transformed with the corresponding pRS315-*pup1* mutant constructs. After counter-selection against the *URA3* gene with 5-FOA cells expressing exclusively the mutant versions of β2 could be isolated. This plasmid shuffling procedure was also used to create a comparable wild-type strain expressing wild-type *PUP1* from plasmid pRS315.

The α3ΔN mutant was generated by exchanging the chromosomal *PRE9* gene by the *pre9-Δ2-10* allele (lacking codons 2-10) via a two-step gene replacement (pop-in/pop-out) procedure. For this, the *pre9-Δ2-10* allele was inserted into the integrative, *URA3*-marked plasmid pRS306 and the resulting construct integrated at the chromosomal *PRE9* locus. 5-FOA selection served to isolate clones which had lost the *URA3* marker again, leaving either the wild-type *PRE9* or the *pre9-Δ2-10* allele on the chromosome. The latter were identified by PCR fragment analysis and verified by sequencing.

5.5 *In vitro* activity assays

5.5.1 Determination of yCP inhibition and & IC_{50} measurements

In vitro proteasome inhibition pointmeasurements were performed by fluorescence assays in 96-well plates. Assay mixtures contained 10 µg/mL of freshly purified yeast CP in 100 mM Tris (pH 8.0) supplemented with or without 0.01% (wt/vol) SDS. For pointmeasurements, inhibitors were added in DMSO to a final concentration of 200 µM in triplets, thereby not surpassing a final concentration of 10% (wt/vol) DMSO. For IC_{50} measurements, serial dilutions of inhibitors in DMSO were prepared. After an incubation time of 45 min, the fluorogenic substrates Suc-Leu-Leu-Val-Tyr-AMC, Boc-Leu-Arg-Arg-AMC or Z-Leu-Leu-Glu-AMC were added for analysis of the ChTL, TL and CL activities, respectively. The assay mixture was incubated for another hour, whereupon the reaction was stopped by addition of 300 µL of buffer (20 mM Tris/HCl pH 7.5) to the wells. Fluorescence was measured on a Varian Cary Eclipse Photofluorometer with excitation and emission wavelengths of 360 and 460 nm, respectively. IC_{50} curves were analyzed by calculating the nonlinear regression using the sigmoidal dose-response equation (variable slope) in GraphPad Prism (v5; San Diego, CA).

5.5.2 HPLC-MS substrate digestion assay

In vitro proteasome inhibition measurements with natural substrates were performed by analyzing the assay mixture by HPLC-MS at various time points. The substrate H-WNNFALY-OH was synthesized with standard solid phase peptide synthesis. Assay mixtures contained 10 µg/mL of freshly purified yCP in 100 mM Tris (pH 8.0) supplemented with or without 0.01% (wt/vol) SDS and 200 µM KM. After an incubation time of 45 min, the substrate H-WNNFALY-OH was added for analysis of the proteasomal β5 activity at a final concentration of 1 mM. After various incubation times, aliquots (100 µL) of the assay mixture were filtered through a 0.2 µm centrifugal filter and analyzed by HPLC-MS to evaluate the ratio of substrate digestion. 10 µL were injected on a C18 column (3.5 µM, 4.6 mm, 30 mm) with a 10 min 5-95% ACN/Water gradient (both with 0.1% formic acid).

5.5.3 Determination of the β5 activity in yeast cells

Yeast strains were grown to stationary phase in YPD medium and cells from a volume corresponding to 6 OD_{600} were harvested by centrifugation. 200 µl of chloroform was added to the cell pellet, followed by shaking for 15 min. After addition of 660 µl of H_2O, 190 µl per assay of the cell suspension were transferred to a fresh tube and either 10 µl of DMSO, 1 mM Bortezomib or 1 mM KM in DMSO was added. After shaking for 30 min at 30 °C, 100 µl of the suspension was mixed with 100 µl of assay buffer (200 mM Tris/HCl pH 8.0, 200 µM Suc-LLVY-AMC substrate) and shaken for further 35 min at 37 °C. The reaction was stopped by adding 1 mL of cold ethanol, the cells spun down and released AMC in the supernatant was measured in a fluorescence photometer with 360 nm excitation and 460 nm emission. Absorbance values from samples pre-incubated with inhibitor were related to the corresponding value from the DMSO incubated sample.

5.5.4 Halo assay for growth inhibition of yeast cells

Yeast cells were grown overnight in liquid CSM medium (1.7 g nitrogen base w/o amino acids and ammonium sulfate, 20 g glucose, 1 g proline per liter plus 0.004% SDS and supplements according to auxotrophic markers), which was shown to enhance the uptake of proteasome inhibitors.[104,105] 100 µl of the stationary grown yeast culture were then mixed into 4 mL of molten CSM agar (2%) at 50 °C and the mixture poured onto a CSM agar plate. Sterile filter disks with 5 mm diameter were placed onto the solidified yeast layer and 2 µl of KM at different concentrations in DMSO were spotted onto the filters. Plates were incubated at 30 °C for 48 hours.

5.6 Cell culture experiments

HeLa cells were cultured and incubated in Dulbecco's modified eagle medium (DMEM) in an atmosphere of 5% CO_2 and 95% air at 37 °C and 100% humidity. The medium contained 10% FBS, inactivated by heating up to 50 °C for 30 min and 1% Penstrep (10000 units penicillin and 10 mg streptomycin per mL in 0.9% NaCl). Cells grew attached to plastic as a monolayer with a doubling time during exponential growth of about 24 hours. Cells for assays were taken from exponential phase culture.

5.6.1 Cell viability assays

MTT-Assay: KM toxicity in HeLa cells was determined using the MTT assay as described previously.[106,107] Cells were seeded in 96-wells plates (Nunc) at 8,000 cells/well. After 24 h, attached cells were exposed to increasing concentrations of the proteasome inhibitors for another 24 h. Thereafter, 20 µl of MTT solution were added per well and the microplate was incubated for a further 3.5 h, followed by removal of medium, addition of 100 µL DMSO and thorough mixing. Optical density was recorded at 590 nm on a microELISA reader (Varian) with a reference measurement at 630 nm. EC_{50} values were defined as the concentrations that correspond to a reduction of cell growth by 50% when compared to values of untreated control cells and depicted as means of relative activity ± standard deviation.

CellTiter-Glo Assay: 5,000 cells were exposed to a range of KM or carfilzomib concentrations in Eppendorf tubes for 105 min and transferred to white 96-wells plates (Nunc). Cell viability was measured by CellTiter-Glo^{TM} luminescent cell viability assay according to manufacturer's instructions (Promega) using the PheraStar^{Plus} (BMG Labtech). Data were normalized to untreated controls and the respective EC_{50} values were estimated by calculating the nonlinear regression using the sigmoidal dose-response equation (variable slope) in GraphPad Prism (v5; San Diego, CA).

5.6.2 Proteasome-Glo® assays

To measure the chymotrypsin-like proteolytic activities of the proteasome in intact cells, the Proteasome-Glo™ Chymotrypsin-like Cell-Based assay (Promega, Madison, WI, U.S.A.) was used according to manufacturer's instructions.[108] Briefly, 5,000 cells were exposed to a range of KM or carfilzomib concentrations in Eppendorf tubes for 105 min and transferred to white 96-wells plates (Nunc). The substrate for the β5 activity (Suc-LLVY-aminoluciferin) was dissolved in Proteasome-Glo™ Cell-Based Reagent and added to intact cells. After 2 min of shaking for permeabilization and further 10 min of incubation luminescence was measured with a PheraStar^{Plus} (BMG Labtech). The respective IC_{50} values were estimated by calculating the nonlinear regression using the sigmoidal dose-response equation (variable slope) in GraphPad Prism (v5; San Diego, CA).

5.7 Synthesis of sulfonamide derivatives

2-(4-ethoxyphenyl)quinoline-4-carboxylic acid (SA-001)

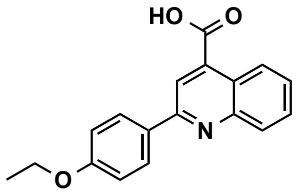

$C_{18}H_{15}NO_3$
M = 293.32 g/mol

In a 100 mL round-bottomed flask, isatin (4.66 g, 32 mmol, 1.3 eq.), potassium hydroxide (4.1 g, 73 mmol, 3 eq.) and 1-(4-ethoxyphenyl)ethanone (4 g, 24 mmol, 1.0 eq.) were refluxed in anhydrous ethanol over molecular sieves (3 Å) for 12 h. The dark red solution was cooled, concentrated *in vacuo* and separated between EtOAc (20 mL) and H_2O (20 mL). The aqueous layer was acidified with hydrochloric acid (10 M, 3.15 mL, excess), and the precipitate collected *via* filtration yielding the desired product as as a beige powder (5.15 g, 17 mmol, 72%).

LRMS: [ESI^+, MeOH] m/z (%): 294.1 (M+H, 100%)

^{1}H NMR (360 MHz, DMSO-d_6) δ 8.70 (ddd, 1H), 8.42 (s, 1H), 8.20 (dd, 2H), 7.80 (ddd, 1H), 7.59 (ddd, 1H), 7.09 (m, 2H), 4.11 (s, 3H), 1.52 (m, 3H).

^{13}C NMR (360 MHz, DMSO-*d$_6$*) δ 167.70, 160.22, 155.48, 148.42, 137.41, 130.17, 130.09, 129.56, 128.70, 127.28, 125.37, 123.10, 118.69, 114.78, 63.28, 40.22, 38.82, 14.62.

***N*-(4-(*N*-acetylsulfamoyl)phenyl)-2-(4-ethoxyphenyl)quinoline-4-carboxamide (SA)**

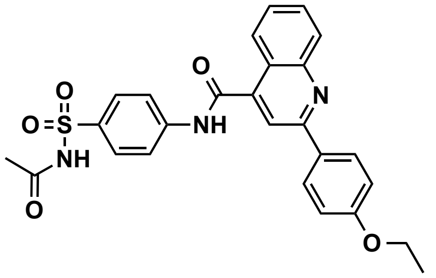

$C_{26}H_{23}N_3O_5S$
M = 489.55 g/mol

A suspension of 2-(4-ethoxyphenyl)quinoline-4-carboxylic acid (SA-001) (250 mg, 0.9 mmol, 1.5 eq.) was refluxed in DCM (15 mL) and thionyl chloride (1.2 mL, 17 mmol, 30 eq.) for 3 h to produce the corresponding acid chloride. Remaining thionyl chloride was removed *in-vacuo* and the acid chloride used immediately without further purification, due to its sensitivity. The acid chloride was suspended in anhydrous DCM and added dropwise to a solution of sulfacetamide (128 mg, 0.6 mmol, 1.0 eq.) in anhydrous DCM (8 mL) containing NMM (125 µL, 1.1 mmol, 2 eq.) at 0 °C, instantly producing a dark orange solution. The reaction was stirred vigorously for a further 12 h, quenched with water, extracted with EtOAc, the organic phases combined and washed with brine, dried over magnesium sulphate, concentrated *in vacuo* and purified *via* FCC (0.5-1% MeOH/DCM) to yield **SA** (30 mg, 0.06 mmol, 10%) as a yellow solid.

R_f = 0.13 (1% MeOH/DCM).

LRMS: [ESI$^+$, MeOH] m/z (%): 290.8 (M+H, 100%)

^{1}H NMR (360 MHz, DMSO-*d$_6$*) δ 12.03 (s, 1H), 11.22 (s, 1H), 8.39 – 8.25 (m, 3H), 8.11 (ddt, J = 8.6, 2.0, 1.1 Hz, 2H), 8.06 – 7.91 (m, 4H), 7.82 (ddd, J = 8.4, 6.9, 1.5 Hz, 1H), 7.62 (ddd, J = 8.3, 6.9, 1.3 Hz, 1H), 7.14 – 7.05 (m, 2H), 4.12 (q, J = 7.0 Hz, 2H), 1.92 (s, 3H), 1.36 (t, J = 7.0 Hz, 3H).

Methyl-2-(4-ethoxyphenyl)quinoline-4-carboxylate (SA-002)

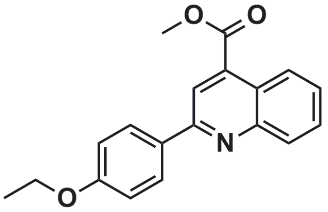

$C_{19}H_{17}NO_3$
M = 307.34 g/mol

To a suspension of **SA-001** (50 mg, 0.17 mmol, 1 eq.) in MeOH was added thionyl chloride (0.25 mL, 3.41 mmol, 20 eq.) and heated to reflux for 2 h. Excess thionyl chloride and MeOH were removed *in vacuo*. The residue was dissolved in EA and washed with water (2 x 5 mL) and brine (1 x 5 mL). The organic phases were dried over $MgSO_4$ and concentrated *in vacuo* to yield SA-002 (41,9 mg, 0,136 mmol, 80 % yield).

LRMS: [ESI^+, MeOH] m/z (%): 308.2 (M+H, 100%)

^{1}H NMR (360 MHz, DMSO-*d$_6$*) δ 8.73 (ddd, 1H), 8.39 (s, 1H), 8.22 (dd, 2H), 7.79 (ddd, 1H), 7.63 (ddd, 1H), 7.07 (m, 2H), 4.15 (q, 2H), 4.10 (s, 3H), 1.47 (m, 3H).

Ethyl-2-(4-ethoxyphenyl)quinoline-4-carboxylate (SA-003)

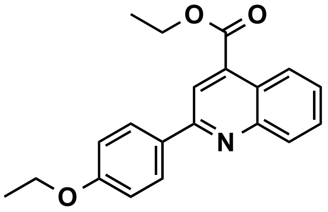

$C_{20}H_{19}NO_3$
M = 321.38 g/mol

To a suspension of **SA-001** (50 mg, 0.17 mmol, 1 eq.) in EtOH was added thionyl chloride (0.25 mL, 3.41 mmol, 20 eq.) and heated to reflux for 2 h. Excess thionyl chloride and EtOH were removed *in vacuo*. The residue was dissolved in EA and washed with water (2 x 5 mL) and brine (1 x 5 mL). The organic phases were dried over $MgSO_4$ and concentrated *in vacuo* to yield SA-003 SA-005 (49 mg, 0.152 mmol, 45 % yield).

LRMS: [ESI^+ , MeOH] m/z (%): 322.3 (M+H, 100%)

^{1}H NMR (360 MHz, DMSO-*d$_6$*) δ 8.73 (ddd, 1H), 8.38 (s, 1H), 8.26 (dd, 2H), 7.82 (ddd, 1H), 7.66 (ddd, 1H), 7.10 (m, 2H), 4.58 (q, 2H), 4.16 (q, 2H), 1.52 (m, 3H).

N-((4-Acetamidophenyl)sulfonyl)acetamide (SA-004)

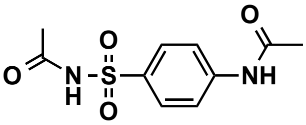

$C_{10}H_{12}N_2O_4S$
M = 256.28 g/mol

A mixture of sulfacetamide (0.2 g, 0.934 mmol, 1 eq), acetic anhydride (0.88 µL, 0.934 mmol, 1 eq.) and pyridine (2.27 mL, 28 mmol, 30 eq.) was heated to reflux for 1 h. After cooling to RT, the reaction mixture was diluted with 30 mL EA and washed with 10% $CuSO_4$ until the aqueous solution remaiend light blue in color. The organic layer was washed with brine, dried over $MgSO_4$ and evaporated to yield a colorless solid (0.034 g, 133 mmol, 14.2%).

LRMS: [ESI$^+$, MeOH] m/z (%): 257.2 (M+H, 100%).

^{1}H NMR (360 MHz, DMSO-*d*$_6$) δ 7.83 (d, 2H), 7.76 (d, 2H), 7.21 (s, 1H), 6.07 (s, 1H), 2.51 (s, 3H), 2.08 (s, 3H).

General method 1: preparation of N-derivatized nitrobenzenesulfonamides

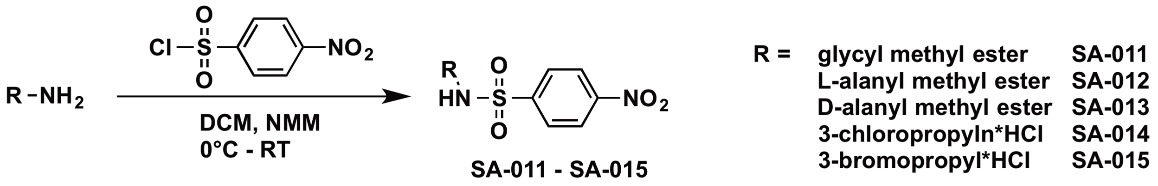
R-NH2
DCM, NMM
0°C - RT
SA-011 - SA-015
R =
glycyl methyl ester SA-011
L-alanyl methyl ester SA-012
D-alanyl methyl ester SA-013
3-chloropropyln*HCl SA-014
3-bromopropyl*HCl SA-015

To a suspension of amine (1 eq.) in DCM (8 mL) at 0°C, NMM (2.25 eq.) followed by *para*-nitrobenzenesulphonyl chloride (1.25 eq.) was added dropwise and allowed to warm to room temperature and stirred for 6 h. The reaction was subsequently quenched with HCl (1 N, 5 mL) and washed with brine, dried over magnesium sulphate and purify *via* FCC (5–25% EtOAc/Hex).

Methyl-((4-nitrophenyl)sulfonyl)glycinate SA-011

Isolated as a yellow crystalline solid (491 mg, 1.8 mmol, 99%).

$C_9H_{10}N_2O_6S$, M = 274.25 g/mol.

R_f = 0.33 (40% EtOAc/Hex).

LRMS: [ESI$^+$, MeOH] m/z (%): 275.9 (M+H, 100%).

^{1}H NMR (500 MHz, DMSO) δ = 8.62 (s, 1H), 8.43 – 8.36 (m, 2H), 8.07 – 7.99 (m, 2H), 3.82 (s, 2H), 3.52 (s, 3H).

Methyl-((4-nitrophenyl)sulfonyl)-L-alaninate SA-012
Isolated as a yellow crystalline solid (487 mg, 1.8 mmol, 94%).

$C_{10}H_{12}N_2O_6S$, M = 288.27 g/mol.

R_f = 0.36 (40% EtOAc/Hex).

LRMS: [ESI$^+$, MeOH] m/z (%): 289.0 (M+H, 100%)

^{1}H NMR (500 MHz, DMSO) δ = 8.73 (s, 1H), 8.50 – 8.35 (m, 2H), 8.22 – 7.83 (m, 2H), 4.00 (q, *J*=7.1, 1H), 3.43 (s, 3H), 1.21 (d, *J*=7.2, 3H).

Methyl-((4-nitrophenyl)sulfonyl)-D-alaninate SA-013
Isolated as a yellow crystalline solid (394 mg, 1.8 mmol, 72%) spectroscopically identical with **SA-012**.

N-(3-Chloropropyl)-4-nitrobenzenesulfonamide SA-014

$C_9H_{11}ClN_2O_4S$, M = 278.71 g/mol.

R_f = 0.19 (20% EtOAc/Hex).

LRMS: [ESI$^+$, MeOH] m/z (%): 279.3 (M+H, 100%).

^{1}H NMR (360 MHz, $CDCl_3$) δ = 8.45 – 8.33 (m, 2H), 8.14 – 8.02 (m, 2H), 5.00 (t, *J*=6.4, 1H), 3.58 (t, *J*=6.1, 2H), 3.26 – 3.15 (m, 2H), 1.99 (p, *J*=6.3, 2H).

^{13}C NMR (91 MHz, $CDCl_3$) δ = 150.27, 145.80, 128.47, 125.17, 124.63, 77.51, 41.75, 40.69, 32.30.

N-(3-Bromopropyl)-4-nitrobenzenesulfonamide SA-015

SA-015 was isolated as a white crystalline solid.

$C_8H_9BrN_2O_4S$, M = 323.16 g/mol.

R_f = 0.65 (2% MeOH/DCM).

LRMS: [ESI$^+$, MeOH] m/z (%): 646.7 (2M+H, 100%).

General method 2: reduction of N-derivatized nitrobenzenesulfonamides

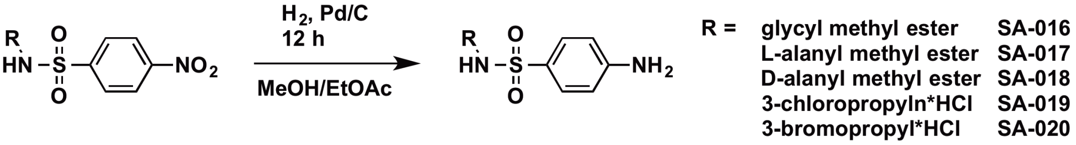
H2, Pd/C
12 h
MeOH/EtOAc
R =
glycyl methyl ester SA-016
L-alanyl methyl ester SA-017
D-alanyl methyl ester SA-018
3-chloropropyln*HCl SA-019
3-bromopropyl*HCl SA-020

N-derivatized nitrobenzenesulfonamides (1.0 eq.) were dissolved in in MeOH:EtOAc (1:1, 10 mL) and stirred with Pd/C (0.015 eq.) under a H_2 atmosphere over 24 h at RT. The progress of the reduction was monitored by TLC and after complete consumption of starting material, the mixture was passed through celite 545. The filtrate was concentrated in vacuo and used in the next step without further purification.

4-Amino-N-(glycylmethylester)benzenesulfonamide SA-016

Isolated as a pale yellow solid (417 mg, 1.6 mmol, 97%).

$C_{10}H_{14}N_2O_4S$, M = 244.26 g/mol.

R_f = 0.36 (60% EtOAc/Hex).

LRMS: [ESI^+, MeOH] m/z (%): 245.1 (M+H, 100%)

^{1}H NMR (500 MHz, DMSO) δ = 7.63 (t, *J*=6.0, 1H), 7.44 – 7.33 (m, 2H), 6.64 – 6.53 (m, 2H), 5.92 (s, 2H), 3.55 (d, *J*=5.6, 2H), 3.54 (s, 3H).

4-Amino-N-(L-alanylmethylester)benzenesulfonamide SA-017

Isolated as a pale yellow solid (417 mg, 1.6 mmol, 97%).

$C_{10}H_{14}N_2O_4S$, M = 258.29 g/mol.

R_f = 0.39 (60% EtOAc/Hex).

LRMS: [ESI^+, MeOH] m/z (%): 259.1 (M+H, 100%).

^{1}H NMR (500 MHz, DMSO) δ = 7.74 (d, *J*=8.3, 1H), 7.41 – 7.34 (m, 2H), 6.62 – 6.55 (m, 2H), 5.91 (s, 2H), 3.72 (dq, *J*=8.2, 7.2, 1H), 3.47 (s, 3H), 1.12 (d, *J*=7.2, 3H).

4-Amino-N-(D-alanylmethylester)benzenesulfonamide SA-018

Isolated as a pale yellow solid (354 mg, 0.66 mmol, 34%) spectroscopically identical to **SA-017**.

4-Amino-N-(3-chloropropyl)benzenesulfonamide SA-019

Isolated as a yellow solid. (1.06 g, 3.5 mmol, 62%).

$C_9H_{13}ClN_2O_2S$, M = 248.72 g/mol.

R_f = 0.31 (40% EtOAc/Hex).

LRMS: [ESI$^+$, MeOH] m/z (%): 278.84 (M+H, 100%).

^{1}H NMR (360 MHz, DMSO) δ = 7.51 – 7.33 (m, 2H), 7.17 (t, *J*=6.0, 1H), 6.62 – 6.56 (m, 2H), 5.93 (s, 2H), 3.61 (t, *J*=6.4, 2H), 2.78 (dt, *J*=6.6, 2H), 1.87 – 1.72 (m, 2H).

LRMS: [ESI$^+$, MeOH] m/z (%): 249.89 (M+H, 100 %)

4-Amino-N-(3-bromopropyl)benzenesulfonamide SA-020

SA-020 was isolated as a pale yellow solid (1.06 g, 3.8 mmol, 82%).

$C_8H_{11}BrN_2O_2S$, M = 279.15 g/mol.

R_f =.31 (40% EtOAc/Hex).

LRMS: [ESI$^+$, MeOH] m/z (%): 278.84 (M+H, 100%).

^{1}H NMR (360 MHz, DMSO) δ = 7.50 – 7.36 (m, 2H), 7.16 (t, *J*=6.0, 1H), 6.58 – 6.54 (m, 2H), 5.91 (s, 2H), 3.55 (t, *J*=6.4, 2H), 2.75 (dt, *J*=6.6, 2H), 1.85 – 1.70 (m, 2H).

General method 3: coupling of biaryl acid SA-001 to 4-aminobenzenesulfonamides SA-016 - SA-020

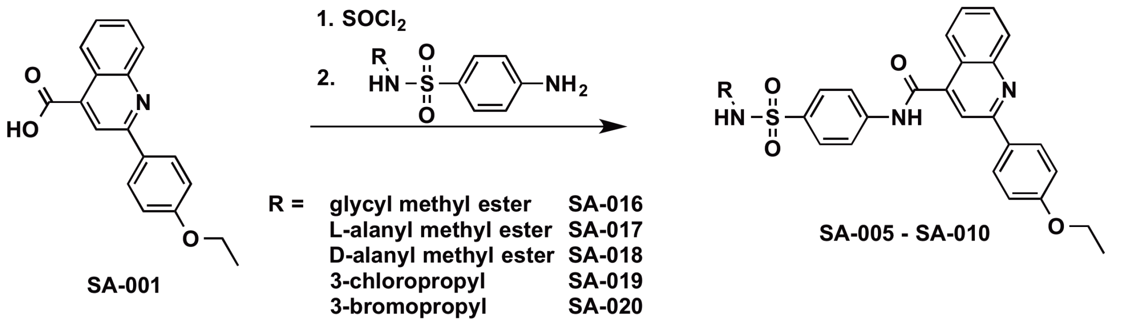
SA-001
1. SOCl2
2.
R
HN
S
O
NH2
R =
glycyl methyl ester SA-016
L-alanyl methyl ester SA-017
D-alanyl methyl ester SA-018
3-chloropropyl SA-019
3-bromopropyl SA-020
NH
N
HO
SA-005 - SA-010

A suspension of **SA-001** (1.1 eq.) and thionyl chloride (30 eq.) was refluxed in DCM (15 mL) for 3 h to yield the corresponding acid chloride. Remaining thionyl chloride was removed *in vacuo* and the acid chlorides were immediately used in the subsequent coupling reaction without further purification. The acid chlorides were suspended in anhydrous DCM and added dropwise to a suspension of **4-aminobenzenesulfonamides** (1.0 eq.) in anhydrous DCM (5 mL) containing NMM (2 eq.) at 0°C. The reaction was stirred vigorously for a further 12 h, quenched with water and extracted with EtOAc (3 x 10 mL). The organic phases were combined, washed with brine, dried over $MgSO_4$ and concentrated *in vacuo*. Purification *via* FCC (0.5-1% MeOH/DCM) gave the final coupling products as pale yellow solids.

Methyl-((4-(2-(4-ethoxyphenyl)quinoline-4-carboxamido)phenyl)sulfonyl)glycinate SA-005

Isolated as a yellow solid (30 mg, 0.06 mmol, 10%).

$C_{27}H_{25}N_3O_6S$, M = 519.57 g/mol.

R_f = 0.15 (1% MeOH/DCM).

LRMS: [ESI$^+$, MeOH] m/z (%): 520.2 (M+H, 100%).

^{1}H NMR (500 MHz, DMSO) δ = 11.15 (s, 1H), 8.44 – 8.28 (m, 3H), 8.25 – 8.07 (m, 3H), 8.06 – 7.93 (m, 2H), 7.90 – 7.78 (m, 3H), 7.63 (m, 1H), 7.19 – 7.04 (m, 2H), 4.14 (q, 2H), 3.72 (d, *J*=6.3, 2H), 3.57 (s, 3H), 1.38 (t, *J*=6.9, 3H).

Methyl-((4-(2-(4-ethoxyphenyl)quinoline-4-carboxamido)phenyl)sulfonyl)-L-alaninate SA-006

Isolated as a yellow solid (85 mg, 0.16 mmol, 28%).

$C_{28}H_{27}N_3O_6S$, M = 533.60 g/mol.

R_f = 0.21 (1% MeOH/DCM).

LRMS: [ESI$^+$, MeOH] m/z (%): 534.4 (M+H, 100%)

^{1}H NMR (500 MHz, DMSO) δ = 11.15 (s, 1H), 8.37 – 8.30 (m, 3H), 8.26 (d, *J*=8.3, 1H), 8.16 – 8.10 (m, 2H), 8.03 – 7.96 (m, 2H), 7.87 – 7.78 (m, 3H), 7.63 (ddd, *J*=8.3, 6.9, 1.2, 1H), 7.15 – 7.08 (m, 2H), 4.14 (q, *J*=6.9, 2H), 3.90 (dq, *J*=9.3, 7.2, 1H), 3.51 (s, 3H), 1.38 (t, *J*=7.0, 3H), 1.18 (d, *J*=7.2, 3H).

Methyl-((4-(2-(4-ethoxyphenyl)quinoline-4-carboxamido)phenyl)sulfonyl)-D-alaninate SA-008

Isolated as a yellow solid (92 mg, 0.16 mmol, 30%), spectroscopically identical with **SA-007**.

N-(4-(*N*-(3-Bromopropyl)sulfamoyl)phenyl)-2-(4-ethoxyphenyl)quinoline-4-carboxamide SA-009

The product was isolated as a yellow solid (210 mg, 0.38 mmol, 22%) as a pale yellow solid.

$C_{26}H_{24}BrN_3O_4S$, M = 554.46 g/mol.

R_f = 0.16 (1% MeOH/DCM).

LRMS: [ESI$^+$, MeOH] m/z (%): 554.35 (M+H, 100%)

N-(4-(*N*-(3-Chloropropyl)sulfamoyl)phenyl)-2-(4-ethoxyphenyl)quinoline-4-carboxamide SA-010

Isolated as a pale yellow solid (210 mg, 0.4 mmol, 85%).

$C_{27}H_{26}ClN_3O_4S$, M = 524.03 g/mol.

R_f = 0.17 (1% MeOH/DCM).

LRMS: [ESI$^+$, MeOH] m/z (%): 524.36 (M+H, 100 %)

2-(4-Ethoxyphenyl)-*N*-(4-(*N*-(3-(4,4,5,5-tetramethyl-1,3,2-dioxaborolan-2-yl)propyl)sulfamoyl)phenyl)quinoline-4-carboxamide SA-007

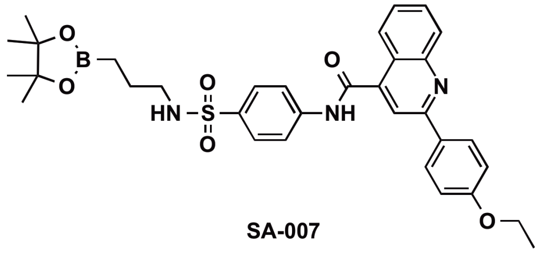

SA-007

$C_{33}H_{38}BN_3O_6S$
M = 615.55 g/mol

Copper(I)iodide (17.15 mg, 0.09 mmol, 10 mol%), triphenylphosphine (31 mg, 0.12 mmol, 13 mol%), lithium methanolate (68 mg, 1.8 mmol, 2 eq.) and bispinacolato diboron (343 mg, 1.35 mmol, 1.5 eq.) were added to DMF (4 mL) in a 25 mL round-bottomed flask. The vessel was purged with three cycles of vacuum before **SA-010** (512 mg, 0.9 mmol, 1.0 eq.) was added. The reaction was stirred at 20 °C for 18 h, diluted with EtOAc (20 mL), filtered through a pad of silica, washed with EtOAc, concentrated *in vacuo* and purified *via* FCC (0-6% MeOH/DCM + 0.5 % TEA) to yield **4** as a white solid (132 mg, 0.216 mmol, 24%).

LRMS: [ESI$^+$, MeOH] m/z (%): 615.3 (M+H, 100%)

5.8 Synthesis of peptidic substrates

5.8.1 Solid phase synthesis

For Fmoc-based solid phase synthesis of peptides, the 2-chlorotrityl alcohol resin was swollen by gentle shaking in dry DCM for two hours in a plastic syringe sealed with a frit and a PTFE stopper. After discarding the DCM, the first amino acid was coupled by adding a solution of 2 eq. of the Fmoc-protected amino acid, HCTU and DIPEA in DCM for 18 h. The reaction was quenched by washing with DCM/MeOH/DIPEA in a 17:2:1 ratio and subsequently with DCM. Evaporation of the remaining solvent gave resins with 80-90% amino acid loading. The amino acid coupling steps were carried out on a peptide synthesizer PS3 (Peptide Technologies) on a 0.2 mmol scale. Briefly, the resin was swollen in DMF for one hour, followed by deprotection in a solution of 20% (v/v) piperidine in DMF for 20 min. After washing with DMF, the resin was incubated with a fresh solution of HCTU and Fmoc-amino acid in 20% (v/v) N-methyl morpholine for 20-40 min and washed again with DMF. After repeated elongation cycles, the N-terminal Fmoc protection group was removed, followed by washing with DMF. The resins were stored at -20 °C.

5.8.2 Resin cleavage and purification

Trityl chloride resins were treated with 95% (v/v) TFA with 2.5% (v/v) TIS and 2.5% (v/v) water. The resin turns deep red upon contact with the cleavage cocktail. The slurry was shaken overnight at room temperature to remove all side chain protection groups. In a final step, the resin was washed thrice with the cleavage cocktails. The collected TFA solutions were cooled on ice and triturated with approximately the same volume of cold diethyl ether. The precipitate was filtrated and the filter cake was redissolved in a small amount of TFA and the precipitation was repeated for several times. Eventually, the precipitate was dried and redissolved in 5% (v/v) ACN in 95% (v/v) water. This solution was applied to preparative HPLC chromatography with a gradient of 5% (v/v) ACN to 40% ACN (v/v) over 100 min. The peptide eluted between 20 and 30% ACN (v/v). HPLC fractions were analyzed by ESI-MS with positive and negative ion detection. Fractions that contained peptide were pooled accordingly and the solvent was removed by lyophilization overnight. The resulting white powder was dissolved in DMSO to concentrations of 100 mM, which were directly applied to digestion assays.

6 Results

6.1 Collection of a focused library for crystallographic screening

A thorough literature search for reports of unusual CP inhibitors from natural and synthetic origins was conducted to collect focused screening library. The emphasis was on ligands that have not been cross-validated by X-ray crystallographic studies before but showed promising preliminary findings regarding CP impairment, such as accumulation of proteasomal substrate proteins (p27, Bax, IκBα), activation of caspase-3, inhibition of transcription factor NF-κB or *in vitro* blockage of the CP. Moreover, the search was limited on compounds with scaffolds that differ from the common di- to tetrapeptidic molecular scaffold of conventional CP inhibitors, since these were not expected to show novel binding modes.

The resulting set of screening candidates is depicted in Figure 14 and represents a broad variety of chemotypes that ranges from complex natural products and semisynthetic derivatives, to more drug-like synthetic small molecules with reduced complexity. If not commercially available, the authors of the respective literature reports generously provided most compounds of the screening library with the exception of SA (Figure 14G), which was resynthesized in the course of this thesis.

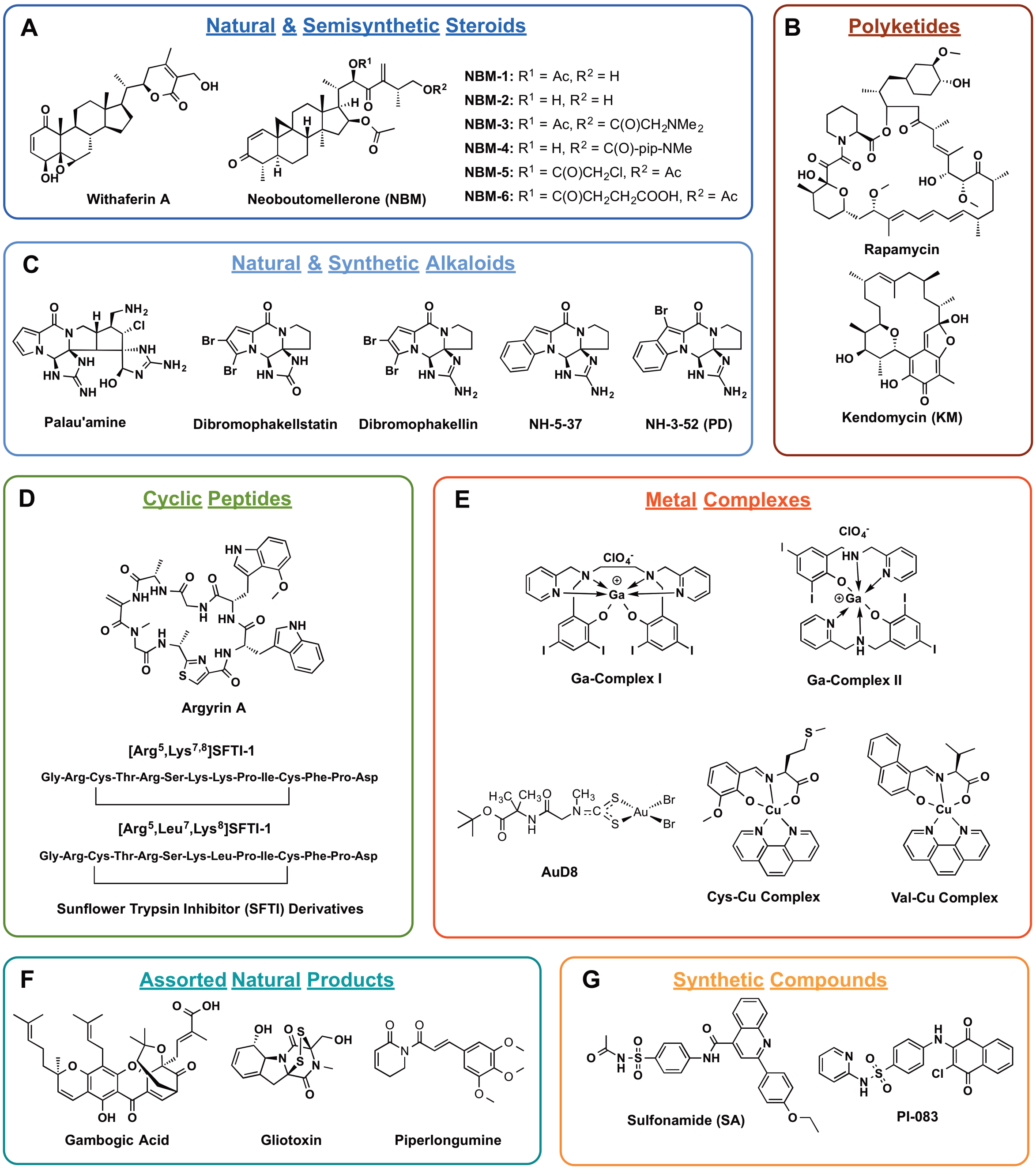
A
Natural & Semisynthetic Steroids
Withaferin A
Neoboutomellerone (NBM)
NBM-1: R1 = Ac, R2 = H
NBM-2: R1 = H, R2 = H
NBM-3: R1 = Ac, R2 = C(O)CH2NMe2
NBM-4: R1 = H, R2 = C(O)-pip-NMe
NBM-5: R1 = C(O)CH2Cl, R2 = Ac
NBM-6: R1 = C(O)CH2CH2COOH, R2 = Ac
B
Polyketides
Rapamycin
Kendomycin (KM)
C
Natural & Synthetic Alkaloids
Palau'amine
Dibromophakellstatin
Dibromophakellin
NH-5-37
NH-3-52 (PD)
D
Cyclic Peptides
Argyrin A
[Arg5,Lys7,8]SFTI-1
Gly-Arg-Cys-Thr-Arg-Ser-Lys-Lys-Pro-Ile-Cys-Phe-Pro-Asp
[Arg5,Leu7,Lys8]SFTI-1
Gly-Arg-Cys-Thr-Arg-Ser-Lys-Leu-Pro-Ile-Cys-Phe-Pro-Asp
Sunflower Trypsin Inhibitor (SFTI) Derivatives
E
Metal Complexes
Ga-Complex I
Ga-Complex II
AuD8
Cys-Cu Complex
Val-Cu Complex
F
Assorted Natural Products
Gambogic Acid
Gliotoxin
Piperlongumine
G
Synthetic Compounds
Sulfonamide (SA)
PI-083

Figure 14: Selected compounds for crystallographic screening against the yCP ordered by molecular scaffold and origin. All compounds were reported as proteasome inhibitors with an unknown molecular mode of action. A: Oxygenated steroidal compounds of natural and semisynthetic origin with α,β-unsaturated carbonyls. B: Ansa-polyketides that bear α-ketoamides (rapamycin) and chinone methides (kendomycin) as the reactive chemical moiety. C: Natural and synthetic alkaloids related to the oroidin class of natural products. D: Cyclic peptides bearing a reactive α,β-unsaturated carbonyl (argyrin A) or disulfide bridges (sunflower trypsin inhibitors, SFTI). E: Synthetic gallium-, copper- and gold complexes with strong cytotoxic properties. F: Miscellaneous natural products with strong cytotoxic effect but unknown cellular target. G: Synthetic hits from in-silico and subsequent in-vitro screening against the yCP.

Class	**Compound**	**Reported data**	**Source**	**Ref**
Steroids (A)	Withaferin A	*In vitro/vivo* CP inhibition, accumulation of ubiquitinated proteins, Bax & IκBα.	Sigma Aldrich	109
	Neoboutomellerones 1-6	Accumulation of ubiquitinated proteins	Pierre Fabre Pharma, France	81,110
Polyketides (B)	Rapamycin	*In vitro* inhibition of human CP	Sigma Aldrich	111
	Kendomycin	*In vitro* inhibition of rabbit CP, accumulation of ubiquitinated proteins, vacuolization of the ER, mitochondrial swelling	Prof. Rolf Müller, Saarland University	112
Natural & synthetic alkaloids (C)	Palau'amine	*In vitro* CP inhibition, blocks degradation of ubiquitinylated proteins	Prof. Phil Baran, The Scripps Research Institute, USA	113
	Dibromo-Palau'amine	Not tested; structurally related to palau'amine	Prof. Phil Baran, The Scripps Research Institute, USA	-
	Dibromophakellin	*In vitro* inhibition of human CP, no activity *in vivo*	Prof. Jetze Tepe, Michigan State University, USA	113
	Dibromophakellstatin	*In vitro* inhibition of human CP, EC_{50} ~1 µM	Prof. Jetze Tepe, Michigan State University, USA	113
	NH-5-52	*In vitro* inhibition of human CP, no activity *in vivo*	Prof. Jetze Tepe, Michigan State University, USA	-
	NH-5-37 (PD)	*In vitro* inhibition of human CP, no activity *in vivo*	Prof. Jetze Tepe, Michigan State University, USA	-
Cyclic Peptides (D)	Scytonemide	*In vitro* CP inhibition, no activity in cell-based assays	-	114
	Sunflower Trypsin Inhibitors (SFTI)	*In vitro* CP inhibition	Prof. Krzysztof Rolka, University of Gdańsk, Poland	-
Metal complexes (E)	Ga-Complex I/II	*In vitro* inhibition of rabbit CP	Prof. Claudio Verani, Wayne State University, USA	115
	Cys-Cu/Val-Cu Complex	*In vitro* CP inhibition, accumulation of ubiquitinated proteins	Q. Ping Dou, Wayne State University, USA	116
	AuD8	*In vitro* inhibition of human CP, antitumor activity *in vivo*, caspase-3 activation, accumulation of p27, IκBα IκBα IκBα and Bax	Prof. Dolores Fregona, University of Padua, Italy	117
Assorted natural products (F)	Gambogic Acid	*In vitro* CP inhibition, caspase-3 activation, accumulation of ubiquitinated proteins	Sigma Aldrich	118
	Gliotoxin	*In vitro* CP inhibition, inhibition of NFkB activation	-	119
	Piperlongumine	Accumulation of ubiquitinated proteins	Sigma Aldrich	120
Synthetic compounds (G)	PI-083	*In vitro* CP inhibition	Prof. Boris Schmidt, TU Darmstadt	121
	Sulfonamide (SA)	*In vitro* CP inhibition	synthesized in house	122

6.1.1 Steroids (A)

Oxygenated steroids represent a group of putative CP inhibitors that were originally isolated from plants and tested for their antitumor activity against different cell lines. Both withaferin A and the neoboutomellerones (NBM) display potent electrophilic structural motifs that are a common feature of CP inhibitors, such as α,β-unsaturated carbonyls, lactones and epoxides (Figure 14A). As a result, both compound classes were investigated as CP inhibitors in previous studies that suffered from the absence of structural data.[81,109–111] However, soaking of yCP crystals with withaferin A or NBM did not result in defined electron density for the ligands.

6.1.2 Polyketides (B)

The complex natural products rapamycin and kendomycin (Figure 14B) both have originally been isolated from streptomyces species.[112,113] The immunosuppressive and antiproliferative properties of rapamycin lead to the FDA-approval of the drug to prevent rejection in organ transplantation. The macrocyclic lactone was shown to inhibit the human CP activity *in vitro* and a recent study indicated allosteric modulation of the proteasome by blocking the gate to the proteolytic core.[114] However, inspection of the electron density of yCP crystals soaked with rapamycin did not reveal ligand-related electron density at either the surface-exposed α rings or any other part of the proteasome.

Kendomycin (KM) is structurally related to rapamycin but exhibits a quinone methide as its key pharmacophoric element. The unique molecular scaffold together with the scarcity and cytotoxic potency of the compound caught the interest of organic chemists, which resulted in numerous approaches to its total synthesis. In a study from 2007, Elnakady *et al.* showed that KM causes the accumulation of ubiquitinated proteins and observed that treatment of U-937 cells resulted in an expression pattern that closely matches that of other tumor cell lines in response to CP inhibition.[115] Consequently, *in vitro* evaluation of KM against rabbit CP activity demonstrated that the natural product inhibits the hydrolysis of proteasome substrates. Soaking of yCP crystals with KM resulted in a unique complex structure that is discussed in chapter 6.3.

6.1.3 Natural and synthetic alkaloids (C)

In a study from 2012, palau'amine and related oroidine alkaloids (Figure 14C) were reported to inhibit the human constitutive as well as immunoproteasome *in vitro*.[116] In addition, palau'amine was found to prevent the degradation of ubiquitinated proteins in cell culture. The authors of the respective study generously resynthesized the parent ligands and provided the material for evaluation in the crystallographic screening. As a surprise, inspection of the electron density map of palau'amine-soaked yCP crystals revealed no ligand-related electron density, although the natural product was reported as an irreversible CP inhibitor. However, the related synthetic compound NH-5-37 was shown to bind to the yCP in a unique way and is discussed in chapter 6.5.

6.1.4 Cyclic Peptides (D)

Since the discovery of the highly potent TMC-95A,[46,117] a variety of other cyclic peptides have been reported as CP inhibitors.[118–120] Nevertheless, none of the presented compounds have been cross-validated with x-ray crystallographic method although the ligands showed promising *in vitro* data. In addition, the unusual large size of the cyclic peptides (7-14 amino acids) implied an unusual binding mode to the CP since the compounds do not adequately fit into the proteasomal substrate binding channels (Figure 14D). However, diffraction data of the yCP crystals that were soaked with Scytonemide or the sunflower trypsin inhibitors (SFTI) did not result in ligand-bound complex structures.

6.1.5 Metal complexes (E)

Various metal complexes (Figure 14E) have been reported to inhibit the CP with micromolar activity both *in vitro* and in cell culture.[121–124] Soaking of yCP crystals with gallium and copper complexes did not result in reproducible liganded structures, whereas crystals that were soaked with the gold complexes were severely damaged upon compound exposure and only diffracted to a maximum resolution of 5 Å. Although the latter compound was extensively investigated as a proteasome inhibitor in previous studies, the extreme oxidative strength of the Au(III) complexes suggests a polypharmacologic mode of action on cancer cells.[124]

6.1.6 Assorted natural products (F)

A variety of natural products that bear reactive functional groups have been reported as CP inhibitors. Indeed, the FDA-approved α',β'-epoxyketone carfilzomib is derived from epoxomicin, which was first isolated from an *actinomycete* strain.[60] While epoxomicin bears a molecular scaffold that is closely related to proteasomal substrates, many of the reported CP inhibitors from natural origin lack a peptidic structure and therefore are promising candidates to display novel binding modes in complex with the CP. Thus, three assorted natural products (gambogic acid,[125] gliotoxin[126] and piperlongumine[127]), that are comprised of unique structural motifs with reactive functional groups have been included in the crystallographic screening (Figure 14F). However, none of the compounds was identified in the resulting electron density maps of the soaked yCP crystals.

6.1.7 Synthetic compounds (G)

A plethora of HTS have been undertaken to identify novel ligands against the CP, but few were able to improve on the initial screening hits.[128–131] One successful example was the identification of *N*-hydroxyureas (HUs) as non-covalent, non-peptidic CP inhibitors. The initial hit exhibited an IC_{50} of 229 µM on purified yCP, whereas subsequent structure guided hit optimization resulted in a lead compound with 1000-fold improved potency (HU10, $IC_{50} = 0.34$ µM). All HU-derivatives leading to the most active inhibitor HU10 were synthesized in the course of the thesis. However, the results are not discussed herein but have been published in Gallastegui *et al.*[132]

The parent case represents a so-far singular exception, since all other studies suffered from the absence of structural knowledge about the binding mode of the respective hit molecules. Thus, two representative compounds from different *in silico* and *in vitro* screenings have been included in the crystallographic screening (Figure 14G). However, soaking of yCP crystals with the chloropnaphthoquinone screening hit PI-083 from the

NCI Diversity Set-1 library was not successful, whereas soaking of the sulfonamide (SA) resulted in a complex structure with 2.5 Å resolution that is discussed in chapter 6.3.

6.2 Evaluation of screening hits

The screening library encumbered a total of 27 compounds that were soaked onto yeast 20S CP crystals. Collection of diffraction data and subsequent evaluation of the F_O-F_C-electron density map resulted in three complex structures with the ligands depicted in Figure 15. All screening hits exhibit completely novel binding modes to the CP and are discussed in detail in the following chapters as separate case studies.

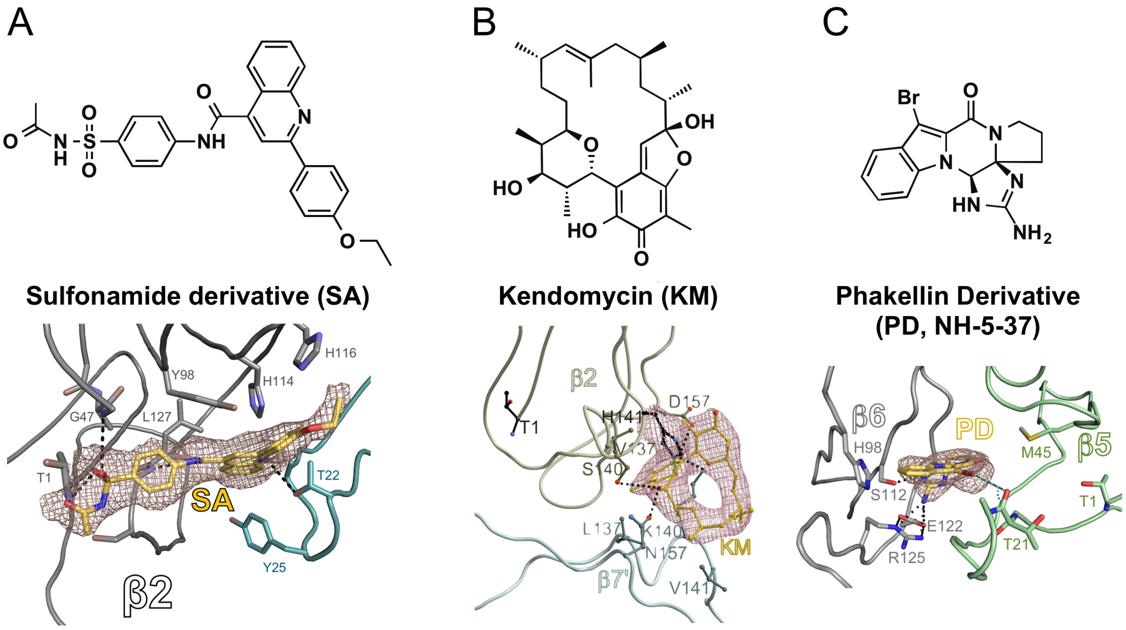
A
B
C
Sulfonamide derivative (SA)
Kendomycin (KM)
Phakellin Derivative (PD, NH-5-37)
H116
Y98
H114
G47
L127
T1
T22
SA
Y25
β2
β2
T1
D157
H141
V137
S140
L137
K140
N157
KM
β7'
V141
β6
PD
M45
β5
H98
S112
T1
E122
R125
T21

Figure 15: Hit compounds of the crystallographic screening. The electron densities are represented as a red mesh and contoured to 1.0 σ. A: Complex structure of SA with the yCP. The ligand (yellow) was shown to bind to the primed β2 substrate binding channel and thus affects both the β1 (gray) and β2 catalytic activity (teal). B: Complex of the ansa-polyketide KM with the yCP. The structure showed the natural product (yellow) covalently bound to β2-H141 in a surface exposed pocket between subunits β2 (wheat) and β7' (light cyan). C: The pyrrole-imidazole scaffold of PD is closely related to the natural product palau'amine. PD (yellow) was found to reversibly bind to the S3 specificity pocket of the β5 substrate binding channel (green).

6.3 Screening hit I: Sulfonamides (SA)

6.3.1 Discovery of SA by in silico screening

An *in silico* screening for nonpeptidic inhibitors of mammalian CP revealed a variety of sulfone- or piperazine-containing hits as noncovalent CP inhibitors.[133] Although the study focused on screening the ChTL active site, some of the identified compounds were found to inhibit the TL and CL activities as well. In addition, most compounds exhibited incoherent structure-activity relationships when compared with closely related compounds. However, a series of three structurally related ligands with a sulfacetamide core motif were described to selectively block the TL and CL activities, whereas the ChTL remained unaffected (Figure 16). These characteristic inhibitory profiles lead to the crystallographic investigation to determine the binding mode of the compounds.

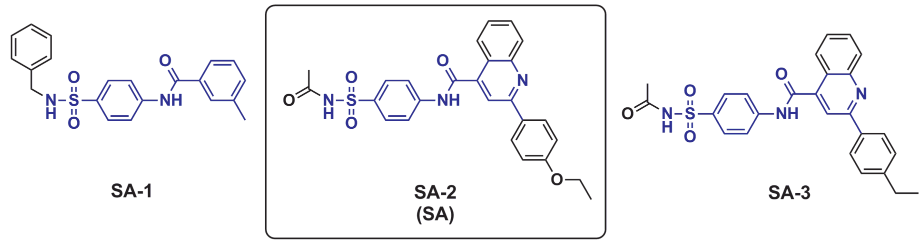

	% inhibition [100 μM]		
	ChTL	TL	CL
SA-1	-	13%	54%
SA-2	-	45%	42%
SA-3	-	15%	45%

Figure 16: Structures of sulfonamide compounds. The unifying sulfacetamide motif is colored in blue. All three compounds share a common inhibition profile by weakly inhibiting the TL and CL activities, while the ChTL catalytic site remains unaffected.

6.3.2 Crystal structure of SA bound to the yCP

Yeast 20S proteasome crystals were soaked with SA and diffraction data was recorded to a maximum resolution of 2.5 Å (R_{free} = 22.2 %). Surprisingly, inspection of the resulting F_O-F_C electron density map revealed that the substrate binding channels of all catalytic sites were lacking any ligand-related electron density. Instead, SA was found to bind to the primed substrate binding channel of subunit β2, which represents a hitherto unobserved binding mode to the yCP. The $2F_O$–F_C electron density map in which the ligand has been omitted prior to phase calculations clearly displays SA well defined in the primed β2 substrate binding channel and thus reveals a novel, non-covalent mode of action on the yCP (Figure 17).

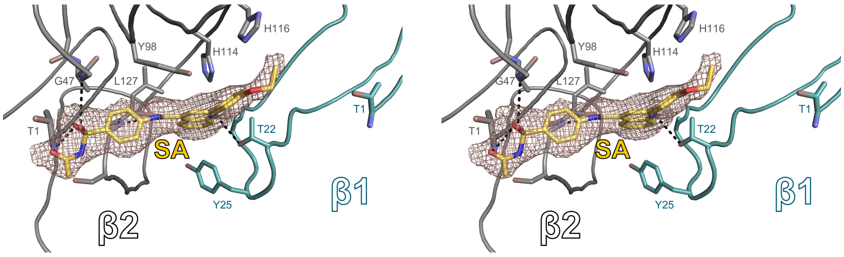
H116
Y98
H114
G47
L127
T1
SA
T22
T1
Y25
β1
β2
H116
Y98
H114
G47
L127
T1
SA
T22
T1
Y25
β1
β2

Figure 17: Stereo representation of the CP:SA crystal structure. The $2F_O-F_C$ omit electron density map (red mesh, 1σ) of SA (yellow) bound to the primed β2 substrate binding channel in proximity to the unprimed binding site of β1 (teal).

The ligand bridges the entire length of the primed β2 substrate binding channel and is stabilized by extensive hydrophilic and hydrophobic interactions. Particularly, the *N*-actetylsulfamoyl moiety of SA is strongly coordinated with β2-Thr1N and β2-Gly47N, thus disrupting the key interactions that stabilize the tetrahedral transition state of substrates during catalytic peptide bond cleavage (Figure 18). The 2,4-substituted quinoline ring system protrudes deeply into a large cavity that is formed by residues of both the β2 and β5 subunit. Thereby, binding of SA is favored by van-der-Waals interactions with L127, Y98, H114 (all β2) as well as β1-Y25, whereas a single polar interaction between β1-T22O^{γ} and the quinoline nitrogen atom provides additional stabilization.

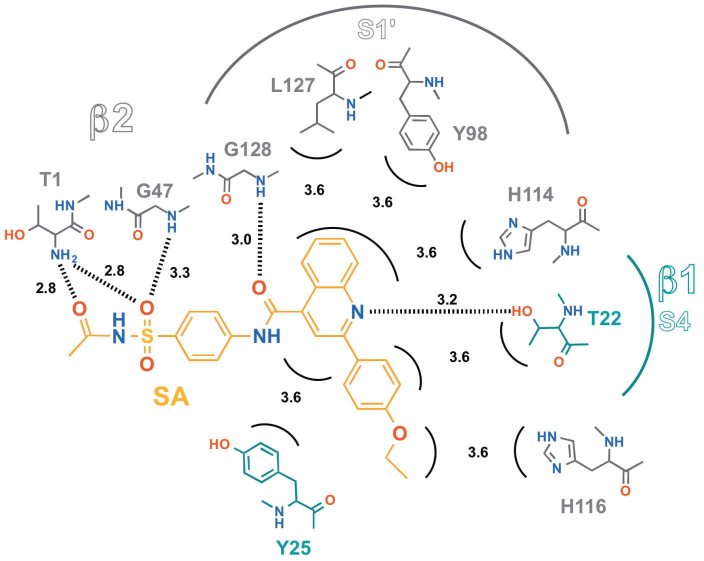
S1'
L127
Y98
β2
G128
T1
G47
H114
β1
S4
T22
SA
Y25
H116
3.6
3.6
3.6
3.0
2.8
2.8
3.3
3.2
3.6
3.6
3.6

Figure 18: Schematic overview of yCP in complex with SA. The interaction distances are shown in Å. The SA ligand is shown in yellow and amino acids of β1 as well as the β2 primed substrate binding site are depicted in teal and gray, repsectively. Residues of the β1 S4 specificity pocket that are in close contact with SA are colored in cyan.

Interestingly, superposition of yCP:SA and yCP in complex with the tetrapeptidic inhibitor ONX 0914 revealed that the 4-ethoxyphenyl moiety of SA is in close contact with β2-H116 that forms the S4 substrate specificity pocket of subunit β1 (Figure 19). These findings explain why SA is able to inhibit both the β1 and β2 catalytic activity to approximately equal extend. First, the ligand forms hydrogen bonds with β2-Thr1N *via* its *N*-acetylsulfamoyl moiety and thus impairs peptide bond hydrolysis by the CL activity. Second, the biaryl system of SA stretches into the substrate binding channel of β1, thereby affecting substrate turnover of the TL activity.

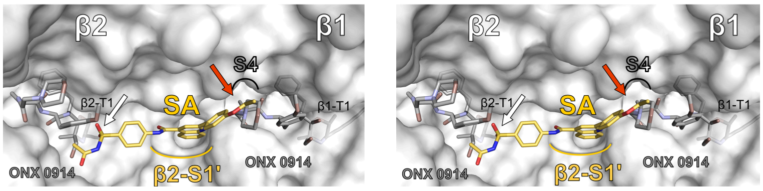

Figure 19: Dual targeting of β1 and β2 by SA (stereo view). Superposition of SA (yellow) and the tetrapeptidic CP inhibitor ONX 0914 (gray) highlights the dual effect of SA on the β1 and β2 catalytic activities. The *N*-acetylsulfamoyl group of SA is in close contact with the catalytic β2-Thr1N (white arrow), while its 4-ethoxyphenyl moiety protrudes into the S4 specificity pocket of β1 (red arrow).

While the unprimed substrate binding channel of β2c and β2i exhibits only marginal structural changes between mammalian CP subtypes, comparison of the primed substrate binding channel highlights an extraordinary structural diversity. Structural superposition of the SA binding site with cCP and iCP revealed that the β2-S' pocket displays a significant alteration in size and polarity among β2c and β2i. Specifically, systematic replacements in the iCP such as β2-S131E, β2-S111E and β1-A27V result in a significantly smaller and more polar environment in the SA binding site and thus opens up the possibility to design β2-type selective ligands.

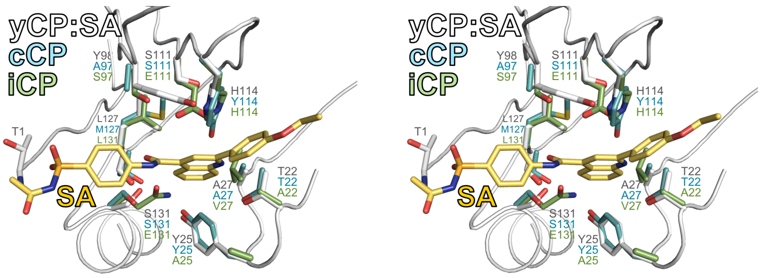
yCP:SA
cCP
iCP
Y98
A97
S97
S111
S111
E111
H114
Y114
H114
L127
M127
L131
T1
SA
S131
S131
E131
Y25
Y25
A25
A27
A27
V27
T22
T22
A22

Figure 20: Structural superposition of the primed β2 pocket of yCP:SA and murine iCP and cCP (stereo view). The primed β2 substrate binding site is structurally highly diverse between cCP (teal) and iCP (green). Thus, the size and polarity of the β2-S1' pocket is significantly altered in iCPs by the β2-S131E, β2-S111E and β1-A27V mutations.

6.3.3 Synthesis of SA and derivatives

In order to probe the interactions that are crucial for the binding affinity of SA, a series of five ligand fragments have been synthesized. The resulting set of compounds consisted of the commercially available sulfacetamide, its *N*-acetylated derivative SA-004 as well as the biaryls SA-001 – SA-003 (Figure 21). However, the compounds were not active against purified yCP *in vitro* and soaking of yCP crystals with the fragments failed to result in cocrystal structures. Thus, it is the entirety of the SA scaffold that is responsible for its binding affinity and may not be altered to a large extend.

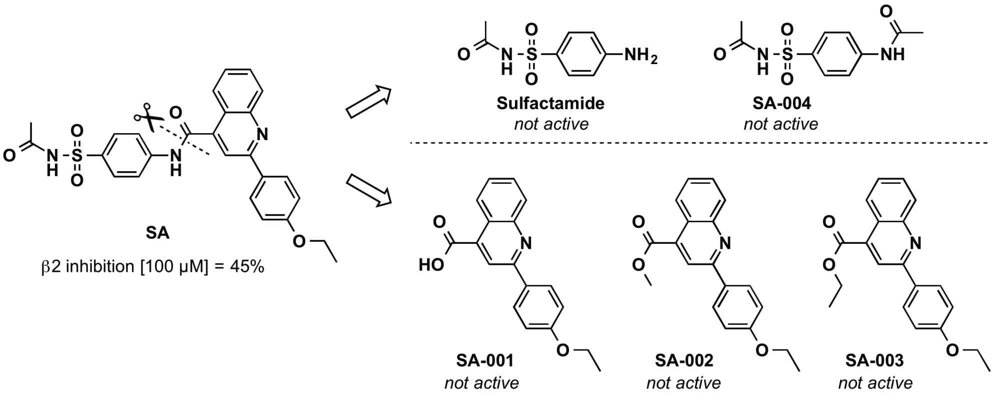
SA
β2 inhibition [100 µM] = 45%
Sulfactamide
not active
SA-004
not active
SA-001
not active
SA-002
not active
SA-003
not active

Figure 21: Ligand fragmentation approach. Structures of synthesized sulfacetamide (upper) and quinoline (lower) SA fragments. Soaking of yCP with the compounds did not result in complex structures. None of the fragments affected β2 or β1 substrate turnover of yCP *in vitro*.

Nevertheless, the weak inhibitory potency of SA represents a crucial vulnerability for the hit development process, since even subtle changes to the SA scaffold can result in complete loss of binding affinity. Therefore, covalent tethering to β2-T1 and extension towards the unprimed substrate binding channel *via* variation of the *N*-acetylsulfamoyl moiety was attempted to increase the ligands potency. In a first step, the SA ligand was synthesized to establish a general route to the SA derivatives (Figure 22). The two-step synthesis starts with a Pfitzinger reaction of isatin and 4-ethoxyacetophenone in refluxing ethanol in the presence of excess potassium hydroxide.[134] The resulting biaryl acid is precipitated with hydrochloric acid and collected *via* filtration. Successive treatment with thionyl chloride and sulfacetamide furnishes the SA ligand in low, albeit acceptable yield.

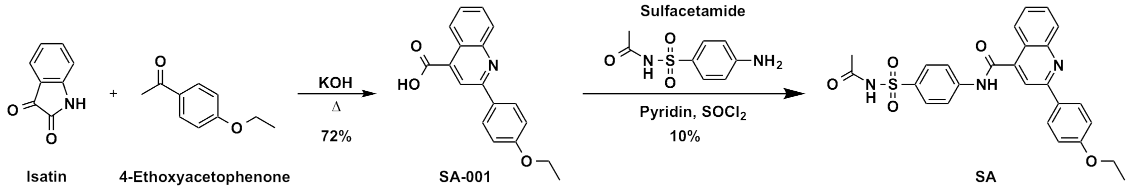

Figure 22: Synthesis of the SA ligand. The molecular scaffold of the SA hit structure is synthesized in two steps, starting with a Pfitzinger reaction of isatin and 4-ethoxyacetophenone to yield the quinoline biaryl ring scaffold. Conversion of the acid into the acid chloride and subsequent addition of sulfacetamide gives the SA ligand with 10% yield.

Subsequently, a convergent synthetic method was developed for the robust synthesis of SA derivatives (Figure 23A). The central sulfacetamide core (blue) is introduced with 4-nitrobenzenesulfonyl chloride, which allows for rapid modification of the acetyl moiety. Thus, various propylamines with leaving groups (SA-005, SA-006) or boronic acids esters (SA-007) were attached for covalent tethering of SA to the catalytic β2-Thr1 (Figure 23B). In a similar fashion, gylcin- and D- or L-alanine esters were introduced to provide stabilization by interacting with the primed β2 substrate binding channel. However, the binding affinity of SA was revealed to be highly sensitive in regard to changes of the *N*-acetyl moiety. Soaking of yCP crystals with the synthesized SA ligands showed that the derivatives were not defined in the electron density map and thus, further efforts for derivatization of this moiety has to be continued in future work.

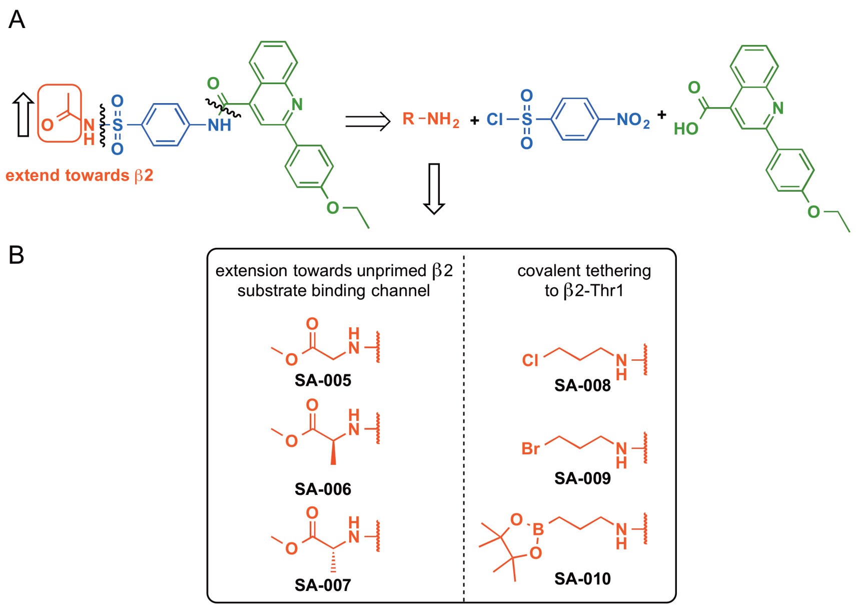
A
extend towards β2
R-NH$_2$ + Cl-SO$_2$-C$_6$H$_4$-NO$_2$ + HO
B
extension towards unprimed β2 substrate binding channel
covalent tethering to β2-Thr1
SA-005
SA-006
SA-007
SA-008
SA-009
SA-010

Figure 23: Synthesized SA derivatives. The *N*-acetylsulfamoyl moiety of SA was modified to target either β2-Thr1 (SA-005 – SA007) or the unprimed β2 substrate binding channel and thus increase the binding affinity of the SA scaffold.

6.4 Screening hit II: kendomycin (KM)

6.4.1 Discovery & cytotoxicity of KM

KM (KM, Figure 24) was first isolated from *Streptomyces violaceoruber* in 1996 and the natural compound was subsequently shown to exert anti-osteoporotic and endothelin recepter antagonistic properties.[112,113,135] Moreover, cytotoxicity tests with the structurally unique ansa-polyketide against human stomach adenocarcinoma (HMO2), hepatocellular carcinoma (HEP G2) and breast adenocarcinoma (MCF-7) cell lines demonstrated its potential for the treatment of cancer.[136] However, the cellular target could not be determined and approaches to enhance KM's cytotoxic effect thus remained limited.[137] In a genome-wide proteomics approach on KM-treated leukemic monocyte lymphoma cells (U-937), the natural product was found to cause accumulation of ubiquitinated proteins and activation of caspase-8, which in turn triggered apoptosis.[115] Thus, it was concluded that the CP might be a target of KM and it was shown that the natural product blocked proteasomal substrate cleavage to 25% residual activity in the presence of low amounts of SDS.

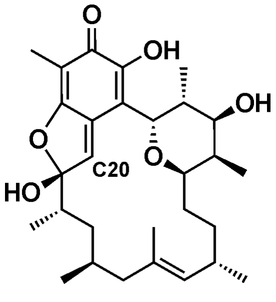

Kendomycin (KM)

Figure 24: Structure of Kendomycin. The ansa-cyclic scaffold of bears reactive chinon methide (C20) as the central pharmacophore.

6.4.2 KM inhibits the CP in the presence of SDS

The effect of KM on the proteasome was confirmed by an *in vitro* point measurement with fluorogenic substrates (Figure 25A). In addition to the previous studies, KM was shown to affect all three catalytic sites of the yCP by inhibiting the substrate cleavage to 25% residual activity at a inhibitor concentration of 200 µM. The IC_{50} for inhibition of the β5 activity was determined as 67.9 µM (Figure 25A). However, the assay results were found to be dependent on the presence of 0.01% SDS that is often used in assays to stimulate cleavage of chromophoric substrates by opening the closed gate to the proteolytic chamber of the CP, therefore providing rapid access of substrates to the cleavage sites (Figure 25).

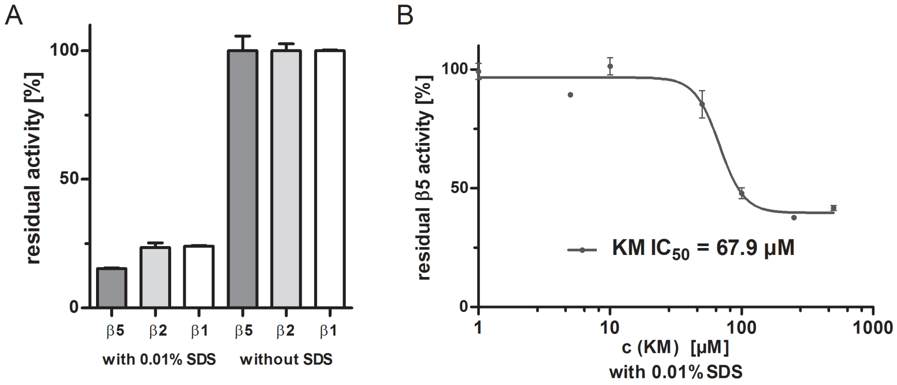

Figure 25: *In vitro* yCP blockage of the proteasome activity by KM. A: Inhibition of yCP β5 (15.3%), β2 (23.5%) and β1 (24.0%) catalytic activities by KM at 200 µM concentration in the presence and absence of SDS. B: Inhibitory potency of KM against the β5 activity of yCP that was incubated with varying concentrations of KM (1-500 µM). Data from three individual experiments were normalized to DMSO treated controls and are presented as means of relative activity ± standard deviation. Figure adopted from Beck *et al.*[138]

Since the inhibitory effect of KM on purified wildtype yCP vanished in the absence of SDS, a CP mutant (α3ΔN) with a permananet open gate conformation was employed in the same assay to render the use of SDS unnecessary.[139] However, the inhibition profile of KM remained similarly dependent on SDS even with the inherently activated α3ΔN mutant (Figure 26A). Moreover, addition of the CP activator PA28α from mouse confirmed that enzyme inhibition by KM only occurs in the presence of the detergent. Furthermore, the SDS-dependence of KM inhibition was observed in a similar experiment with ATP-activated human 26S proteasome (Figure 26B).

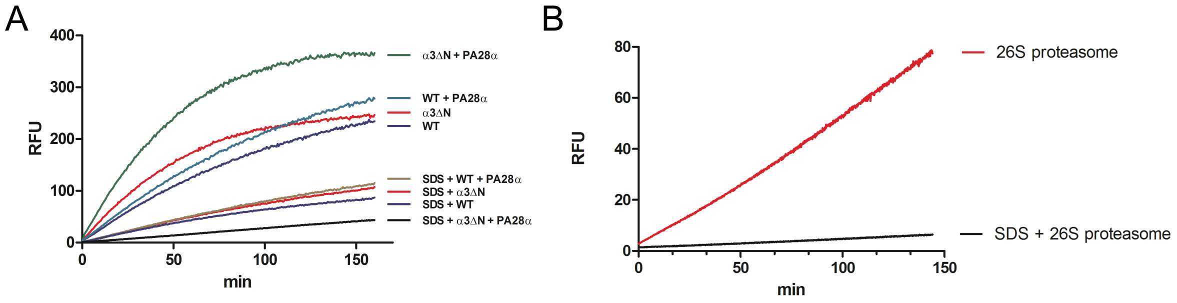

Figure 26: Time dependent comparison of Suc-LLVY-AMC digestion by the proteasomal β5 activity after preincubation with KM (200 µM). A: Addition of 0.01% SDS to the assay buffer significantly impairs substrate turnover, independent of employing wildtype (WT), open-gate α3ΔN yCPs or the addition of the proteasome activator PA28α. B: Substrate digestion of human 26S-activated proteasome is impaired in the presence of 0.01% SDS (black), whereas omission of detergent results in normal substrate hydrolysis (red). Figure adopted from Beck *et al.*[138]

To eliminate any artificial interference of KM or SDS with the chromogenic substrates that are used in the activity assays, an HPLC/MS-coupled digestion assay was conducted. Here, the peptide WNNFALY was employed to mimic a natural substrate for the CP that hydrolyses the natural substrate through a specific single cleavage by the β5 activity into the products WNNF ($[M+H]^+$ = 580.12 m/z) and ALY ($[M+H]^+$ = 365.97 m/z) (Figure 27A).[84] The peptide was synthesized on solid phase on a trityl-chloride resin *via* standard Fmoc-based coupling chemistry and purified *via* a C18 column. Yeast wildtype CP was treated with KM (200 µM) for 60 minutes before substrate addition (1 mM) and incubated at 37 °C for various timeframes. The reaction was stopped by ultrafiltration through a 100 kDa cut-off membrane and a standardized amount (40 µL) of the filtrate was injected for HPLC/MS analysis. In the presence of SDS, WNNFALY was hydrolyzed within 30 min, whereas omission of SDS leads to a reduced but steady rate of substrate cleavage by the CP (Figure 27B/C). Thus, turnover of oligopeptides by the proteasome is unaffected in the presence of KM, indicating that the natural product does not alter the substrate binding channel of the proteolytic activities of the CP.

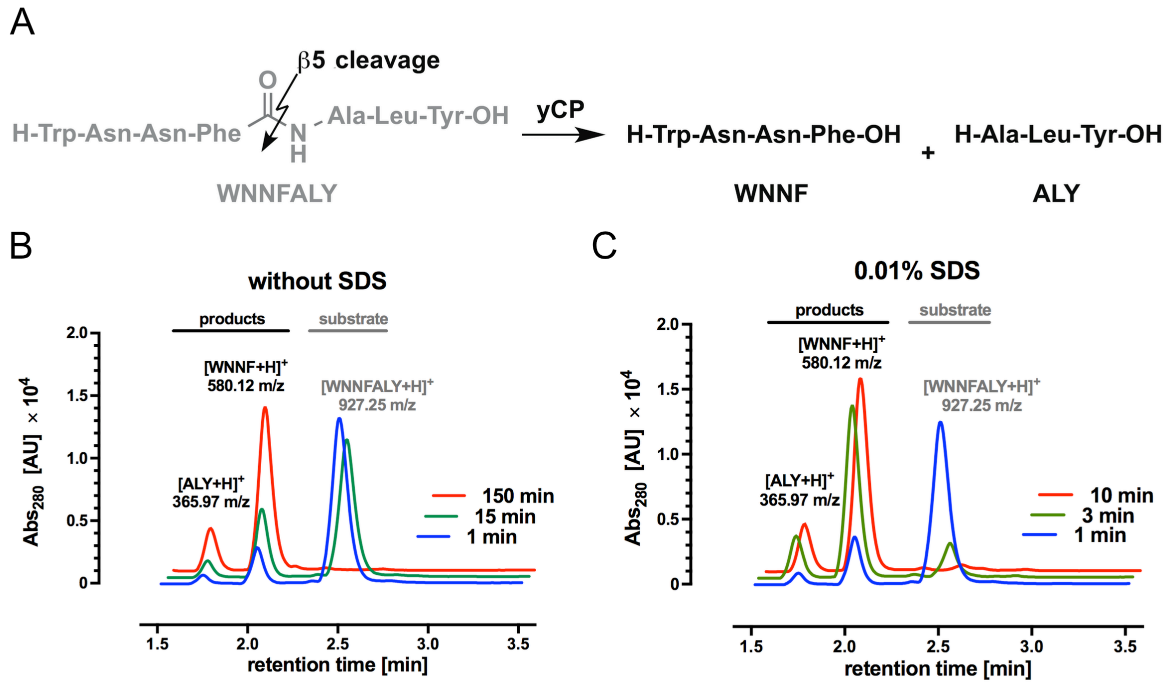

Figure 27: HPLC/MS peptide digestion assay. A: The substrate WNNFALY with the scissile peptide bond is depicted in gray and the hydrolysis products WNNF and ALY coloured in black. B: HPLC chromatograms of substrate digestions by yCP after preincubation with KM (200 µM) without or with 0.01% SDS (B/C, respectively). The undigested substrate peak (gray, 2.51 min, 927.25 m/z) and the hydrolysis product peaks of WNNF (black, 2.01 min, 580.12 m/z) and ALY (black, 1.43 min, 365.97 m/z), are shown, respectively. Omission of the detergent results in a reduced but steady rate of peptide cleavage (B), while addition of 0.01% SDS results in complete substrate hydrolysis within 10 min (C). Figure adopted from Beck *et al.*[138]

6.4.3 Crystal structure of KM bound to the yCP

For further investigation of KM's mode of action on the proteasome, the CP:KM complex structure was elucidated. yCP crystals were soaked with KM for 24 h at a final concentration of 5 mM and diffraction data were recorded to a maximum resolution of 2.6 Å (R_{free} = 22.4 %, PDB ID 4Q1S). As a surprise, inspection of the resulting electron density map revealed that the catalytic sites were free of any electron density derived from the natural product. Instead, an automated search of the F_O-F_C-difference electron density map unambiguously identified KM in a surface exposed pocket formed by the subunits β2 and β7' at the interface of the two β-β' rings (Figure 28).

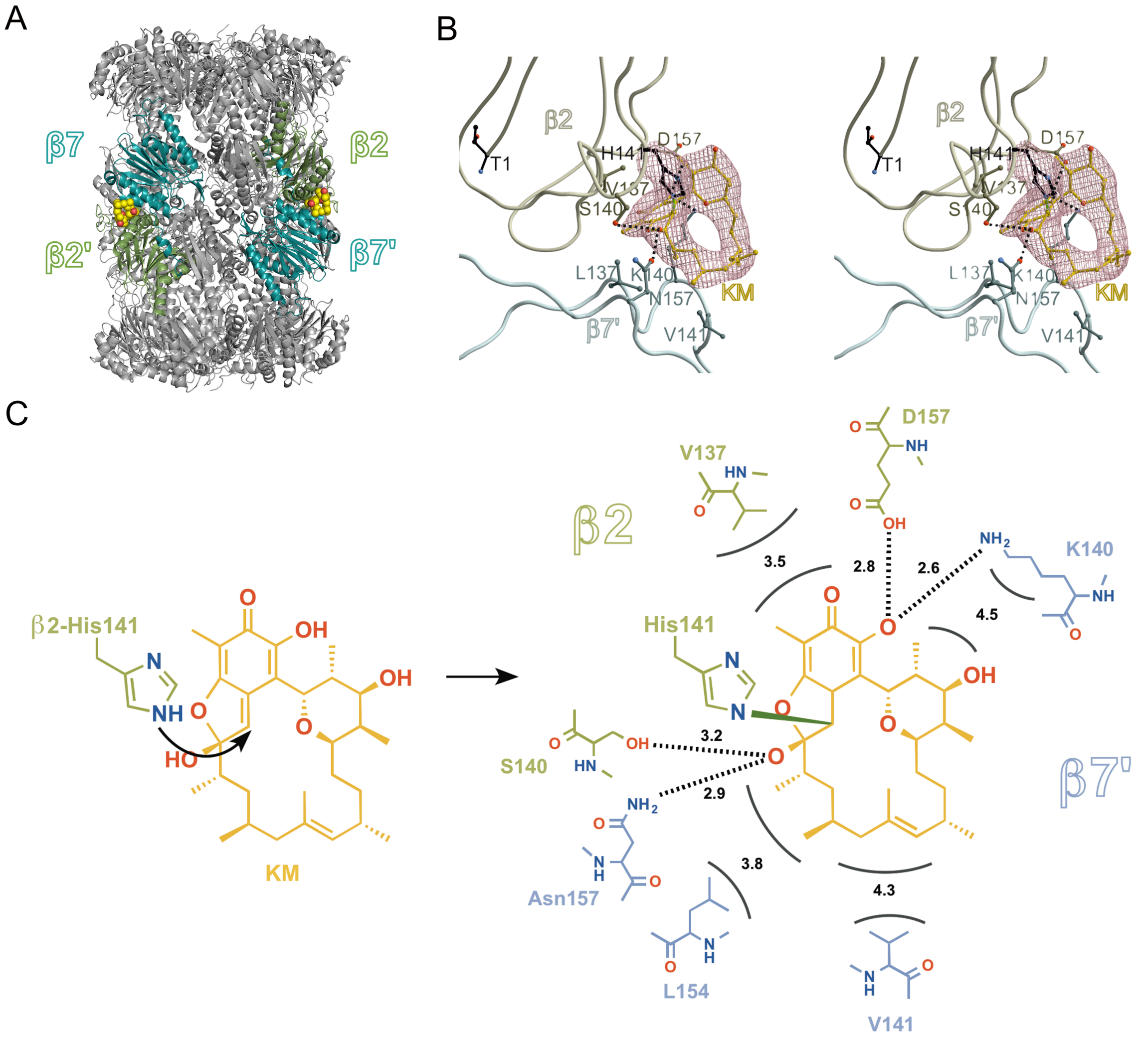
A
β7
β2
β2'
β7'
B
β2
T1
H141
D157
V137
S140
L137
K140
N157
KM
β7'
V141
C
β2-His141
N
NH
O
HO
O
OH
O
OH
KM
V137
HN
O
D157
NH
O
O
OH
β2
NH2
K140
NH
O
3.5
2.8
2.6
4.5
His141
N
N
O
O
OH
O
O
S140
OH
HN
3.2
O
NH2
2.9
O
N
H
O
Asn157
3.8
4.3
L154
V141
β7'

Figure 28: KM bound to the surface exposed pocket at the interface between subunits β2 and β7' of the yCP. A: Cartoon representation of the CP:KM crystal structure with KM (yellow) presented as a sphere model in the surface exposed binding site at the intersection of the β-β' rings. The β2 and β7 subunits are represented in green and teal, respectively. B: Stereo representation of the CP:KM crystal structure with the $2F_O{-}F_C$ omit electron density map (red mesh, 1σ) of KM (yellow) bound to β2-His141N$^\gamma$ at the interface of β2 (light green) and β7' (light blue). C: Scheme of the adduct formation mechanism. Binding of KM (yellow) to the yCP results in covalent bond formation of β2-H141N$^\gamma$ and the chinone methide pharmacophore of KM. The interaction distances are shown in Å. Amino acids of subunits β2 and β7' are depicted in green and blue, respectively. Figure adopted from Beck *et al.*[138]Figure adopted from Beck *et al.*[138]

The polyketide is covalently bound by its reactive quinone methide C20 via β2-His141N$^\gamma$ and further stabilized by hydrophilic and hydrophobic interactions by its quinone chromophore that deeply protrudes into a cavity (Figure 28A). The flexible ansa-chain is fully defined in the electron density map and does not adopt any alternative conformations. Likewise, the tetrahydropyran ring is fixed in a perpendicular position to the quinone. As shown by superposition of the apo and holo structures, binding of KM to the yCP does not induce major structural alterations; only β2-K157 and β2-L154 are slightly shifted upon ligand binding (Figure 29). Thus, the absence of major structural rearrangements does not hint at an allosteric modulation of the CP upon binding of KM.

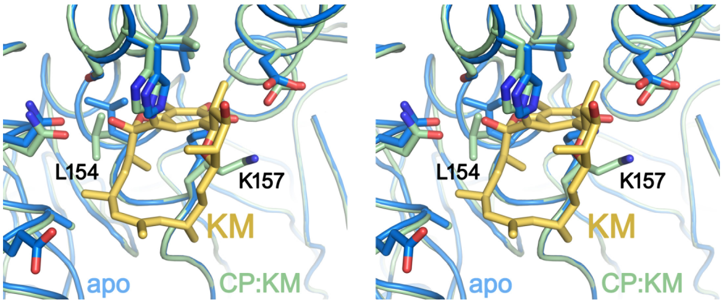

Figure 29: Superposition of apo- and holo yCP crystal structures. Binding of KM (yellow) to the CP (green) merely shifts β2-K157 and β2-L154 out of their original position compared to the apo structure (blue).

Since KM possesses a bulky molecular scaffold and might not fit through the wildtype yCP pore gate, the yeast α3ΔN open-gate yCP mutant was crystallized and soaked with KM. The resulting complex structure once more revealed that all active sites remained free of ligand-derived electron density, whereas KM again was bound at the exosite via β2-H141N$^{\gamma}$.

Structural superposition of yCP with murine cCP and iCP shows that the newly identified binding pocket at the intersection of subunits β2 and β7' is highly conserved in its architecture (Figure 30). Strikingly, in mammals β2-His141 is substituted by Lys141 in constitutive and Arg141 in immunoproteasomes, respectively.[38] In contrast, sequence alignment of the β2 subunit shows that the amino acids surrounding position 141 are strictly conserved. Consequently, the β2-H141R and β2-H141K yeast mutants were created that should mimic the cCP and iCP structures in regard to KM’s binding site.

```
          1        10        20        30        40        50        60
yβ2       TTIVGVKFNNGVVIAADTRSTQGPIVADKNCAKLHRISPKIWCAGAGTAADTEAVTQLIG
mβ2c      TTIAGVVYKDGIVLGADTRATEGMVVADKNCSKIHFISPNIYCCGAGTAADTDMTTQLIS
mβ2i      TTIAGLVFRDGVILGADTRATNDSVVADKSCEKIHFIAPKIYCCGAGVAADTEMTTRMAA
hβ2c      TTIAGVVYKDGIVLGADTRATEGMVVADKNCSKIHFISPNIYCCGAGTAADTDMTTQLIS
hβ2i      TTIAGLVFQDGVILGADTRATNDSVVADKSCEKIHFIAPKIYCCGAGVAADAEMTTRMVA
          ***.*: :.:*:::.****:*:  :****.* *:* *:*:*:*.***.***:: .*:: .

          61       70        80        90        100       110       120
yβ2       SNIELHSLYTSREPRVVSALQMLKQHLFKYQGHIGAYLIVAGVDPTGSHLFSIHAHGSTD
mβ2c      SNLELHSLTTGRLPRVVTANRMLKQMLFRYQGYIGAALVLGGVDVTGPHLYSIYPHGSTD
mβ2i      SKMELHALSTGREPRVATVTRILRQTLFRYQGHVGASLVVGGVDLNGPQLYEVHPHGSYS
hβ2c      SNLELHSLSTGRLPRVVTANRMLKQMLFRYQGYIGAALVLGGVDVTGPHLYSIYPHGSTD
hβ2i      SKMELHALSTGREPRVATVTRILRQTLFRYQGHVGASLIVGGVDLTGPQLYGVHPHGSYS
          *::***:* *.* ***.:. ::*:* **:*:*::** *::.***  * :*: :: *** .

                   130       140       150       160       170       180
yβ2       VGYYLSLGSGSLAAMAVLESHWKQDLTKEEAIKLASDAIQAGIWNDLGSGSNVDVCVMEI
mβ2c      KLPYVTMGSGSLAAMAVFEDKFRPDMEEEEAKKLVSEAIAAGIFNDLGSGSNIDLCVISK
mβ2i      RLPFTALGSGQGAAVALLEDRFQPNMTLEAAQELLVEAITAGILSDLGSGGNVDACVITA
hβ2c      KLPYVTMGSGSLAAMAVFEDKFRPDMEEEEAKNLVSEAIAAGIFNDLGSGSNIDLCVISK
hβ2i      RLPFTALGSGQDAALAVLEDRFQPNMTLEAAQGLLVEAVTAGILGDLGSGGNVDACVITK
             : ::***. **:*::*.:::: ::  * *  *  :*: ***  *****..:* **:

                   190       200       210       220        230
yβ2       GKDAEYLRNYLTPNVREEKQKSYKFPRGTTAVLKESIVNICD-IQEEQVDITA- 232
mβ2c      S-KLDFLRPFSVPNKKGTRLGRYRCEKGTTAVLTEKVTPLEIEVLEETVQTMDT 233
mβ2i      G-GAKLQRALSTPTEPVQRAGRYRFAPGTTPVLTREVRPLTLELLEETVQAMEV 233
hβ2c      N-KLDFLRPYTVPNKKGTRLGRYRCEKGTTAVLTEKITPLEIEVLEETVQTMDT 233
hβ2i      T-GAKLLRTLSSPTEPVKRSGRYHFVPGTTAVLTQTVKPLTLELVEETVQAMEV 233
              .  *    *.    :   *    *** **.. :  :   : ** *:
```

Figure 30: Sequence conservation of the β2 subunits in yeast, mouse and human. Sequence alignment of subunit β2 from yeast (yβ2), murine (mβ2c/mβ2i) and human (hβ2c/hβ2i) constitutive and immuno proteasomes. The strictly conserved amino acid exchanges in the immune subunit compared to the constitutive counterparts are marked in green. Figure adopted from Beck *et al.*[138]

The crystal structures of the corresponding KM-soaked β2-H141R and β2-H141K yeast mutants lacked any defined electron density for the ligand and a non-covalent binding mode in a β2-H141A mutant was not observed (Figure 31). However, KM exhibited comparable inhibition rates on all tested proteasome mutants but only in the presence of 0.01% SDS.

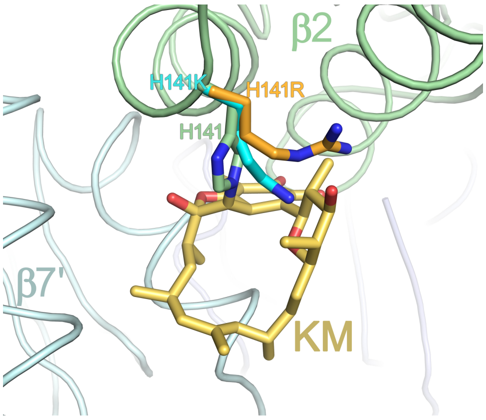

Figure 31: Comparison of the wildtypc yCP and mutant KM binding pockets. Structural superposition of the KM binding pockets of wildtype and mutant yeast proteasome crystal structures. The protein subunits β2/β7' are represented as coils (green and teal, respectively), whereas KM (yellow), β2-H141 (green), β2-H141R (orange) and β2-H141K (cyan) are shown as sticks. Note that KM causes a steric clash in the mutants with the elongated side chains of Arg and Lys in position 141. Figure adopted from Beck *et al.*[138]

6.4.4 *In vivo* effect of KM on HeLa and yeast cells

Since the crystallographic studies and *in vitro* assays with purified CP gave only ambiguous results regarding KM's mode of action, the natural product was subjected to in vivo assays with cultured yeast cells. First, inhibition of the β5 activity in permeabilized wildtype and β2-H141A mutant yeast cells upon treatment with KM was evaluated. Treatment with KM did not result in a significant decrease in Suc-LLVY-AMC substrate hydrolysis, whereas bortezomib blocked the β5 cleavage activity of both wildtype and mutant yeast cells (Figure 32).

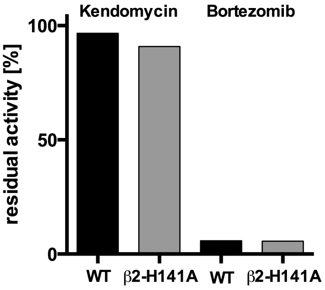

Figure 32: Inhibition of β5 activity in yeast by KM and bortezomib. Inhibition of proteasomal β5 activity of wildtype (WT) and β2-H141A mutant yeast cells by KM and Bortezomib at 50 μM final concentration standardized to DMSO control. Figure adopted from Beck *et al.*[138]

In contrast, KM potently affected yeast cell colony formation of both mutants (Figure 33). Various concentrations of KM were applied on a filter paper and placed on top of agar that was seeded with either wildtype or the β2-H141A mutant yeast. The activity was determined by measuring the magnitude of the zone of inhibition of cell colony formation around the filter paper disk (Figure 33). The growth inhibition caused by KM was significant and, most importantly, affected both wildtype and mutant cells, suggesting that the β2-H141-KM adduct is not responsible for growth inhibition in yeast.

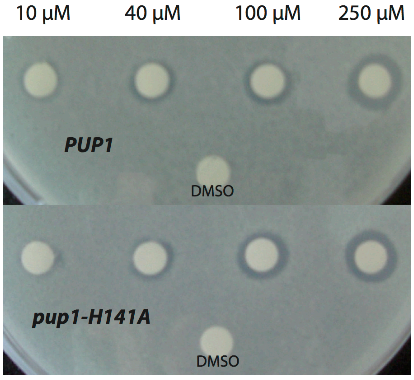

Figure 33: Inhibition of yeast growth in the presence of KM. Inhibition of cell colony formation in wildtype (PUP1, top) or β2-H141A (pup1-H141A, bottom) mutant yeast after treatment with various concentrations of KM compared with the negative control (DMSO). No significant difference in growth inhibition of wildtype or mutant yeast cultures is observed. Figure adopted from Beck *et al.*[138]

The effect of KM on HeLa cell viability was then evaluated in an MTT assay (Figure 34). After two days of incubation, KM inhibits the cell viability of human cervical cancer cells with an EC_{50} of 0.94 µM. This result is comparable to KM's EC_{50} on leukemic monocyte lymphoma (U-937) cells that were reported in earlier studies by Elnakady et al.[115]

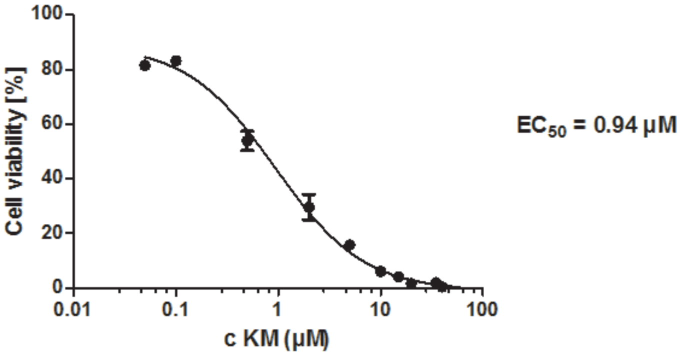

Figure 34: Effect of KM on HeLa cell viability as measured by MTT. KM inhibits the cell viability of human cervical cancer cells with an EC_{50} of 0.94 µM.

To investigate whether the observed EC_{50} results from CP inhibition, the in-situ activity of the protease was evaluated with the Proteasome-Glo^{TM} assay (Promega). Hereby, CP impairment can be observed in situ with luminogenic peptide substrates in a buffer optimized for cell permeabilization, CP activity and luciferase activity. This allows for a more sophisticated, direct control of the proteasomal activity to avoid misinterpretation of polypharmacological effects of putative inhibitors. Intact HeLa cells were incubated with various concentrations of KM for 105 min and IC_{50} of 6.4 µM for the β5 activity was recorded (Figure 35). Simultaneously, a cell viability assay (CellTiter-Glo, Promega) revealed that the viability curve (EC_{50} = 5.4 µM) superimposes well with the IC_{50} curve (Figure 35). Comparison with the FDA-approved CP inhibitor carfilzomib in an analogous experiment reveals that strong inhibition of the proteasomal β5 activity (IC_{50} of 0.019 µM) does not induce cell death within the assay timeframe of 105 min. Hence, the detected proteasomal IC_{50} of KM *in vivo* is not mediated by CP impairment, but rather a consequence of a rapid overall cytotoxic effect of KM.

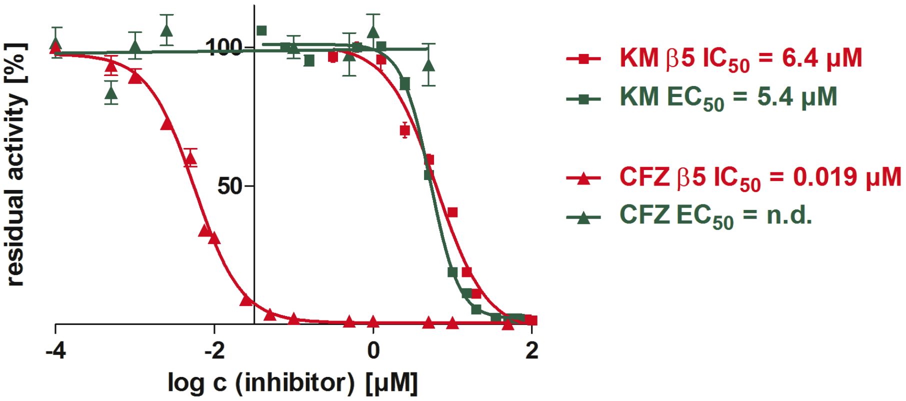

Figure 35: HeLa cell viability and in situ proteasome activity upon KM treatment. Comparison of proteasomal β5 inhibition (red) in intact HeLa cells and cell viability (green) upon treatment with KM (squares) or carfilzomib (triangles) evaluated by Proteasome-Glo and CellTiter-Glo assays, respectively. The superposition of the EC_{50} (green) and IC_{50} (red) curves indicates that the IC_{50} value for KM is a result of cell death rather than specific proteasome inhibition. n.d. = not determined. Figure adopted from Beck *et al.*[138]

6.5 Screening hit III: Phakellin Derivative (PD)

6.5.1 Origin and discovery of phakellins and phakellstatins as CP inhibitors

Phakellins and phakellstatins belong to a highly diverse family of biologically active pyrrole-imidazole marine alkaloids that share a tetracyclic framework with a uniquely bent topology (Figure 36A). The most well-known member of this class of compounds is palau'amine, a cytotoxic and immunosuppressive hexacyclic bisguanidine that was isolated from the sea sponge *stylotella agminata* (Figure 36B).[140] Cytotoxicity tests with dibromophakellstatin against a panel of human cancer cell lines demonstrated the potential application for the treatment of cancer.[141] However, only recently the cellular target was identified in a study that revealed palau'amine as well as dibromophakellin and dibromophakellstatin as inhibitors of the ChTL activity of purified human 20S proteasome.[116] In addition, palau'amine was found to bind irreversibly to the CP and cause accumulation of ubiquitinated proteins in cell culture at low micromolar concentrations.[116]

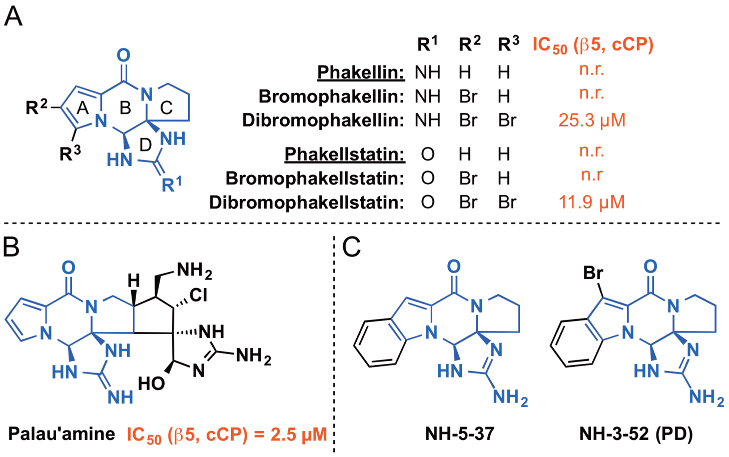
A
R1 R2 R3 IC50 (β5, cCP)
Phakellin: NH H H n.r.
Bromophakellin: NH Br H n.r.
Dibromophakellin: NH Br Br 25.3 μM
Phakellstatin: O H H n.r.
Bromophakellstatin: O Br H n.r
Dibromophakellstatin: O Br Br 11.9 μM
B
Palau'amine IC50 (β5, cCP) = 2.5 μM
C
NH-5-37
NH-3-52 (PD)

Figure 36: Structures of phakellin, phakellistatin and palau'amine. A: Phakellins and phakellstatins are differentiated by the amino- or oxo-substitution of the imidazole ring. The bent pyrrole-imidazole core structure with the ABCD tetracycle is colored in blue. B: Palau'amine exhibits the same pyrrole-imidazole scaffold as phakellin (blue), whereas it's C-ring is substituted with two additional five-membered rings. C: Indole analogues of dibromophakellin that comprise an additional benzene core fused to ring A.

The cytotoxic properties of this compound family inspired the group of Jetze Tepe (Wayne State University, Michigan) to synthesize indole analogues of dibromophakellin (Figure 36C). The compounds showed comparable inhibitory potency to palau'amine and were thus included in the screening library.

6.5.2 Crystal structure of PD bound to the yCP

In total, five members of the pyrrole-imidazole family of compounds were investigated in the crystallographic screening (Figure 14C). yCP crystals were soaked with the respective compounds and diffraction data were recorded to a maximum resolution of 2.5 Å (R_{free} = 21.6 %). As a surprise, inspection of the resulting F_O-F_C-electron density map revealed that the brominated indole phakellin derivative NH-5-37 (PD, Figure 36C) forms a unique complex structure with the yCP. PD is well defined in the S3 pocket of the ChTL active site and revealed a novel, non-covalent binding mode (Figure 37).

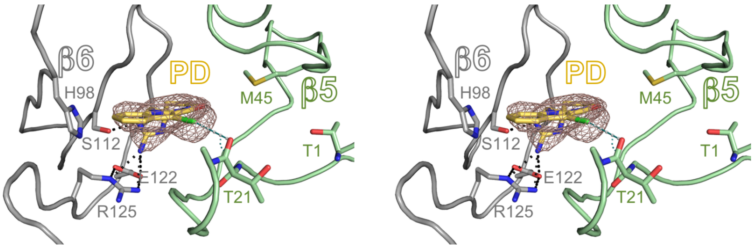

Figure 37: Crystal structure of the yCP in complex with PD. Stereo representation of the yCP:PD crystal structure with the $2F_O{-}F_C$ omit electron density map (red mesh, 1σ) of PD (yellow) bound to the *sub*-S3 specificity pocket of the β5 substrate binding channel (green). The 2-aminoimidazoline group forms a network of hydrogen bonds (black dashed lines) with the side chains of S124, R137 and E134 of the β6 subunit (gray). β6-H98 and β5-V31 display van-der-Waals interactions with PD, whereas the carbonyl oxygen of β5-T21 is perfectly oriented to stabilize the ligand *via* a halogen bond formation (teal) with the bromine substituent of PD (lime).

PD does not interact with the Thr1O^{γ} active site nucleophile of the β5 subunit. Furthermore, the ligand solely resides in the spacious S3 binding pocket and perfectly fits the size and polarity of the cavity. The characteristic 2-aminoimidazole moiety protrudes deeply into the sub-S3 pocket and is stabilized by tight hydrophilic interactions with S112, E122 and R125 of subunit β6 (Figure 38B). The overall rigid scaffold of phakellins and phakellstatins lacks any rotable bonds and thus adopts no alternative conformation, resulting in a minimal entropic penalty upon binding. In addition, the planar tetracyclic system of PD is stabilized by van-der-Waals interactions with the side chains of β6-H98 and β5-V31, both flanking the ligand at the indole- and C-ring, respectively.

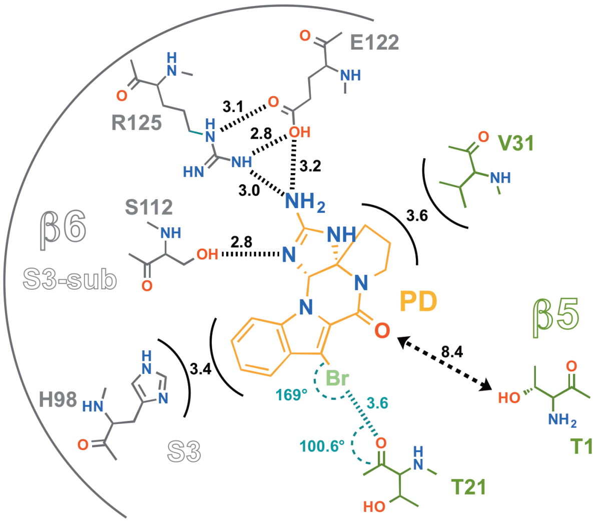

Figure 38: Schematic overview of PD binding. The interaction distances are shown in Å. The specificity pocket *sub*-S3 of the ChTL substrate binding channel and their corresponding amino acids are depicted in gray. Residues of the β5 subunit that are in close contact with PD are colored in green. The halogen bond between β5-T21CO and PD-Br (lime) is illustrated in teal. The distance between the ligand and the catalytically active β5-T1 is highlighted with a double headed arrow (black).

Interestingly, PD breaks with a hitherto accepted dogma of common CP inhibitors that are all substantially stabilized by the formation of an antiparallel β sheet with the substrate binding channel and interaction with the S1 specificity pocket. Superposition of PD with the FDA-approved bortezomib (BTZ) exemplifies the unique binding mode of PD in comparison with peptidic proteasome inhibitors (Figure 39A-C). BTZ only marginally protrudes into the S3 pocket and thereby does not take full advantage of the spacious cavity, although previous studies with non-covalent inhibitors underlined its importance for the stabilization of ligands in the active site.[83,132,142] For example, structural superposition of the non-covalent reversible CP inhibitor HU10 with PD reveals that the bulky adamantyl moiety of HU10 closely matches the position of PD's 2-aminoimidazole ring (Figure 39D/E). Importantly, removal of the adamantyloxy group from HU10 results in complete loss of potency and thus highlights the importance of the P3 site for inhibitor stabilization.

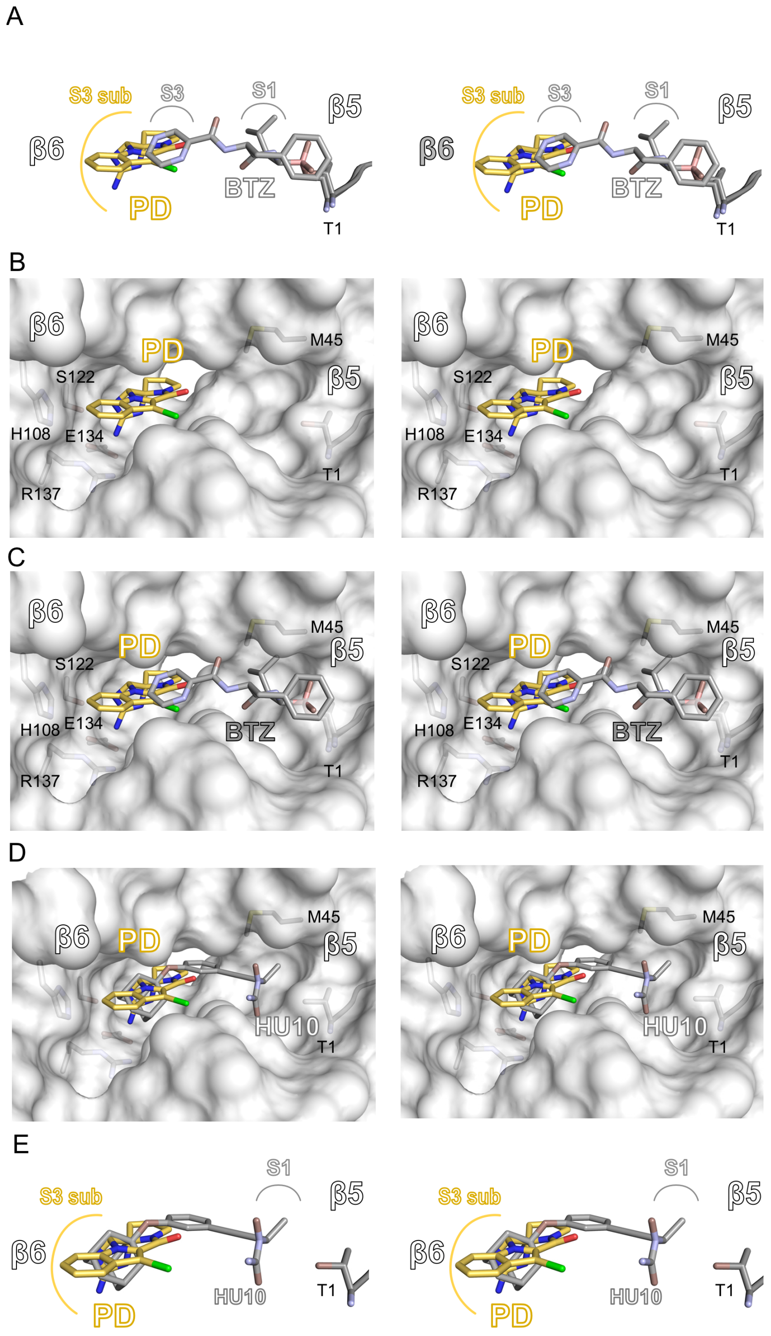
A
S3 sub
S3
S1
β5
β6
PD
BTZ
T1
B
β6
PD
M45
β5
S122
H108
E134
T1
R137
C
β6
M45
PD
β5
S122
H108
E134
BTZ
T1
R137
D
M45
β6
PD
β5
HU10
T1
E
S1
S3 sub
β5
β6
HU10
T1
PD

Figure 39: Binding mode of PD in comparison with BTZ and HU10. A: Superposition of PD (yellow) and bortezomib (BTZ, gray) bound to the ChTL active site, illustrating the location of the specificity pockets in the β5 substrate binding channel. The binding mode of PD significantly differs from that of peptide ligands and all previously analysed ligands. B/C: Surface representation of the ChTL substrate binding channel (white surface) with and without BTZ (B and C, respectively). β5-M45 forms the bottom of the S1 specificity pocket. The PD binding site in the sub-S3 cavity is formed by H108, S124, E134 and R137 of β6 (gray). D/E: Superposition of PD with HU10, highlighting the influence of the sub-S3 pocket for stabilization. The adamantyloxy moiety of HU10 fits perfectly into the cavity,[132] whereas the 2-aminoimidazole residue of PD preferentially matches the highly polar nature of the pocket. Notably, HU10 is tightly coordinated near T1 *via* its *N*-hydroxyurea residue, while PD is only stabilized in the sub-S3 pocket.

6.5.3 Influence of the halogen bond for ligand stabilization

Most remarkably, the inhibitor's imidazole ring is perfectly orientated for the formation of a halogen bond between the bromine atom of PD and the carbonyl oxygen of β5-Thr21. With a Br···O distance of 3.6 Å and an approximately colinear alignment of the acceptor/donor atoms (C—O···X angle = 169°), the observed metrics of the PD-Thr21CO interaction closely fulfill the requirements for ideal halogen bonding.[143–145] Thus, the donor atom is able to orient its electron density into the σ-hole, which resembles the s*-orbital of the C—Br bond (Figure 40).

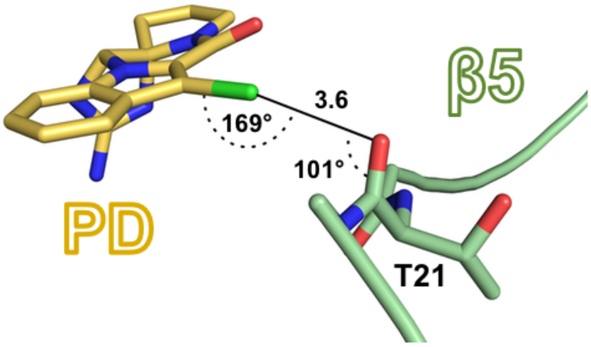

Figure 40: Halogen bonding of PD with β5-T21CO. PD (yellow) is perfectly oriented to form a Br···O=C interaction with T21 of subunit β5 (green); the bromine atom is colored in lime. Distances are given in Å.

The influence of the halogen bond for the stabilization in the cavity was evaluated by comparison with the debrominated PD analogue NH-5-52 (debromo-PD). Inspection of the electron density map of yCP crystals that were soaked with NH-5-52 (Figure 36C) revealed that the ligand is only marginally defined although its scaffold is highly similar to PD. In accordance with the structural observations, the inhibitory potency debromo-PD against purified human cCP (IC_{50} = 25 ± 2.5 µM) is decreased by one order of magnitude in comparison to PD (IC_{50} = 3.5 ± 0.7 µM). Thus, the halogen bond of PD with the protein backbone is a major motif for PD's stabilization in the sub-S3 pocket.

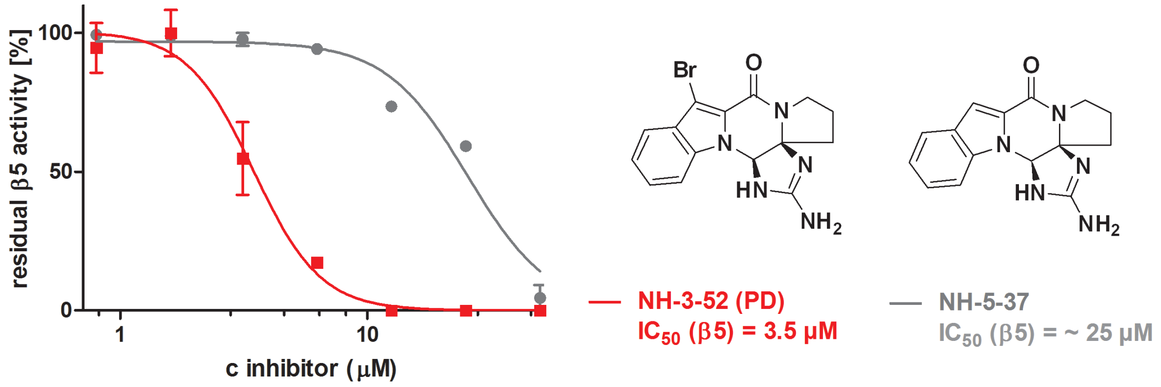

Figure 41: Inhibitory potency of PD and NH-5-37 for the β5 activity of human cCP. The binding affinity of PD largely relies on formation of the halogen bond with the protein backbone. NH-5-37 is lacking the bromine-substituent on the imidazole ring and thus displays a decreased affinity to purified human cCP.

Since the molecular scaffold of PDs are inspired by naturally occurring molecules like dibromophakellin, dibromophakellstatins and palau'amine, these were expected to exhibit a binding mode similar to PD. Conversely, evaluation of yCP crystals that were soaked with the natural products did not result in complex structures. This finding is especially surprising in the case of palau'amine that was reported as an irreversible inhibitor of human cCP. However, the crystallographic observations are in line with the observed lack of inhibitory potency against purified yCP.

7 Discussion

The herein presented crystallographic screening of inhibitors against the CP emphasizes the importance of biostructural approaches in the hit discovery process. Commonly used biochemical HTS methods are lacking sensitivity, produce false-positive results and give no information about the binding mode of ligands. Although the herein applied methodology provides valuable information to the medicinal chemist, development of lead compounds from crystallographic screening hits and translation of the *in vitro* activity into living systems still represents the major obstacle in the early stages of drug discovery.

7.1 Discovery of three CP ligands with novel binding modes

Previous crystallographic studies predominantly focused on the evaluation of peptidic CP inhibitors that exhibit a conventional binding mode by formation of an antiparallel β sheet in the substrate binding channel of the distinct active sites.

The present thesis led to the discovery of CP ligands with so far unobserved modes of actions by performing a crystallographic screening of a focused compound library. In addition, an orthogonal set of assays for hit validation was developed in the course of this thesis as exemplified on the natural product kendomycin. The biostructural approach to CP ligand discovery is less prone to artifacts caused by compound aggregation, fluorescence quenching, autofluorescence or complicated assay setups which are responsible for the plentitude of false-positive reports of CP inhibitors from studies that solely used biochemical assays. In comparison with common biophysical techniques like surface plasmon resonance, isothermal titration calorimetry or NMR, crystallographic screenings are able to detect a broader spectrum of inhibitors since the method is not hampered by low sensitivity, particle size, or inability to detect reversible ligands. However, due to the limited availability of CP crystals, the size of the screening library is limited. Thus, careful pre-selection of the screening candidates is mandatory to constrain the library to promising compounds with validated effect on the UPS.

From the initial 27-membered library, three compounds resulted in complex structures with the CP. Cross-validation with biochemical assays revealed that two of the three compounds actively impair proteasomal substrate degradation, representing an overall hit rate of 7.4%.

Sulfonamide

To date, most CP inhibitors target the unprimed substrate binding channels of the catalytically active sites and thus exploit the S1-S4 specificity pockets to achieve CP subtype selectivity. However, the unprimed substrate binding channel is only subtly altered between iCP and cCP, resulting in a lack of specific inhibitors in particular for the CL activity. Although the primed sites of the catalytic centers display remarkable differences, inhibitors could so far not exploit these alterations due to a lack of structural data.

The presented yCP:SA complex structure shows for the first time a ligand solely bound to the primed site of the substrate binding channel. Moreover, SA selectively targets the CL and TL activities and binds into a pocket that exhibits significant alterations between iCP and cCP. In combination with the facile two-step chemical synthesis of SA, the ligand provides a possibility to selectively impair the β2c or β2i activity of the CP and thus represents a promising candidate for lead development.

A variety of SA fragments as well as derivatives were synthesized and subjected to crystallographic studies followed by *in vitro* activity tests against the CP. Crystal soaking experiments with the SA fragments confirmed that only the complete SA ligand is able to bind to the CP. Additionally, the fragments showed no activity against the CP *in vitro* and thus, it is the entire SA molecule that acts as a promising candidate for further hit development.

Kendomycin

The bacterial secondary metabolite KM was shown to uniquely bind to an exosite of CP in a surface exposed pocket. However, hit validation with orthogonal *in vitro* and *in vivo* assays revealed that binding of KM to the CP is not responsible for the cytotoxic effect of KM on cancer cells. Nevertheless, the set of assays for hit validation that was developed during the investigation of KM is now applied as a helpful tool to determine false positive and -negative proteasome inhibitors.

Phakellin Derivative

The pentacyclic PD exhibits a complex scaffold and shares its overall structural motif with the natural product palau'amine. Although the latter has been reported as an irreversible proteasome inhibitor, soaking of yCP crystals did not result in defined electron density for the ligand. Owing to the complexity of this compound class, only a limited number of derivatives were tested in the crystallographic screening. Thus, a more facile synthesis has to be developed for the rapid generation of related compounds. Structural superposition of PD with the more potent, reversible HU10 ligand revealed that the 2-aminoimidazole moiety aligns with the position of the adamantyloxy residue. However, ligand merging approaches by attachment of the 2-aminoimidazole moiety to the hydrodroxyurea scaffold are hampered by the instability of this compound class, showing that fragment evolution of screening hits with natural origin faces demanding challenges regarding chemical synthesis. However, the CP:PD crystal structure provides valuable information for rational design of new CP inhibitors, since it has been shown for the first time that exploiting the size and polarity of the proteasomal S3 specificity pocket is sufficient to cause selective proteasomal blockage. In addition, PD comprises a non-peptidic scaffold and is thus not expected to show any cross-reactivity with other proteases like common proteasome inhibitors.

7.2 Guidelines for the rational design of CP inhibitors

Various autoimmune disorders as well as the development of resistances by cancers against CP inhibitors are associated with modified levels of iCP or expression of proteasomal subunits with mutationally altered substrate binding channels. Thus, iCP-/cCP-selective compounds and inhibitors that are able to overcome resistances against common CP blockers are promising candidates to avoid serious pitfalls in the clinical application of proteasome inhibitors.

Previous crystallographic studies focused on structural analysis of holo- or apo CP crystal structures and their interaction with peptide based inhibitors. However, it was shown that the differences between iCP and cCP structures in the unprimed site of the substrate binding channels and the corresponding specificity pockets are only subtle. Consequently, development of specific inhibitors requires extensive fine-tuning and mutations of single amino acids of the proteasomal substrate binding channels, rapidly causing resistance phenomena against the highly optimized drugs. The herein presented cocrystal structures of the yCP in complex with SA and PD provide structural information for the rational design of CP inhibitors with completely new binding modes. Thereby, the ligands serve as starting points for the design of novel drugs that can overcome the drawbacks associated with conventional CP inhibitors.

7.2.1 SA: CP subtype specificty and dual targeting of β1 and β2

The SA ligand was shown to entirely bind in the primed region of the β2 subunit. Furthermore, the quinoline ring system protrudes deeply into the S1’ pocket that significantly differs in size and polarity between the immune and constitutive CP. Variation of the fused ring system to smaller residues might result in CP subtype selectivity that is not affected by the commonly observed mutations in the unprimed substrate binding channel (Figure 42).

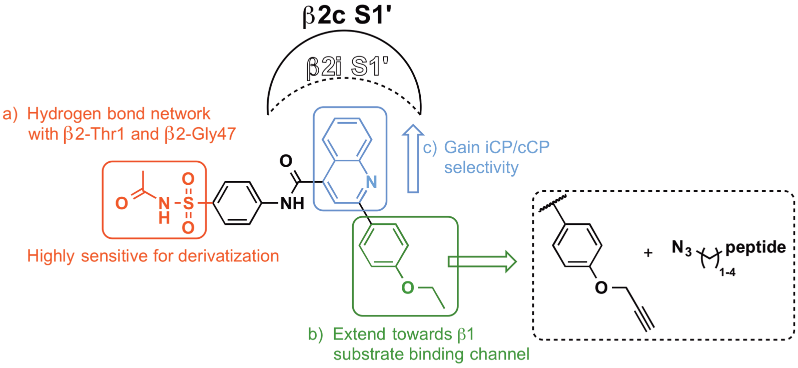
β2c S1'
β2i S1'
a) Hydrogen bond network with β2-Thr1 and β2-Gly47
Highly sensitive for derivatization
c) Gain iCP/cCP selectivity
b) Extend towards β1 substrate binding channel
O
N
H
S
NH
+
N3
peptide
1-4

Figure 42: Design directions for the development of inhibitors based on SA. The molecular scaffold of SA provides different directions for hit evolution strategies. a) Variation of the *N*-acetylsulfamoyl disturbs the tight hydrogen bond network with the catalytic β2Thr1N and β2-Gly47N, which serves as the oxyanion hole during peptide bond cleavage. b) Ligand potency can be increased *via* exploitation of the β1 substrate binding channel by extension of the ethoxyphenyl residue by means of click chemistry. c) Variation of the quinoline ring system to target the β2-S1' pocket, which significantly differs in iCP and cCPs (dashed/solid line, respectively).

However, fine-tuning of the ligand's iCP/cCP specificity demands an increased level of potency (sub-micromolar) for better interpretation of the influence of subtle changes to the quinoline ring system. In this regard, the molecular scaffold of SA provides two possible routes by a) anchoring the ligand to the catalytic β2-Thr1 through extension of the sulfacetamide moiety and b) growing of the biaryl system into the β1 substrate binding channel (Figure 42). The former route was attempted within this thesis, but changes to the *N*-acetylsulfamolyl moiety were shown to be detrimental to ligand binding. In contrast, the proposed route b) requires only minimal changes to the ligand at the phenylethoxy moiety that is not in close contact with the protein and thus less likely to disturb ligand binding. Addition of azidopeptides to the alkyne-derivatized SA ligand *via* huisgen 1,3-dipolar cycloadditions might enhance the binding affinity through stabilization in the β1 substrate binding channel (Figure 42).

7.2.2 PD: a scaffold for β5-selective inhibitors

The CP:PD cocrystal structure revealed that the ligand entirely and exclusively binds to the *sub*-S3 pocket formed by the β5 and β6 subunits. With its five fused rings, PD comprises a rigid overall scaffold and thus minimizes the entropic penalty upon binding to the *sub*-S3 pocket. Strikingly, comparison of a debromo-PD derivative ($IC_{50} = 25 \pm 2.5\ \mu M$) with the PD hit molecule ($IC_{50} = 3.5 \pm 0.7\ \mu M$) confirmed that the ligand's potency mainly relies on the formation of a C=O···Br halogen bond to β5-Thr21. Thus, a ligand merging approach that combines the unique binding mode of the HU inhibitors with just the 2-aminoimidazole moiety of PD is likely to fail, even though the polar five-membered ring perfectly fits the *sub*-S3 pocket.

However, the synthesis of PD requires just 5 steps starting from commercially available compounds, derivatization of the ligand is challenging since the sensitive scaffold is formed in the first steps of the synthesis. Nevertheless, substitution of the indole core structural motif at position 5 provides a possibility for the synthesis of more potent derivatives.

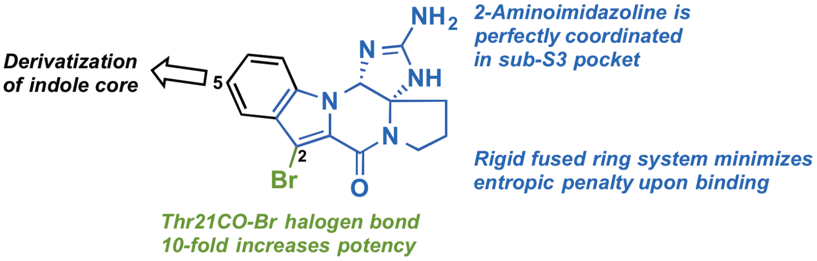
Derivatization of indole core
5
2
Br
O
N
N
N
NH
NH2
2-Aminoimidazoline is perfectly coordinated in sub-S3 pocket
Rigid fused ring system minimizes entropic penalty upon binding
Thr21CO-Br halogen bond 10-fold increases potency

Figure 43: Structural features of PD and their impact on ligand binding. The rigid molecular scaffold of PD has no rotatable bonds and consists of five fused rings. The 2-aminoimidazoline moiety is well coordinated of the residues that form the *sub*-S3 pocket. Attachment of bromine (green) at position 2 of the indole core results in a 10-fold increase in potency, whereas substitution at position 5 provides a possibility for easy derivatization of the ligand.

The simple molecular scaffold of PD is related to the complex natural product palau'amine. Structural superposition of the PD ligand with a model of palau'amine showed that both molecules share an identical overall topology that would allow palau'amine to fit into the *sub*-S3 pocket. However, soaking of CP crystals with the natural product did not result in defined electron density of the latter, thus, it is the overall architecture of the ligand which dictates the docking and binding mode to its target.

The herein described screening hits significantly contribute to the structural knowledge for future development of advanced CP inhibitors. In particular, the SA and PD ligands expand the druggable space that can be targeted by proteasome inhibitors and thus can be exploited as starting points for the structure-based design of novel drugs with potential application for the treatment of various CP-related diseases as well as tool compounds for biochemical research.

8 Bibliography

1. Voorhees, P.M., Dees, E.C., O'Neil, B. & Orlowski, R.Z. (2003). The proteasome as a target for cancer therapy. *Clin. Cancer Res.* **9**, 6316–25
2. Driscoll, J., Brown, M. & Finley, D. (1993). MHC-linked LMP gene products specifically alter peptidase activities of the proteasome. *Nature* **365**, 262–264
3. Finley, D. (2009). Recognition and processing of ubiquitin-protein conjugates by the proteasome. *Annu. Rev. Biochem.* **78**, 477–513
4. Etlinger, J. & Goldberg, A. (1977). A soluble ATP-dependent proteolytic system responsible for the degradation of abnormal proteins in reticulocytes. *Proc. Natl. Acad. Sci. U. S. A.* **74**, 54–8
5. Hershko, A. & Ciechanover, A. (1998). The ubiquitin system. *Annu. Rev. Biochem.* **67**, 425–79
6. Hershko, a & Ciechanover, a (1992). The ubiquitin system for protein degradation. *Annu. Rev. Biochem.* **61**, 761–807
7. Hochstrasser, M. (2006). Lingering mysteries of ubiquitin-chain assembly. *Cell* **124**, 27–34
8. Kerscher, O., Felberbaum, R. & Hochstrasser, M. (2006). Modification of proteins by ubiquitin and ubiquitin-like proteins. *Annu. Rev. Cell Dev. Biol.* **22**, 159–80
9. Hamilton, K., Ellison, M., Barber, K., Williams, R., Huzil, J., McKenna, S., Ptak, C., Glover, M. & Shaw, G. (2001). Structure of a Conjugating Enzyme-Ubiquitin Thiolester Intermediate Reveals a Novel Role for the Ubiquitin Tail. *Structure* **9**, 897–904
10. Kamadurai, H.B., Souphron, J., Scott, D.C., Duda, D.M., Miller, D.J., Stringer, D., Piper, R.C. & Schulman, B.A. (2009). Insights into ubiquitin transfer cascades from a structure of a UbcH5B approximately ubiquitin-HECT(NEDD4L) complex. *Mol. Cell* **36**, 1095–102
11. Hershko, A., Ciechanover, A., Heller, H., Haas, A.L. & Rose, I.A. (1980). Proposed role of ATP in protein breakdown : Conjugation of proteins with multiple chains of the polypeptide of ATP-dependent proteolysis. *Proc. Natl. Acad. Sci. U.S.A.* **77**, 1783–1786
12. Thrower, J.S., Hoffman, L., Rechsteiner, M. & Pickart, C.M. (2000). Recognition of the polyubiquitin proteolytic signal. *EMBO J.* **19**, 94–102
13. Komander, D. (2009). The emerging complexity of protein ubiquitination. *Biochem. Soc. Trans.* **37**, 937–53
14. Pickart, C.M. (2001). Mechanisms underlying ubiquitination. *Annu. Rev. Biochem.* **70**, 503–33
15. Voges, D., Zwickl, P. & Baumeister, W. (1999). The 26S proteasome: a molecular machine designed for controlled proteolysis. *Annu. Rev. Biochem.* **68**, 1015–68
16. Glickman, M.H., Rubin, D.M., Coux, O., Wefes, I., Pfeifer, G., Cjeka, Z., Baumeister, W., Fried, V. a & Finley, D. (1998). A subcomplex of the proteasome regulatory particle required for ubiquitin-conjugate degradation and related to the COP9-signalosome and eIF3. *Cell* **94**, 615–23
17. Bochtler, M., Ditzel, L., Groll, M., Hartmann, C. & Huber, R. (1999). The proteasome. *Annu. Rev. Biophys. Biomol. Struct.* **28**, 295–317
18. Groll, M., Ditzel, L., Lowe, J., Stock, D., Bochtler, M., Bartunik, H.D. & Huber, R. (1997). Structure of 20S Proteasome from yeast at 2.4 Å resolution. *Nature* **386**, 463–471

19. Brannigan, J.A., Dodson, H.J., Moody, P.C.E., Smith, J.L., Tomchick, D.R. & Murzin, A.G. (1995). A protein catalytic framework with an N-terminal nucleophile is capable of self-activation. *Nature* **378**, 416–419
20. Seemuller, E., Lupas, A., Stock, D., Lowe, J., Huber, R. & Baumeister, W. (1995). Proteasome from Thermoplasma acidophilum: a threonine protease. *Science (80-.).* **268**, 579–582
21. Nussbaum, A.K., Dick, T.P., Keilholz, W., Schirle, M., Stevanović, S., Dietz, K., Heinemeyer, W., Groll, M., Wolf, D.H., Huber, R., Rammensee, H.G. & Schild, H. (1998). Cleavage motifs of the yeast 20S proteasome beta subunits deduced from digests of enolase 1. *Proc. Natl. Acad. Sci. U.S.A.* **95**, 12504–12509
22. Goldberg, A.L. & Rock, K.L. (1992). Proteolysis, proteasomes and antigen presentation. *Nature* **357**, 375–9
23. Borissenko, L. & Groll, M. (2007). Diversity of proteasomal missions: fine tuning of the immune response. *Biol. Chem.* **388**, 947–955
24. Beck, P., Dubiella, C. & Groll, M. (2012). Covalent and non-covalent reversible proteasome inhibition. *Biol. Chem.* **393**, 1101–1120
25. Orlowski, M., Cardozo, C. & Michaud, C. (1993). Evidence for the presence of five distinct proteolytic components in the pituitary multicatalytic proteinase complex. Properties of two components cleaving bonds on the carboxyl side of branched chain and small neutral amino acids. *Biochemistry* **32**, 1563–1572
26. Nazif, T. & Bogyo, M. (2001). Global analysis of proteasomal substrate specificity using positional-scanning libraries of covalent inhibitors. *Proc. Natl. Acad. Sci. U.S.A.* **98**, 2967–72
27. Groll, M., Nazif, T., Huber, R. & Bogyo, M. (2002). Probing structural determinants distal to the site of hydrolysis that control substrate specificity of the 20S proteasome. *Chem. Biol.* **9**, 655–662
28. Groll, M., Larionov, O. V, Huber, R. & de Meijere, A. (2006). Inhibitor-binding mode of homobelactosin C to proteasomes: new insights into class I MHC ligand generation. *Proc. Natl. Acad. Sci. U.S.A.* **103**, 4576–4579
29. Bürgi, H., Dunitz, J. & Shefter, E. (1973). Geometrical reaction coordinates. II. Nucleophilic addition to a carbonyl group. *J. Am. Chem. Soc.* **587**, 5065–5067
30. Groll, M., Huber, R. & Potts, B.C.M. (2006). Crystal structures of Salinosporamide A (NPI-0052) and B (NPI-0047) in complex with the 20S proteasome reveal important consequences of beta-lactone ring opening and a mechanism for irreversible binding. *J. Am. Chem. Soc.* **128**, 5136–41
31. Murata, S., Sasaki, K., Kishimoto, T., Niwa, S.-I., Hayashi, H., Takahama, Y. & Tanaka, K. (2007). Regulation of CD8+ T cell development by thymus-specific proteasomes. *Science (80-.).* **316**, 1349–53
32. Aki, M., Shimbara, N., Takashina, M., Akiyama, K., Kagawa, S., Tamura, T., Tanahashi, N., Yoshimura, T., Tanaka, K. & Ichihara, A. (1994). Interferon-γ Induces Different Subunit Organizations and Functional Diversity of Proteasomes. *J. Biochem.* **115** , 257–269
33. Rock, K.L. & Goldberg, A.L. (1999). Degradation of cell proteins and the generation of MHC class I-presented peptides. *Annu. Rev. Immunol.* **17**, 739–79
34. Unno, M., Mizushima, T., Morimoto, Y., Tomisugi, Y., Tanaka, K., Yasuoka, N. & Tsukihara, T. (2002). The Structure of the Mammalian 20S Proteasome at 2.75 Å Resolution. *Structure* **10**, 609–618
35. Groettrup, M., Kraft, R., Kostka, S., Standera, S., Stohwasser, R. & Kloetzel, P.-M. (1996). A third interferon-γ-induced subunit exchange in the 20S proteasome. *Eur. J. Immunol.* **26**, 863–869

36. Cascio, P., Call, M., Petre, B.M., Walz, T. & Goldberg, A.L. (2002). Properties of the hybrid form of the 26S proteasome containing both 19S and PA28 complexes. *EMBO J.* **21**, 2636–45
37. Rammensee, H.-G., Friede, T. & Stevanovic, S. (1995). MHC ligands and peptide motifs : first listing. *Immunogenetics* **41**, 178–228
38. Huber, E.M., Basler, M., Schwab, R., Heinemeyer, W., Kirk, C.J., Groettrup, M. & Groll, M. (2012). Immuno- and constitutive proteasome crystal structures reveal differences in substrate and inhibitor specificity. *Cell* **148**, 727–38
39. Chauhan, D., Singh, A. V, Aujay, M., Kirk, C.J., Bandi, M., Ciccarelli, B., Raje, N., Richardson, P. & Anderson, K.C. (2010). A novel orally active proteasome inhibitor ONX 0912 triggers in vitro and in vivo cytotoxicity in multiple myeloma. *Blood* **116**, 4906–15
40. Nawrocki, S.T., Carew, J.S., Dunner, K., Boise, L.H., Chiao, P.J., Huang, P., Abbruzzese, J.L. & McConkey, D.J. (2005). Bortezomib inhibits PKR-like endoplasmic reticulum (ER) kinase and induces apoptosis via ER stress in human pancreatic cancer cells. *Cancer Res.* **65**, 11510–9
41. Bianchi, G., Oliva, L., Cascio, P., Pengo, N., Fontana, F., Cerruti, F., Orsi, A., Pasqualetto, E., Mezghrani, A., Calbi, V., Palladini, G., Giuliani, N., Anderson, K.C., Sitia, R. & Cenci, S. (2009). The proteasome load versus capacity balance determines apoptotic sensitivity of multiple myeloma cells to proteasome inhibition. *Blood* **113**, 3040–9
42. Muchamuel, T., Basler, M., Aujay, M.A., Suzuki, E., Kalim, K.W., Lauer, C., Sylvain, C., Ring, E.R., Shields, J., Jiang, J., Shwonek, P., Parlati, F., Demo, S.D., Bennett, M.K., Kirk, C.J. & Groettrup, M. (2009). A selective inhibitor of the immunoproteasome subunit LMP7 blocks cytokine production and attenuates progression of experimental arthritis. *Nat. Med.* **15**, 781–7
43. Basler, M., Dajee, M., Moll, C., Groettrup, M. & Kirk, C.J. (2010). Prevention of experimental colitis by a selective inhibitor of the immunoproteasome. *J. Immunol.* **185**, 634–41
44. Ichikawa, H.T., Conley, T., Muchamuel, T., Jiang, J., Lee, S., Owen, T., Barnard, J., Nevarez, S., Goldman, B.I., Kirk, C.J., Looney, R.J. & Anolik, J.H. (2011). Novel proteasome inhibitors have a beneficial effect in murine lupus via the dual inhibition of type i interferon and autoantibody secreting cells. *Arthritis Rheum.* **64**, 493–503
45. Groll, M., Kim, K.B., Kairies, N., Huber, R. & Crews, C.M. (2000). Crystal Structure of Epoxomicin:20S Proteasome Reveals a Molecular Basis for Selectivity of α‘,β‘-Epoxyketone Proteasome Inhibitors. *J. Am. Chem. Soc.* **122**, 1237–1238
46. Groll, M., Koguchi, Y., Huber, R. & Kohno, J. (2001). Crystal structure of the 20 S proteasome:TMC-95A complex: a non-covalent proteasome inhibitor. *J. Mol. Biol.* **311**, 543–548
47. Vinitsky, A., Michaud, C., Powers, J.C. & Orlowski, M. (1992). Inhibition of the chymotrypsin-like activity of the pituitary multicatalytic proteinase complex. *Biochemistry* **31**, 9421–8.
48. Kisselev, A.F. & Goldberg, A.L. (2001). Proteasome inhibitors: from research tools to drug candidates. *Chem. Biol.* **8**, 739–58
49. Bross, P., Farrell, A. & Pazdur, R. (2003). Velcade(R): U.S. FDA Approval for the Treatment of Multiple Myeloma Progressing on Prior Therapy. *Oncologist* **8**, 508–513

50. Kane, R.C., Dagher, R., Farrell, A., Ko, C.-W., Sridhara, R., Justice, R. & Pazdur, R. (2007). Bortezomib for the treatment of mantle cell lymphoma. *Clin. Cancer Res.* **13**, 5291–4
51. Groll, M., Berkers, C.R., Ploegh, H.L. & Ovaa, H. (2006). Crystal structure of the boronic acid-based proteasome inhibitor bortezomib in complex with the yeast 20S proteasome. *Structure* **14**, 451–456
52. Arastu-Kapur, S., Anderl, J.L., Kraus, M., Parlati, F., Shenk, K.D., Lee, S.J., Muchamuel, T., Bennett, M.K., Driessen, C., Ball, A.J. & Kirk, C.J. (2011). Nonproteasomal targets of the proteasome inhibitors bortezomib and carfilzomib: a link to clinical adverse events. *Clin. Cancer Res.* **17**, 2734–43
53. Piva, R., Ruggeri, B., Williams, M., Costa, G., Tamagno, I., Ferrero, D., Giai, V., Coscia, M., Peola, S., Massaia, M., Pezzoni, G., Allievi, C., Pescalli, N., Cassin, M., di Giovine, S., Nicoli, P., de Feudis, P., Strepponi, I., Roato, I., Ferracini, R., Bussolati, B., Camussi, G., Jones-Bolin, S., Hunter, K., Zhao, H., Neri, A., Palumbo, A., Berkers, C., Ovaa, H., Bernareggi, A. & Inghirami, G. (2008). CEP-18770: A novel, orally active proteasome inhibitor with a tumor-selective pharmacologic profile competitive with bortezomib. *Blood* **111**, 2765–75
54. Kupperman, E., Lee, E.C., Cao, Y., Bannerman, B., Fitzgerald, M., Berger, A., Yu, J., Yang, Y., Hales, P., Bruzzese, F., Liu, J., Blank, J., Garcia, K., Tsu, C., Dick, L., Fleming, P., Yu, L., Manfredi, M., Rolfe, M. & Bolen, J. (2010). Evaluation of the proteasome inhibitor MLN9708 in preclinical models of human cancer. *Cancer Res.* **70**, 1970–80
55. Chauhan, D., Tian, Z., Zhou, B., Kuhn, D., Orlowski, R., Raje, N., Richardson, P. & Anderson, K.C. (2011). In vitro and in vivo selective antitumor activity of a novel orally bioavailable proteasome inhibitor MLN9708 against multiple myeloma cells. *Clin. Caner Res.* **17**, 5311–21
56. Kuhn, D., Orlowski, R. & Bjorklund, C. (2011). Second Generation Proteasome Inhibitors: Carfilzomib and Immunoproteasome-Specific Inhibitors (IPSIs). *Curr. Cancer Drug Targets* **11**, 285–295
57. Demo, S.D., Kirk, C.J., Aujay, M.A., Buchholz, T.J., Dajee, M., Ho, M.N., Jiang, J., Laidig, G.J., Lewis, E.R., Parlati, F., Shenk, K.D., Smyth, M.S., Sun, C.M., Vallone, M.K., Woo, T.M., Molineaux, C.J. & Bennett, M.K. (2007). Antitumor activity of PR-171, a novel irreversible inhibitor of the proteasome. *Cancer Res.* **67**, 6383–91
58. Huber, E.M. & Groll, M. (2012). Inhibitors for the Immuno- and Constitutive Proteasome: Current and Future Trends in Drug Development. *Angew. Chem. Int. Ed. Engl.* **200**, 10.1002/anie.201201616, in press
59. Basler, M., Mundt, S., Muchamuel, T., Moll, C., Jiang, J., Groettrup, M. & Kirk, C.J. (2014). Inhibition of the immunoproteasome ameliorates experimental autoimmune encephalomyelitis. *EMBO Mol. Med.* **6**, 226–38
60. Hanada, M., Sugawara, K., Kaneta, K., Toda, S., Nishiyama, Y., Tomita, K., Yamamoto, H., Konishi, M. & Oki, T. (1992). Epoxomicin, a new antitumor agent of microbial origin. *J. Antibiot. (Tokyo).* **45**, 1746–1752
61. Rubio-Aliaga, I. & Daniel, H. (2008). Peptide transporters and their roles in physiological processes and drug disposition. *Xenobiotica.* **38**, 1022–42
62. Parlati, F., Lee, S.J., Aujay, M., Suzuki, E., Levitsky, K., Lorens, J.B., Micklem, D.R., Ruurs, P., Sylvain, C., Lu, Y., Shenk, K.D. & Bennett, M.K. (2009). Carfilzomib can induce tumor cell death through selective inhibition of the chymotrypsin-like activity of the proteasome. **114**, 3439–3447
63. Singh, A. V, Bandi, M., Aujay, M. a, Kirk, C.J., Hark, D.E., Raje, N., Chauhan, D. & Anderson, K.C. (2011). PR-924, a selective inhibitor of the immunoproteasome

subunit LMP-7, blocks multiple myeloma cell growth both in vitro and in vivo. *Br. J. Haematol.* **152**, 155–63

64. Niewerth, D., van Meerloo, J., Jansen, G., Assaraf, Y.G., Hendrickx, T.C., Kirk, C.J., Anderl, J.L., Zweegman, S., Kaspers, G.J.L. & Cloos, J. (2014). Anti-leukemic activity and mechanisms underlying resistance to the novel immunoproteasome inhibitor PR-924. *Biochem. Pharmacol.* **924**,
65. Dorsey, B.D., Iqbal, M., Chatterjee, S., Menta, E., Bernardini, R., Bernareggi, A., Cassarà, P.G., D'Arasmo, G., Ferretti, E., De Munari, S., Oliva, A., Pezzoni, G., Allievi, C., Strepponi, I., Ruggeri, B., Ator, M. a, Williams, M. & Mallamo, J.P. (2008). Discovery of a potent, selective, and orally active proteasome inhibitor for the treatment of cancer. *J. Med. Chem.* **51**, 1068–72
66. Quader, S., Cabral, H., Mochida, Y., Ishii, T., Liu, X., Toh, K., Kinoh, H., Miura, Y., Nishiyama, N. & Kataoka, K. (2014). Selective intracellular delivery of proteasome inhibitors through pH-sensitive polymeric micelles directed to efficient antitumor therapy. *J. Control. Release* doi:10.1016/j.jconrel.2014.05.048
67. Ashley, J. & Stefanick, J. (2014). Liposomal Bortezomib Nanoparticles Via Boronic Ester Prodrug Formulation for Improved Therapeutic Efficacy In Vivo. *J. Med. ...* doi:10.1021/jm500352v
68. Younes, A., Bartlett, N.L., Leonard, J.P., Kennedy, D.A., Lynch, C.M., Sievers, E.L. & Forero-Torres, A. (2010). Brentuximab vedotin (SGN-35) for relapsed CD30-positive lymphomas. *N. Engl. J. Med.* **363**, 1812–21
69. Verma, S., Miles, D., Gianni, L., Krop, I.E., Welslau, M., Baselga, J., Pegram, M., Oh, D.-Y., Diéras, V., Guardino, E., Fang, L., Lu, M.W., Olsen, S. & Blackwell, K. (2012). Trastuzumab emtansine for HER2-positive advanced breast cancer. *N. Engl. J. Med.* **367**, 1783–91
70. Hamann, P.R., Hinman, L.M., Hollander, I., Beyer, C.F., Lindh, D., Holcomb, R., Hallett, W., Tsou, H.-R., Upeslacis, J., Shochat, D., Mountain, A., Flowers, D. a & Bernstein, I. (2002). Gemtuzumab ozogamicin, a potent and selective anti-CD33 antibody-calicheamicin conjugate for treatment of acute myeloid leukemia. *Bioconjug. Chem.* **13**, 47–58
71. Stein, M.L. & Groll, M. (2014). Applied techniques for mining natural proteasome inhibitors. *Biochim. Biophys. Acta* **1843**, 26–38
72. Nienaber, V.L., Richardson, P.L., Klighofer, V., Bouska, J.J., Giranda, V.L. & Greer, J. (2000). Discovering novel ligands for macromolecules using X-ray crystallographic screening. *Nat. Biotechnol.* **18**, 1105–8
73. Yamane, J., Ohyabu, N., Yao, M., Takemoto, H. & Tanaka, I. (2010). In-crystal chemical ligation for lead compound generation. *J. Appl. Crystallogr.* **43**, 1329–1337
74. Liggett, a, Crawford, L.J., Walker, B., Morris, T.C.M. & Irvine, a E. (2010). Methods for measuring proteasome activity: current limitations and future developments. *Leuk. Res.* **34**, 1403–9
75. Bosch, M., Sanchez, A., Rojas, F. & Ojeda, C. (2007). Optical Chemical Biosensors for High Throughput Screening of Drugs. *Comb. Chem. High Throughput Screen.* **10**, 413–432
76. Tu, Y., Jeffries, C., Ruan, H., Nelson, C., Smithson, D., Shelat, A. a, Brown, K.M., Li, X.-C., Hester, J.P., Smillie, T., Khan, I. a, Walker, L., Guy, K. & Yan, B. (2010). Automated high-throughput system to fractionate plant natural products for drug discovery. *J. Nat. Prod.* **73**, 751–4

77. Götze, S., Bose, A., Abele, D., Sokolova, I.M. & Saborowski, R. (2013). Pitfalls in invertebrate proteasome assays. *J. Exp. Biol.* **216**, 1351–4
78. Verdoes, M., Hillaert, U., Florea, B.I., Sae-Heng, M., Risseeuw, M.D.P., Filippov, D. V, van der Marel, G. a & Overkleeft, H.S. (2007). Acetylene functionalized BODIPY dyes and their application in the synthesis of activity based proteasome probes. *Bioorg. Med. Chem. Lett.* **17**, 6169–71
79. Clerc, J., Florea, B.I., Kraus, M., Groll, M., Huber, R., Bachmann, A.S., Dudler, R., Driessen, C., Overkleeft, H.S. & Kaiser, M. (2009). Syringolin A selectively labels the 20 S proteasome in murine EL4 and wild-type and bortezomib-adapted leukaemic cell lines. *Chembiochem* **10**, 2638–43
80. Figueiredo-Pereira, M.E., Berg, K.A. & Wilk, S. (1994). A New Inhibitor of the Chymotrypsin-Like Activity of the Multicatalytic Proteinase Complex (20S Proteasome) Induces Accumulation of Ubiquitin-Protein Conjugates in a Neuronal Cell. *J. Neurochem.* **63**, 1578–1581
81. Long, C., Beck, J., Cantagrel, F., Marcourt, L., Vendier, L., David, B., Plisson, F., Derguini, F., Vandenberghe, I., Aussagues, Y., Ausseil, F., Lavaud, C., Sautel, F. & Massiot, G. (2012). Proteasome inhibitors from Neoboutonia melleri. *J. Nat. Prod.* **75**, 34–47
82. Traenckner, E., Wilk, S. & Baeuerle, P. (1994). A proteasome inhibitor prevents activation of NF-kappa B and stabilizes a newly phosphorylated form of I kappa B-alpha that is still bound to NF-kappa B. *EMBO J.* **13**, 5433–5441
83. Blackburn, C., Gigstad, K.M., Hales, P., Garcia, K., Jones, M., Bruzzese, F.J., Barrett, C., Liu, J.X., Soucy, T. a, Sappal, D.S., Bump, N., Olhava, E.J., Fleming, P., Dick, L.R., Tsu, C., Sintchak, M.D. & Blank, J.L. (2010). Characterization of a new series of non-covalent proteasome inhibitors with exquisite potency and selectivity for the 20S beta5-subunit. *Biochem. J.* **430**, 461–76
84. Stein, M.L., Beck, P., Kaiser, M., Dudler, R., Becker, C.F.W. & Groll, M. (2012). One-shot NMR analysis of microbial secretions identifies highly potent proteasome inhibitor. *Proc. Natl. Acad. Sci. U. S. A.* **109**, 18367–71
85. Dalvit, C., Fogliatto, G., Stewart, a, Veronesi, M. & Stockman, B. (2001). WaterLOGSY as a method for primary NMR screening: practical aspects and range of applicability. *J. Biomol. NMR* **21**, 349–59
86. Jahnke, W. (2007). Perspectives of biomolecular NMR in drug discovery: the blessing and curse of versatility. *J. Biomol. NMR* **39**, 87–90
87. Pellecchia, M., Bertini, I., Cowburn, D., Dalvit, C., Giralt, E., Jahnke, W., James, T.L., Homans, S.W., Kessler, H., Luchinat, C., Meyer, B., Oschkinat, H., Peng, J., Schwalbe, H. & Siegal, G. (2008). Perspectives on NMR in drug discovery: a technique comes of age. *Nat. Rev. Drug Discov.* **7**, 738–45
88. Ladbury, J.E., Klebe, G. & Freire, E. (2010). Adding calorimetric data to decision making in lead discovery: a hot tip. *Nat. Rev. Drug Discov.* **9**, 23–7
89. Freire, E. (2008). Do enthalpy and entropy distinguish first in class from best in class? *Drug Discov. Today* **13**, 869–74
90. Johnsson, B., Löfås, S. & Lindquist, G. (1991). Immobilization of proteins to a carboxymethyldextran-modified gold surface for biospecific interaction analysis in surface plasmon resonance sensors. *Anal. Biochem.* **198**, 268–77
91. Gorodkiewicz, E., Ostrowska, H. & Sankiewicz, A. (2011). SPR imaging biosensor for the 20S proteasome: sensor development and application to measurement of proteasomes in human blood plasma. *Mikrochim. Acta* **175**, 177–184

92. Annis, D.A., Nickbarg, E., Yang, X., Ziebell, M.R. & Whitehurst, C.E. (2007). Affinity selection-mass spectrometry screening techniques for small molecule drug discovery. *Curr. Opin. Chem. Biol.* **11**, 518–26
93. Dechavanne, V., Vilbois, F., Glez, L. & Antonsson, B. (2013). Purification and separation of the 20S immunoproteasome from the constitutive proteasome and identification of the subunits by LC-MS. *Protein Expr. Purif.* **87**, 100–10
94. Heinemeyer, W. & Kleinschmidt, J. (1991). Proteinase yscE, the yeast proteasome/multicatalytic-multifunctional proteinase: mutants unravel its function in stress induced proteolysis and uncover its necessity for cell survival. *EMBO J.* **10**, 555–562
95. Winn, M.D., Ballard, C.C., Cowtan, K.D., Dodson, E.J., Emsley, P., Evans, P.R., Keegan, R.M., Krissinel, E.B., Leslie, A.G.W., McCoy, A., McNicholas, S.J., Murshudov, G.N., Pannu, N.S., Potterton, E.A., Powell, H.R., Read, R.J., Vagin, A. & Wilson, K.S. (2011). Overview of the CCP4 suite and current developments. *Acta Crystallogr. D. Biol. Crystallogr.* **67**, 235–242
96. Emsley, P., Lohkamp, B., Scott, W.G. & Cowtan, K. (2010). Features and development of Coot. *Acta Crystallogr. D. Biol. Crystallogr.* **66**, 486–501
97. DeLano, W.L. (2002). The PyMOL Molecular Graphics System. *Schrödinger LLC wwwpymolorg* **Version 1.**, http://www.pymol.org
98. Kabsch, W. (2010). XDS. *Acta Crystallogr. D. Biol. Crystallogr.* **66**, 125–32
99. Groll, M. & Huber, R. (2005). Purification, crystallization, and X-ray analysis of the yeast 20S proteasome. *Methods Enzymol.* **398**, 329–36
100. Vagin, A.A., Steiner, R.A., Lebedev, A.A., Potterton, L., McNicholas, S., Long, F. & Murshudov, G.N. (2004). REFMAC5 dictionary: organization of prior chemical knowledge and guidelines for its use. *Acta Crystallogr. D. Biol. Crystallogr.* **60**, 2184–2195
101. Homer, R.W., Swanson, J., Jilek, R.J., Hurst, T. & Clark, R.D. (2008). SYBYL line notation (SLN): a single notation to represent chemical structures, queries, reactions, and virtual libraries. *J. Chem. Inf. Model.* **48**, 2294–2307
102. Turk, D. (2013). MAIN software for density averaging, model building, structure refinement and validation. *Acta Crystallogr. D. Biol. Crystallogr.* **69**, 1342–57
103. Heinemeyer, W., Fischer, M., Krimmer, T., Stachon, U. & Wolf, D. (1997). The Active Sites of the Eukaryotic 20 S Proteasome and Their Involvement in Subunit Precursor Processing. *J. Biol. Chem.* **272**, 25200–25209
104. Liu, C., Apodaca, J., Davis, L. & Rao, H. (2007). Proteasome inhibition in wild-type yeast Saccharomyces cerevisiae cells. *Biotechniques* **42**, 158–162
105. Howard, G.C., Collins, G.A. & Tansey, W.P. (2012). Letter to the Editor. *Yeast* **29**, 93–94
106. Mosmann, T. (1983). Rapid colorimetric assay for cellular growth and survival: application to proliferation and cytotoxicity assays. *J. Immunol. Methods* **65**, 55–63
107. Gerlier, D. & Thomasset, N. (1986). Use of MTT colorimetric assay to measure cell activation. *J. Immunol. Methods* **94**, 57–63
108. Moravec, R. a, O'Brien, M. a, Daily, W.J., Scurria, M. a, Bernad, L. & Riss, T.L. (2009). Cell-based bioluminescent assays for all three proteasome activities in a homogeneous format. *Anal. Biochem.* **387**, 294–302
109. Ozorowski, G., Ryan, C.M., Whitelegge, J.P. & Luecke, H. (2012). Withaferin A binds covalently to the N-terminal domain of annexin A2. *Biol. Chem.* **393**, 1151–1163

110. Yang, H., Shi, G. & Dou, Q.P. (2007). The tumor proteasome is a primary target for the natural anticancer compound Withaferin A isolated from "Indian winter cherry". *Mol. Pharmacol.* **71**, 426–37
111. Beck, J., Guminski, Y., Long, C., Marcourt, L., Derguini, F., Plisson, F., Grondin, A., Vandenberghe, I., Vispé, S., Brel, V., Aussagues, Y., Ausseil, F., Arimondo, P.B., Massiot, G., Sautel, F. & Cantagrel, F. (2012). Semisynthetic neoboutomellerone derivatives as ubiquitin-proteasome pathway inhibitors. *Bioorg. Med. Chem.* **20**, 819–31
112. Yasunori, F., Noriaki, K. & Takenori, I. (1996). 19-Membered ring compound, its production and use thereof.
113. Yasunori, F., Noriaki, K. & Takenori, I. (1996). 18-Membered ring compound, its production and use.
114. Osmulski, P.A. & Gaczynska, M. (2013). Rapamycin allosterically inhibits the proteasome. *Mol. Pharmacol.* **84**, 104–13
115. Elnakady, Y., Rohde, M., Sasse, F., Backes, C., Keller, A., Lenhof, H.-P., Weissman, K.J. & Müller, R. (2007). Evidence for the mode of action of the highly cytotoxic Streptomyces polyketide kendomycin. *ChemBioChem* **8**, 1261–72
116. Lansdell, T.A., Hewlett, N.M., Skoumbourdis, A.P., Fodor, M.D., Seiple, I.B., Su, S., Baran, P.S., Feldman, K.S. & Tepe, J.J. (2012). Palau'amine and related oroidin alkaloids dibromophakellin and dibromophakellstatin inhibit the human 20S proteasome. *J. Nat. Prod.* **75**, 980–5
117. Koguchi, Y., Kohno, J., Nishio, M., Takagashi, K., Okuda, T., Ohnuki, T. & Komatsubara, S. (2000). TMC-95A, B, C, and D, Novel Proteasome Inhibitors Produced by Apiospora montagnei Sacc. TC 1093. Taxonomy, Production, Isolation, and Biological Activities. *J. Antibiot. (Tokyo).* **53**, 105–109
118. Krunic, A., Vallat, A., Mo, S., Lantvit, D.D., Swanson, S.M. & Orjala, J. (2010). Scytonemides A and B, cyclic peptides with 20S proteasome inhibitory activity from the cultured cyanobacterium Scytonema hofmanii. *J. Nat. Prod.* **73**, 1927–32
119. Nickeleit, I., Zender, S., Sasse, F., Geffers, R., Brandes, G., Sörensen, I., Steinmetz, H., Kubicka, S., Carlomagno, T., Menche, D., Gütgemann, I., Buer, J., Gossler, A., Manns, M.P., Kalesse, M., Frank, R. & Malek, N.P. (2008). Argyrin A reveals a critical role for the tumor suppressor protein p27(kip1) in mediating antitumor activities in response to proteasome inhibition. *Cancer Cell* **14**, 23–35
120. Yabe, K. & Koide, T. (2009). Inhibition of the 20S proteosome by a protein proteinase inhibitor: evidence that a natural serine proteinase inhibitor can inhibit a threonine proteinase. *J. Biochem.* **145**, 217–27
121. Chen, D., Frezza, M., Shakya, R., Cui, Q.C., Milacic, V., Verani, C.N. & Dou, Q.P. (2007). Inhibition of the proteasome activity by gallium(III) complexes contributes to their anti prostate tumor effects. *Cancer Res.* **67**, 9258–65
122. Zhang, Z., Bi, C., Schmitt, S.M., Fan, Y., Dong, L., Zuo, J. & Dou, Q.P. (2012). 1,10-Phenanthroline promotes copper complexes into tumor cells and induces apoptosis by inhibiting the proteasome activity. *J. Biol. Inorg. Chem.* **17**, 1257–67
123. Xiao, Y.A.N., Bi, C., Fan, Y., Cui, C., Zhang, X.I.A. & Dou, Q.P. (1992). L-glutamine Schiff base copper complex as a proteasome inhibitor and an apoptosis inducer in human cancer cells. *Int. J. Oncol.* 1073–1079doi:10.3892/ijo_00000096
124. Nardon, C., Schmitt, S.M., Yang, H., Zuo, J., Fregona, D. & Dou, Q.P. (2014). Gold(III)-dithiocarbamato peptidomimetics in the forefront of the targeted anticancer therapy: preclinical studies against human breast neoplasia. *PLoS One* **9**,
125. Li, X., Liu, S., Huang, H., Liu, N., Zhao, C., Liao, S., Yang, C., Liu, Y., Zhao, C., Li, S., Lu, X., Liu, C., Guan, L., Zhao, K., Shi, X., Song, W., Zhou, P., Dong, X.,

Guo, H., Wen, G., Zhang, C., Jiang, L., Ma, N., Li, B., Wang, S., Tan, H., Wang, X., Dou, Q.P. & Liu, J. (2012). Gambogic Acid Is a Tissue-Specific Proteasome Inhibitor In Vitro and In Vivo. *Cell Rep.* 1–12doi:10.1016/j.celrep.2012.11.023

126. Kroll, M., Arenzana-Seisdedos, F., Bachelerie, F., Thomas, D., Friguet, B. & Conconi, M. (1999). The secondary fungal metabolite gliotoxin targets proteolytic activities of the proteasome. *Chem. Biol.* **6**, 689–98
127. Jarvius, M., Fryknäs, M., D'Arcy, P., Sun, C., Rickardson, L., Gullbo, J., Haglund, C., Nygren, P., Linder, S. & Larsson, R. (2013). Piperlongumine induces inhibition of the ubiquitin-proteasome system in cancer cells. *Biochem. Biophys. Res. Commun.* **431**, 117–23
128. Mishto, M., Luciani, F., Holzhütter, H.-G., Bellavista, E., Santoro, A., Textoris-Taube, K., Franceschi, C., Kloetzel, P.M. & Zaikin, A. (2008). Modeling the in vitro 20S proteasome activity: the effect of PA28-alphabeta and of the sequence and length of polypeptides on the degradation kinetics. *J. Mol. Biol.* **377**, 1607–17
129. Kazi, A., Lawrence, H., Guida, W.C., McLaughlin, M.L., Springett, G.M., Berndt, N., Yip, R.M.L. & Sebti, S.M. (2009). Discovery of a novel proteasome inhibitor selective for cancer cells over non-transformed cells. *Cell Cycle* **8**, 1940–51
130. Lawrence, H.R., Kazi, A., Luo, Y., Kendig, R., Ge, Y., Jain, S., Daniel, K., Santiago, D., Guida, W.C. & Sebti, S.M. (2010). Synthesis and biological evaluation of naphthoquinone analogs as a novel class of proteasome inhibitors. *Bioorg. Med. Chem.* **18**, 5576–5592
131. Ge, Y., Kazi, A., Marsilio, F., Luo, Y., Jain, S., Brooks, W., Daniel, K.G., Guida, W.C., Sebti, S.M. & Lawrence, H.R. (2012). Discovery and synthesis of hydronaphthoquinones as novel proteasome inhibitors. *J. Med. Chem.* **55**, 1978–98
132. Gallastegui, N., Beck, P., Arciniega, M., Huber, R., Hillebrand, S. & Groll, M. (2012). Hydroxyureas as noncovalent proteasome inhibitors. *Angew. Chem. Int. Ed. Engl.* **51**, 247–9
133. Basse, N., Montes, M., Maréchal, X., Qin, L., Bouvier-Durand, M., Genin, E., Vidal, J., Villoutreix, B.O. & Reboud-Ravaux, M. (2010). Novel organic proteasome inhibitors identified by virtual and in vitro screening. *J. Med. Chem.* **53**, 509–13
134. Li, J., Chen, J., Gui, C., Zhang, L., Qin, Y., Xu, Q., Zhang, J., Liu, H., Shen, X. & Jiang, H. (2006). Discovering novel chemical inhibitors of human cyclophilin A: virtual screening, synthesis, and bioassay. *Bioorg. Med. Chem.* **14**, 2209–24
135. Su, M.H., Hosken, M.I., Hotovec, B.J. & Johnston, T.L. (1998). Antiosteoporotic compound.
136. Bode, H.B. & Zeeck, A. (2000). Biosynthesis of kendomycin: origin of the oxygen atoms and further investigations. *J. Chem. Soc. Perkin Trans. 1* 2665–2670doi:10.1039/b003362f
137. Janssen, C.O., Lim, S., Lo, E.P., Wan, K.F., Yu, V.C., Lee, M.A., Ng, S.B., Everett, M.J., Buss, A.D., Lane, D.P. & Boyce, R.S. (2008). Interaction of kendomycin and semi-synthetic analogues with the anti-apoptotic protein Bcl-xl. *Bioorg. Med. Chem. Lett.* **18**, 5771–3
138. Beck, P., Heinemeyer, W., Späth, A.-L., Elnakady, Y., Müller, R. & Groll, M. (2014). Structural and biochemical characterization of the natural product kendomycin and the 20S proteasome. *J. Mol. Biol.*
139. Groll, M., Bajorek, M., Köhler, A., Moroder, L., Rubin, D.M., Huber, R., Glickman, M.H. & Finley, D. (2000). A gated channel into the proteasome core particle. *Nat. Struct. Biol.* **7**, 1062–7

140. Kinnel, R.B., Gehrken, H.P. & Scheuer, P.J. (1993). Palau'amine: a cytotoxic and immunosuppressive hexacyclic bisguanidine antibiotic from the sponge Stylotella agminata. *J. Am. Chem. Soc.* **115**, 3376–3377

141. Zöllinger, M., Kelter, G., Fiebig, H. & Lindel, T. (2007). Antitumor activity of the marine natural product dibromophakellstatin in vitro. *Bioorg. Med. Chem. Lett.* **17**, 346–9

142. Blackburn, C., Barrett, C., Blank, J.L., Bruzzese, F.J., Bump, N., Dick, L.R., Fleming, P., Garcia, K., Hales, P., Jones, M., Liu, J.X., Nagayoshi, M., Sappal, D.S., Sintchak, M.D., Tsu, C., Xia, C., Zhou, X. & Gigstad, K.M. (2012). Optimization of a series of dipeptides with a P3 β-neopentyl asparagine residue as non-covalent inhibitors of the chymotrypsin-like activity of human 20S proteasome. *Medchemcomm* **3**, 710

143. Hardegger, L. a., Kuhn, B., Spinnler, B., Anselm, L., Ecabert, R., Stihle, M., Gsell, B., Thoma, R., Diez, J., Benz, J., Plancher, J.-M., Hartmann, G., Banner, D.W., Haap, W. & Diederich, F. (2010). Systematic Investigation of Halogen Bonding in Protein-Ligand Interactions. *Angew. Chemie Int. Ed.* **50**, 314–318

144. Wilcken, R., Zimmermann, M.O., Lange, A., Joerger, A.C. & Boeckler, F.M. (2013). Principles and Applications of Halogen Bonding in Medicinal Chemistry and Chemical Biology. *J. Med. Chem.* doi:10.1021/jm3012068

145. Wilcken, R., Zimmermann, M.O., Lange, A., Zahn, S. & Boeckler, F.M. (2012). Using halogen bonds to address the protein backbone: a systematic evaluation. *J. Comput. Aided. Mol. Des.* **26**, 935–45

9 Appendix

Crystallographic data collection and refinement statistics of the yCP in complex with the sulfonamide ligand (SA), Kendmycin (KM) and the phakelline derivative (PD).

Crystallographic data	yCP:SA*	yCP:KM*	yCP:PD*
Crystal parameters			
Space group	$P2_1$	$P2_1$	$P2_1$
Cell constants (Å/°)	a = 135.8	a = 136.4	a = 136.1
(dataset was collected from	b = 301.0	b = 301.1	b = 300.1
1 crystal / 1 CP per AU	c = 146.3	c = 145.6	c = 146.0
	β =113.3	β = 113.2	β = 113.1
Data collection			
Beamline	X06SA, SLS	X06SA, SLS	X06SA, SLS
Wavelength, Å	1.0	1.0	1.0
Resolution range, Å[†]	30- 2.5 (2.6-2.5)	30-2.6 (2.7-2.6)	30-2.5 (2.6-2.5)
No. observations	1045521	988940	1122779
No. unique reflections[‡]	353170	324230	366252
Completeness, %[†]	93.5 (95.2)	98.2 (99.3)	96.5 (98.7)
R_{merge}[†,§]	6.2 (64.5)	6.0 (48.5)	6.4 (52.4)
I/σ (I)[†]	13.7 (2.5)	14.3 (2.7)	11.9 (2.25)
Refinement			
Resolution range, Å	15-2.5	15-2.6	15-2.5
No. reflections working set	335511	308018	347939
No. reflections test set	24205	16212	18313
No. nonhydrogen	50894	49542	50914
No. of ligand atoms	60	70	44
Water molecules	1321	1310	1322
R_{work}/R_{free} %[¶]	17.6/22.2	17.6/22.4	17.4/21.6
Rmsd bond (Å)/(°)**	0.012/1.61	0.010/1.61	0.016/1.80
Ramachandran plot, %		96.4/3.2/0.4	

*Dataset has been collected on a single crystal.

†Values in parentheses of resolution range, completeness, Rmerge, and I/σ (I) correspond to the last resolution shell.

‡Friedel pairs were treated as identical reflections.

§Rmerge (I) = $\Sigma_{hkl}\Sigma_j\ |[I(hkl)_j - I(hkl)]|/\ \Sigma_{hkl}\ I_{hkl}$, where $I(hkl)_j$ is the measurement of the intensity of reflection hkl and <I(hkl)> is the average intensity.

¶R = $\Sigma_{hkl}||F_{obs}| - |F_{calc}||/\Sigma_{hkl}|F_{obs}|$, where R_{free} is calculated without a sigma cut off for a randomly chosen 5% of reflections, which were not used for structure refinement, and R_{work} is calculated for the remaining reflections.

**Deviations from ideal bond lengths/angles.

10 Abbreviations

Å	Ångström
A_{280}	Absorption at 280 nm
AAA	ATPases associated with diverse cellular activities
ACN	Acetonitrile
AMC	7-Amino-4-methyl-coumarin
ATP	Adenosine triphosphate
FBS	Fetal bovine serum
ChTL	Chymotrypsin-like
°C	degree Celsius
CL	Caspase-like
cCP	Constitutive 20S proteasome
CP	Core particle
CSM	Complete supplement mixture
Da	Dalton
DIPEA	N,N-diisopropylethylamine
DMEM	Dulbecco’s Modified Eagle Medium
DMF	N,N-dimethylformamide
DMSO	Dimethylsulfoxide
DNA	Desoxyribunucleic acid
EDTA	Ethylenediaminetetraacetic acid
ELISA	Enzyme-linked immunosorbent assay
ESI	Electron spray ionisation
EtOH	Ethanol
FBS	Fetal Bovine Serum
Fmoc	Fluoromethyloxycarbonyl
h	hour(s)
HCl	Hydrochloric acid
HCTU	O-(1H-6-Chlorobenzotriazole-1-yl)-1,1,3,3-tetramethyluronium hexafluorophosphate
HPLC(/MS)	(Mass spectroscopy coupled) High performance liquid chromatography
HTS	High-throughput screening
iCP	20S immunoproteasome
ITC	Isothermal calorimentry
MeOH	Methanol
MDa	mega Dalton
MES	2-(N-morpholino)ethanesulfonic acid
MHC-I	Major histocompatibility complex I
min	minute(s)

MPD	2-methyl-2,4-penatediol
MTT	(3-[4,5-dimethylthiazol-2-yl]-2,5-diphenyl) tetrazolium bromide
MWt	Molecular weight
NMR	Nuclear magnetic resonance
ORF	Open reading frame
PBS	Phosphate buffered saline
PDB	Protein data bank
PCR	Polymerase chain reaction
rmsd	Root mean square deviation
RT	Room temperature
SLS	Swiss light source
SDS	Sodium dodecylsulfate
SPR	Surface plasmon resonance
tCP	20S thymoproteasome
TFA	trifluoro acetic acid
TL	Trypsin-like
Tris	Tris(hydroxymethyl)-aminomethane
Ub	Ubiquitin
UV	Ultra violet
Vis	visible
WT	Wild type
YPD	Yeast extract peptone dextrose

11 Publications

The present thesis has been conducted from November 2010 till June 2014 under the supervision of Prof. Dr. Michael Groll, Chair of Biochemistry, TUM.

Parts of this thesis have been published:

1) Gallastegui, N., Beck, P., Arciniega, M., Huber, R., Hillebrand, S., Groll, M.
Hydroxyureas as noncovalent proteasome inhibitors.
Angewandte Chemie (International Ed. in English), 2012, **124**, 251–254.

2) Beck, P., Dubiella, C., Groll, M.
Covalent and non-covalent reversible proteasome inhibition.
Biological Chemistry, 2012, **393**, 1101–1120.

3) Stein, M. L., Beck, P., Kaiser, M., Dudler, R., Becker, C. F. W., Groll, M.
One-shot NMR analysis of microbial secretions identifies highly potent proteasome inhibitor.
Proc. Natl. Acad. Sci. USA, 2012, **109**, 18367–71.

4) Quitterer, F., List, A., Beck, P., Bacher, A., Groll, M.
Biosynthesis of the 22nd genetically encoded amino acid pyrrolysine: structure and reaction mechanism of PylC at 1.5Å resolution.
Journal of Molecular Biology, 2012, **424**, 270–82.

5) Quitterer, F., Beck, P., Bacher, A., Groll, M.
Structure and reaction mechanism of pyrrolysine synthase (PylD).
Angewandte Chemie (International Ed. in English), 2013, **52**, 7033-7.

6) Stein, M. L., Cui, H., Beck, P., Dubiella, C., Voss, C., Krüger, A., Schmidt, B., Groll, M.
Systematic Comparison of Peptidic Proteasome Inhibitors Highlights the α-Ketoamide Electrophile as an Auspicious Reversible Lead Motif.
Angewandte Chemie (International Ed. in English), 2014, **53**, 1679–83.

7) Quitterer, F.,* Beck, P.,* Bacher, A., Groll, M. (* equally contributed)
The Formation of Pyrroline and Tetrahydropyridine Rings in Amino Acids Catalyzed by Pyrrolysine Synthase (PylD).
Angewandte Chemie (International Ed. in English), 2014, DOI: 10.1002/anie.201402595

8) Beck, P., Heinemeyer, W., Späth, A.-L., Elnakady, Y., Müller, R., Groll, M.
Structural and biochemical characterization of the natural product kendomycin and the 20S proteasome.
Journal of Molecular Biology, 2014, *in print.*

9) Arciniega, M., Beck, P., Lange, O. F., Groll, M., Huber, R.
Differential global structural changes in the core particle of yeast and mouse proteasome induced by ligand binding.
Proc. Natl. Acad. Sci. USA, 2014, **111**, 9479-9484.

12 Acknowledgement

First and foremost, I would like to thank my supervisor Prof. Michael Groll for granting me the opportunity to work in his excellent team at the intersection of crystallography and chemistry. The confidence he placed in me for setting up the chair's laboratory for organic chemistry was not only a huge honor but also a great pleasure to fulfill. His enormous enthusiasm and encouragement in the event of even slightest progress helped me to bridge the times when my projects did not proceed as desired. I have greatly appreciated the freedoms he granted to me regarding my research focus and the timing of my everyday work. I'm especially thankful for his enormous support through the last year of my thesis.

Furthermore, I want to thank PD Dr. Wolfgang Heinemeyer for creating the proteasome mutants and performing yeast experiments that ultimately shed light into a very cloudy research project.

Richard Feicht deserves a special acknowledgement for all the yeast proteasome purifications and the amazing crystals he produced. This thesis heavily relied on his magic skills with handling proteins and without his enormous efforts, this work would not have been possible. I am also thankful to Astrid König, who supported me regarding a variety of aspects during my thesis.

I am also especially in debt to all the students that joined me in the lab. In particular, I thank Anna-Lena Späth for her excellent work in the cell culture lab that hugely enriched the kendomycin project. Additional thanks go to Thomas Fleming, who heavily supported the sulfonamide research project with his unrelenting commitment and perseverance.

Special credit goes to my colleague Christian Dubiella for joining me in the organic chemistry lab at the chair. Our lively discussions most often broadened my scope and I enjoyed every of the many hilarious moments in the lab.

Last but not least, I want to thank all members of the Groll group, especially my PhD colleagues that I had the pleasure to work with. I am very thankful for the fruitful collaborations but also for the relaxed atmosphere and lively discussions in our group that sparked so much inspiration.

A special thank goes to my parents for their support and providing me with every opportunity that I could have hoped for.

Finally, I am especially grateful for the love and support of my wife Laura and daughter Katharina.

13 Declaration

I, Philipp Beck, hereby declare that I independently prepared the present thesis, using only the references and resources stated. This work has not been submitted to any examination board yet. Parts of this work have been or will be published in scientific journals.

Munich, July 2014